SPSD II

ROLE OF OCEANIC PRODUCTION AND DISSOLUTION OF CALCIUM CARBONATE IN CLIMATE CHANGE (CCCC)

L. CHOU, M.-H. DARO, R. VAN GRIEKEN

PART 2

GLOBAL CHANGE, ECOSYSTEMS AND BIODIVERSITY ——— ● **ATMOSPHERE AND CLIMATE**

MARINE ECOSYSTEMS AND BIODIVERSITY

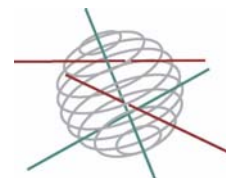TERRESTRIAL ECOSYSTEMS AND BIODIVERSITY

NORTH SEA

ANTARCTICA

BIODIVERSITY

.be

Part 2:
Global change, Ecosystems and Biodiversity

FINAL REPORT

**ROLE OF OCEANIC PRODUCTION AND DISSOLUTION OF
CALCIUM CARBONATE IN CLIMATE CHANGE**

(CCCC)

EV/05

**Lei Chou, Jérôme Harlay, Nathalie Roevros,
Delphine Lannuzel, Laura Rebreanu, Claar van der Zee**

Université Libre de Bruxelles, Laboratoire d'Océanographie
Chimique et Géochimie des Eaux
Campus Plaine – CP 208, Bd du Triomphe, B-1050 Brussels, Belgium

Pascale-Emmanuelle Lapernat, Marie-Herman Daro
Vrije Universiteit Brussel, Laboratorium voor Ecologie en Systematiek
Pleinlaan 2, B-1050 Brussels, Belgium

Katrien Aerts, Ricardo Godoi, René Van Grieken
Universiteit Antwerpen, Micro and Trace Analysis Centre
Universiteitsplein 1, B-2610 Antwerp, Belgium

BELGIAN SCIENCE POLICY

ULB

Vrije Universiteit Brussel

Universiteit Antwerpen

BELGIAN SCIENCE POLICY

TABLE OF CONTENTS

1. ABSTRACT

CCCC (Role of oceanic production and dissolution of calcium carbonate in climate change) was an interdisciplinary consortium composed of biologists, chemists, (bio)geochemists. The overall objective of this research project was to gain a better understanding of the oceanic inorganic carbon cycle and its role in climate change. We aimed, in particular, at quantifying the role of calcifying phytoplanktonic organisms in sequestering CO_2. To achieve this aim, we combined the laboratory experiments with field investigations, focusing on process-oriented studies.

Laboratory chemostat experiments were performed to investigate the effect of increasing pCO_2 on cellular calcification of an N-limited culture of *Emiliania huxleyi (E. huxleyi)*. Our investigation differed from previous studies reported in the literature by its regulation of pCO_2 based on the bubbling of gas mixtures and the maintenance of phytoplankton in the required steady-state conditions of nutrient limitation. Experimental evidence indicated that a sudden doubling in pCO_2 had a rapid effect on the cell physiology, leading to a decrease in cellular calcification rates by 25 %, which took place within two generations. The magnitude of decrease in calcification rates in this work agrees with the results found in the literature. The decrease of calcification rates in our study was not accompanied, however, by a significant decrease in the particulate inorganic carbon (PIC) to particulate organic carbon (POC) ratio because the production of organic matter paralleled the decrease in biogenic calcium carbonate precipitation.

Primary production and calcification in response to different partial pressures of CO_2 (pCO_2) ("glacial," "present," and "year 2100" atmospheric CO_2 concentrations) were also investigated during a mesocosm bloom dominated by *E. huxleyi*. The net community production (NCP) and net community calcification (NCC) were assessed during the bloom development and decline, together with oxygen production and ^{14}C incorporation. No significant change in net NCP was observed with increasing pCO_2, while the NCC was reduced by 40%. The higher pCO_2 caused a delay in the onset of calcification. A change in the ratio of PIC to POC production and thus in export fluxes could be expected with rising atmospheric pCO_2.

Three field investigations, assisted by remote sensing, were carried out during April-May 2002, April-May 2003 and June 2004 onboard the *RV Belgica* in the Gulf of Biscay where the occurrence of frequent and recurrent coccolithophore blooms had been observed. Biogeochemical parameters were measured and rates of primary production and calcification were determined. The three cruises with respect to the seasonal cycle of phytoplanktonic biomass covered distinct phases of the spring bloom. The cruise carried out in 2002 characterised an early-bloom situation, during which high rates of primary production were sustained. The subsequent cruises

(2003 and 2004) took place after the first peak of phytoplanktonic biomass (2003) or during the late-stage of the bloom (2004) and showed a lower C incorporation in the organic matter. As observed for primary production, calcification was also sustained at different rates between the three cruises and followed the pattern of primary production. Averaged calcification to primary production ratio (C:P) was estimated to be 0.34 during the 2002 early-bloom period, and decreased to 0.11 and 0.16 in 2003 and 2004, respectively.

Various degrees of $CaCO_3$ preservation were observed by SEM for samples collected during the 2004 cruise, but overall they appeared to be well preserved. A contrario, bad preservation of coccoliths was encountered within the high reflectance patch, where good $CaCO_3$ preservation was rarely found in the top 40 m of the water column. Such a low preservation may represent dissolution of $CaCO_3$ above the lysocline, as previously evoked in the literature for the same area.

Based on C incorporation data, a tentative mass balance for C can be derived for the continental shelf and slope in the Northern Gulf of Biscay area. The intensity of the biological pump is modulated by the carbonate counter-pump, which is enhanced in areas where coccolithophores develop important blooms. In early-stage conditions, the potential sequestration of C due to phytoplanktonic activity in surface waters is significant and the continental shelf behaves as a sink for atmospheric CO_2. The oceanic sink decreased with aging of the phytoplanktonic bloom either on the shelf or on the slope. Nevertheless, the potential impact of transparent exopolymer particle (TEP) formation, as suggested by our results may play an important role in C sequestration since they may contribute to suspended matter aggregation and hence to the export of C.

Finally a conceptual model is proposed to describe the implication of the production of polysaccharides (PCHO) in the metabolism of the *E. huxleyi*. The uptake of C under nutrient-replete conditions leads to the biosynthesis of functional and structural compounds that allows cells to divide during the exponential growth phase. After nutrient exhaustion, the metabolic activity is sustained by photosynthesis (maintenance functions) and, in absence of photolimitation, the excess of C taken up by photosynthesis is exuded in the form of PCHO or other C-rich compounds. Among this pool of PCHO, the acidic ones have a particular affinity for Ca^{2+} and allow $CaCO_3$ to precipitate internally. These acidic polysaccharides are then extruded with the coccoliths and are found in the external coating of the cells.

Key words: C-cycle, calcium carbonate, coccolithophores, calcification, carbonate dissolution, primary production, nutrients, Gulf of Biscay

2.   INTRODUCTION

Concentrations of carbon dioxide (CO_2), one of the most important greenhouse gases contributing to global warming, have increased by almost 30% from about 280 ppmV in the late 18th century to 370 ppmV at present-day. This increase is primarily due to combustion of fossil fuel, to cement production, and to land-use change. Recognising the societal problems which could result from climate change, the Kyoto Protocol was signed so far by 84 countries including Belgium, in response to the United Nations Framework Convention on Climate Change, in order to limit future release of CO_2 to the atmosphere.

The fate of the anthropogenic CO_2 has been intensively studied. Various sinks have been identified and quantified. Most recent estimates show that anthropogenic emission of CO_2 represents 7.1 ± 1.1 Gt C y^{-1} (1 Gt = 10^{15} g), of which 46% resides in the atmosphere, 28% is taken up by the ocean and the remaining 26% is absorbed by the terrestrial biosphere (IPCC, 1995). Being the largest reservoir of reactive carbon, the ocean acts as an important sink (2.0 ± 0.8 Gt C y^{-1}) for anthropogenic CO_2 and plays a significant role in the global biogeochemical cycle of carbon and its perturbations.

The anthropogenic CO_2 can be transferred into or out of the ocean via air-sea exchange as a result of various processes (Volk and Hoffert, 1985). They include (1) dissolution of $CO_{2(g)}$ in seawater (solubility pump), (2) photosynthesis and respiration (soft-tissue pump), and (3) precipitation and dissolution of carbonate particles (carbonate pump). The quantitative understanding of the key biogeochemical and physical processes controlling the carbon fluxes, across the air-sea interface and in the water column, is thus of primary importance in assessing the role of the ocean in climate and environmental change.

The marine biogeochemical processes seem to have responded in measurable ways to the atmospheric increase in CO_2. But the associated mechanisms are still poorly quantified and not fully understood. Considerable efforts have been made by the JGOFS community to assess the marine primary productivity and the export of organic carbon to the deep ocean (e.g. Hansen et al., 2000). The efficiency of this "biological pump" plays a crucial role in sequestering CO_2. There are, however, still large uncertainties associated with the global estimate of primary production in the ocean and its fraction exported to deep waters and buried in the sediments.

Related to the "biological pump" is the so-called "carbonate pump" involving the production and dissolution of marine calcifying algae and animals (e.g. coccolithophores, foraminifera) which form "hard" test composed of calcium carbonate ($CaCO_3$) mainly in the form of calcite, aragonite and magnesian calcites. The role of carbonate secreting phytoplankton in the marine carbon cycle is very

complex. In broadest terms, $CaCO_3$ is precipitated during photosynthesis and this carbonate sinks out of the surface layer along with the exported organic carbon. The calcification process will consume alkalinity, while the dissolution will produce alkalinity and thus modify the dissolved inorganic carbonate system according to the following reaction:

$$Ca^{2+} + 2\,HCO_3^- \Leftrightarrow CaCO_3 + CO_{2(g)} + H_2O$$

Marine carbon research in the past decade has been mainly devoted to the understanding and quantification of processes controlling the fluxes of organic matter in the ocean. Little attention has been paid, however, presently to the inorganic carbon whose net fluxes to the sediments are comparable to those of the organic matter. There is a growing awareness of the importance of the calcification process in the global carbon cycle (Bates et al., 1996; Balch and Kilpatrick, 1996; Gattuso *et al.*, 1996). Recent data based on the vertical distribution of $CaCO_3$ and sediment trap studies (Bishop *et al.*, 1980; Sherrel *et al.*, 1998; Wollast and Chou, 1998) suggest that significant dissolution of $CaCO_3$ is occurring in the upper 1000 m of the water column under conditions oversaturated with respect to calcite or aragonite. This process could act as a potential sink for atmospheric CO_2 (Sabine and Mackenzie, 1993; Milliman *et al.*, 1999). A better assessment of the production and dissolution of calcium carbonate is thus of global climatic significance.

Within this context, an interdisciplinary consortium was formed, which consisted of biologists, chemists, (bio)geochemists to carry out the CCCC (Role of oceanic production and dissolution of calcium carbonate in climate change) project. The overall objective of this research project is to gain a better understanding of the oceanic inorganic carbon cycle and its role in climate change. We aim, in particular, at quantifying the role of calcifying phytoplanktonic organisms in sequestering CO_2.

The present report presents and discusses the main results obtained by the CCCC project during laboratory experiments and field investigations. It focuses on processes associated with the oceanic production and dissolution of calcium carbonate, an important component of the marine inorganic carbon cycle. The results acquired could improve the parameterisation of processes affecting the carbon cycles in the existing coupled hydrodynamic-biogeochemical models for the prediction of the response of the marine system to increasing atmospheric CO_2 concentrations.

3.   MATERIALS AND METHODS

3.1   Laboratory chemostat experiments

The chemostat experiment is characterized by the use of continuous nitrate limited cultures of the *Emiliania huxleyi (E. huxleyi)* strain TW1 (university of Caen). The experiment of this Mediterranean strain of *E. huxleyi* was performed with K/2 culture medium based on natural filtered and sterilized Mediterranean seawater enriched with vitamins and metals, without ammonium addition. One of the major particularities of this medium, compared to other F media (Guillard and Ryther, 1962) is given by the presence of selenium that is shown to bear importance in biogenic precipitation of calcium carbonate in coccolithophores (Danbara and Shiraiwa, 1999; Obata *et al.*, 2005). Nutrient concentrations in the growth medium were set to 14-15.5 μmol.l^{-1} nitrates and 5 μmol.l^{-1} phosphates.

A chemostat is a bioreactor in which constant growth conditions for micro-organisms are maintained over prolonged periods of time by supplying the reactor with a continuous input of nutrients and continuous removal of medium. The fresh medium is supplied to the reactors by peristaltic pumping at a constant rate and the excess of cultured medium is removed. In order to reach stable conditions, the cultured medium needs to be homogenous. The chemostat properties allow converting quantities into fluxes.

Figure 1. Setup of the chemostat experiments.

The experimental setting consisted of two water-jacketed 10 l cylinders (filled to 9.5 l) connected to a circulating thermostated bath (17 ± 0.5°C) as shown in Figure 1. The

experiment was conducted at constant dilution rate of 0.5 d^{-1} under continuous irradiance (570-580 $\mu mol.m^{-2}.s^{-1}$, simulated daylight). In the case of our study, the use of continuous culture allows the maintenance of phytoplankton in steady conditions of nutrient limitation, intensive and frequent sampling over a longer period than allowed in batch cultures.

We ran two axenic cultures of *E. huxleyi* in two chemostats, under similar pCO_2 conditions and, after adaptation time, we tuned one of them (LH for Low to high pCO_2) to 700 μatm (t_0) while the other (LL for Low to Low pCO_2) was let to evolve by atmospheric CO_2 control. After 15 days of experiment, the dilution was stopped and the chemostats were turned to batch cultures.

The pCO_2 in the chemostats was achieved, using a pH-stat based approach. The desired pCO_2 was calculated from the coupled total alkalinity (TA) and pH, using dissociation constant from Roy *et al.* (1993). Because TA varied in cultures, depending on the magnitude of biological processes (principally calcification), TA was sampled daily and determined on triplicate samples in chemostats and in the culture medium. The target pH, calculated accordingly, was obtained by bubbling gas mixtures (pure CO_2, atmospheric air and CO_2-free air) by an automated system.

The pH was maintained under atmospheric air bubbling before the shift of pCO_2. In the LH (low-to-high) chemostat, the bubbling of a gas mixture enriched with CO_2 decreased the pH of seawater. The target pH, corresponding to a two-fold pCO_2 compared to actual levels, was reached within few hours and maintained by the use of a pH-stat control system. The pH regulation was done every minute in the LH chemostat while in the control one (low-to-low or LL), atmospheric air was bubbled and pH checked twice a day. Figures 2 and 3 show respectively the evolution of pH and pCO_2 during the chemostat experiments.

A complete description of the methods for the measurements of the various parameters studied can be found in Sciandra *et al.* (2003).
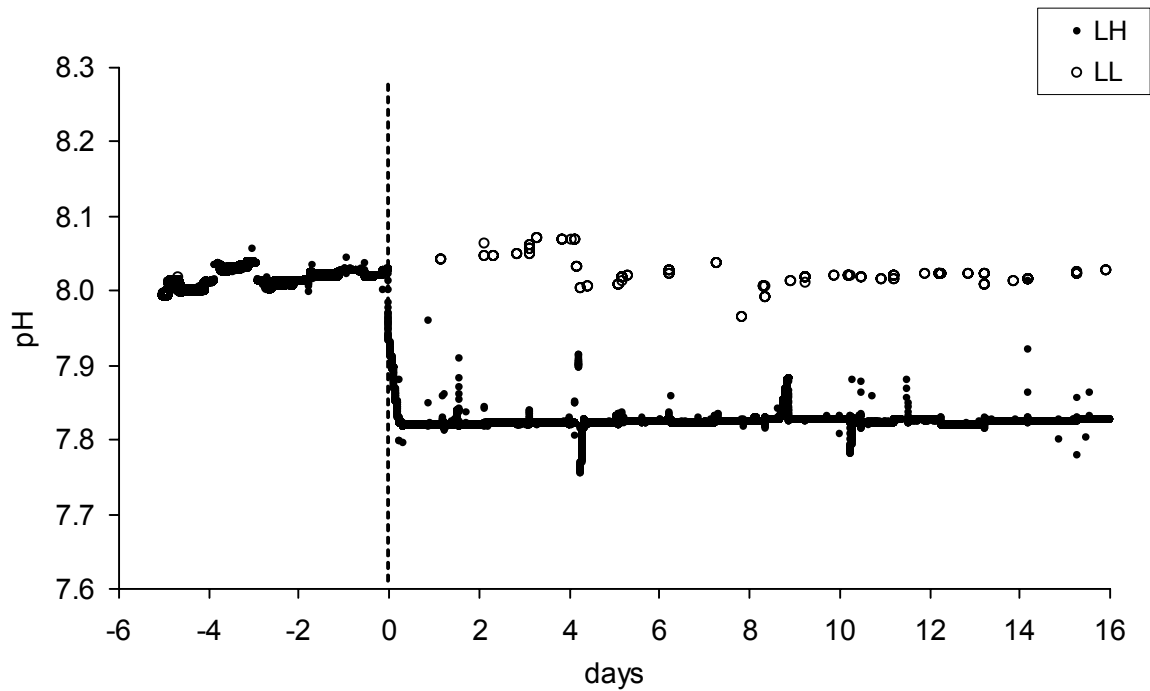
Figure 2. Measured seawater pH (seawater scale) in the low-to-high (LH solid circles) and low-to-low (LL open circles) chemostats during the experiment.
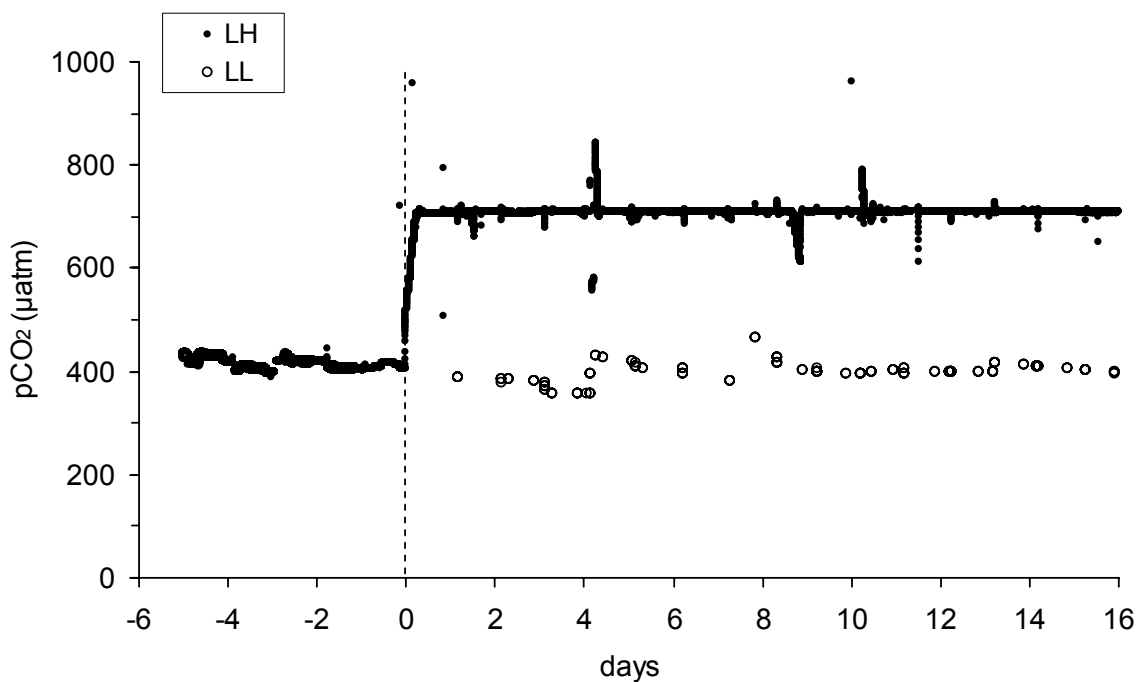
Figure 3. Calculated partial pressure in CO_2 in the low-to-high (LH solid circles) and low-to-low (LL open circles) chemostats during the experiment (dissociation constants Roy *et al.*, 1993).

Table 1. Parameters presented in Sciandra *et al.* (2003)

Parameter	Symbol	Unit	Technique
Total alkalinity	TA	$\mu mol.l^{-1}$	potentiometric Gran titration
pH	pH	sws	potentiometric TRIS-AMP
cell number		$cell.l^{-1}$	optical counting
particle diameter		μm	optical counting
Particulate organic carbon	POC	$\mu gC.l^{-1}$	elemental analysis
Particulate inorganic carbon	PIC	$\mu gC.l^{-1}$	elemental analysis
Particulate organic nitrogen	PON	$\mu gN.l^{-1}$	elemental analysis
Nitrate	NO_2	$\mu mol.l^{-1}$	spectrophotometric (auto-analyser)
Nitrite	NO_3	$\mu mol.l^{-1}$	spectrophotometric (auto-analyser)
Net Commuinty Production	NCP	$\mu mol.l^{-1}$	Winkler 0_2 measurement
Dark Community Respiration	DCR	$\mu mol.l^{-1}$	Winkler 0_2 measurement

Table 1 summarises the parameters presented in Sciandra *et al.* (2003). In addition, ^{14}C fixation in organic and inorganic matter was measured on duplicates (10 ml) for each chemostat during short-term incubations (6 hours). The spike of $NaH^{14}CO_3$ was done immediately after sample collection and the samples were kept placed into a thermostated incubator at the same light intensity as in the chemostats. The samples were filtered onto nuclepore 0.2 μm filters. ^{14}C fixation in organic matter was measured on filters after HCl 0.01 N addition while fixation in inorganic matter was measured after oxidation of the organic matter with a strong base. The filters were rinsed with filtered seawater before radioactivity counting in a Beckman counter.

3.2   Mesocosm experiment

The experiment was conducted between 31 May and 25 June 2001 in a Norwegian fjord where coccolithophore blooms occur recurrently. It consisted of isolating an 11 m^3 volume of unfiltered nutrient-poor post-bloom water from external forcings and inducing a phytoplankton bloom by adding nutrients. The aim of the experiment was to enhance a bloom of coccolithophores, which was done by adding nutrients in adequate proportions (nitrate and phosphate, without silicate). Various pCO_2 conditions were achieved by bubbling air mixtures with different concentrations of CO_2 according to the constant-alkalinity technique prior to nutrient addition. Mesocosms 1-3 were representative of the expected pCO_2 condition in the next century ("year 2100" 713 ± 6.0 ppmV), according to IPCC's "Business as usual" IS92a scenario. Mesocosms 4-6 and 7-9 were representative of present ("present" 414 ± 11.0 ppmV) and pre-industrial ("glacial" 190 ± 2.4 ppmV) conditions, respectively. The atmospheric pCO_2 corresponded to *in situ* pH$_{sws}$ of 8.209 (± 0.162), 8.016 (± 0.010) and 7.788 (± 0.025) for the "year 2100", "present" and "glacial" mesocosms, respectively.

The mesocosms were gently mixed with an airlift system in order to ensure an efficient mixing of dissolved parameters (Figure 4). An overlying volume of air was kept in equilibrium with seawater pCO_2 by the use of transparent tents, adapted at the top of the mesocosms. A complete description of the experimental setup is given in Engel *et al.* (2005).
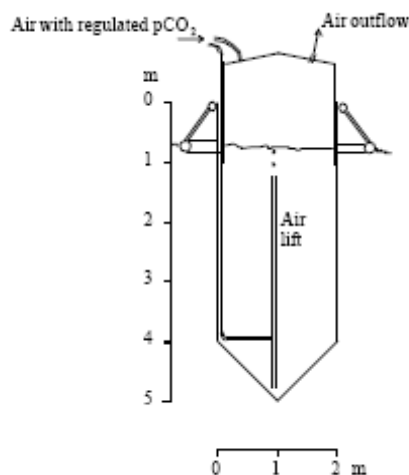
Figure 4. Set-up of the mesocosm experiments.

The large volume allowed intensive daily sampling for the description of various variables (Table 2) describing the initiation, exponential growing phase and the bloom termination.

The set of variables consisted of daily measured parameters for the description of the bloom development (Chl a, algal cell density, nutrients, elemental composition of particulate matter, viral density), in correlation with carbonate system parameters (pH, TA and pCO_2) (Engel *et al.*, 2005).

In some occasions during the bloom, the net community production and respiration were determined through oxygen production in the light and consumption in dark incubations. The net community production and calcification were determined from daily DIC and TA changes (Delille *et al.*, 2005). Primary production and calcification were determined by ^{14}C incorporation.

Subsurface seawater for incubation experiments was sampled in the mesocosms 1, 4 and 9 before sunrise. All water samples were pre-sieved through a 200µm nylon mesh to remove zooplankton species.

Table 2. Biogeochemical variables determined during the mesocosm study.

Variable	Method	Reference
Algal cell density	Flow cytometry	Engel *et al.*, 2005
Alkalinity	Gran potentiometric titration	Delille *et al.*, 2005
Alkenone concentration	Gas chromatography	A. Benthien unpubl. data
Alkenone d^{13}C	GCirmMS	A. Benthien unpubl. data
Bacterial abundance	Epifluorescence microscopy	Rochelle-Newall *et al.*, 2004
^{14}C primary production	Radiography	Delille *et al.*, 2005
Chromophoric DOM	Spectrophotometry	Rochelle-Newall *et al.*, 2004
Chl a	Fluorometry	Engel *et al.*, 2005
Coccosphere/Coccolith size	SEM	Engel *et al.*, 2005
Coccolith weight	Image analysis	Engel *et al.*, 2005
pCO$_2$	Infrared analyser (LiCor 6262)	Delille *et al.*, 2005
DOC	Shimadzu TOC analyser	Engel *et al.*, 2004a
DIC	calculated from pH, pCO2 and TA	Delille *et al.*, 2005
Light intensity	LiCor spherical sensor (Li-193SA)	Engel *et al.*, 2005
Mono-/polysaccharides	Colorimetric analysis with TPZ	Engel *et al.*, 2004b
Nutrients	Autoanalyser	Engel *et al.*, 2005
O$_2$	Winkler titration	Delille *et al.*, 2005
pH	Potentiometry	Delille *et al.*, 2005
PIC	CHN analyser (TPC-POC)	Engel *et al.*, 2005
POC	CHN analyser	Engel *et al.*, 2005
PON	CHN analyser	Engel *et al.*, 2005
POP	Acid combustrion	Engel *et al.*, 2005
d^{13}C POC	Mass spectrometry	Riebesell unpubl.
Salinity	CTD	Engel *et al.*, 2005
temperature	CTD	Engel *et al.*, 2005
TEP	Colorimetric analysis, microscopy	Engel *et al.*, 2004a
Viral density	Flow cytometry	Delille *et al.*, 2005

In situ incubations were carried out in 60-ml culture bottles inoculated with H^{14}CO$_3$ (~20 µCi per 500 ml) and incubated for 24 hours at a depth of 1.5 m in the water of the fjord adjacent to the mesocosms. Concomitant incubations were made in dark bottles.

In vitro incubations were carried out on the same inoculated batch. The samples were incubated in 75ml culture flasks for 6 hours under constant illumination (180 µmol.m-2.s-1), in incubators at the *in situ* temperature. Parallel incubations were carried out in the dark. 24-hours kinetics of ^{14}C incorporation was conducted on days 9, 12, 14, 15 and 16.

After incubation, the samples were filtered on Whatman$^{©}$ GF/F filters under gentle vacuum. Duplicate filters were collected for each sample incubated. One set of filters was treated with 100 µl HCl (0.01 N) to eliminate the inorganic radiocarbon incorporated. Radioactivity of filters was measured by scintillation counting to determine the uptake of ^{14}C both in organic and inorganic phases.

The samples treated with acid were used to quantify the production of organic carbon. The amount of inorganic carbon produced was calculated from the difference of radioactivity between organic and total carbon phases and corrected for incorporation in the dark.

Finally, the continuum between dissolved and particulate matter was studied through the determination of dissolved polysaccharides concentration (Engel *et al.*, 2004b), TEP and DOC (Engel *et al.*, 2004a). The concentrations of chromophoric dissolved organic matter (CDOM) were determined in relation with bacterial abundance (Rochelle-Newall *et al.*, 2004).

3.3   Laboratory dissolution experiments of coccolithophores

E. huxleyi was first grown in culture medium and then resuspended in seawater at various pHs to investigate the dissolution process of the carbonate skeletons. The solution pH was adjusted by the addition of HCl. Figure 5 shows the experimental set-up.
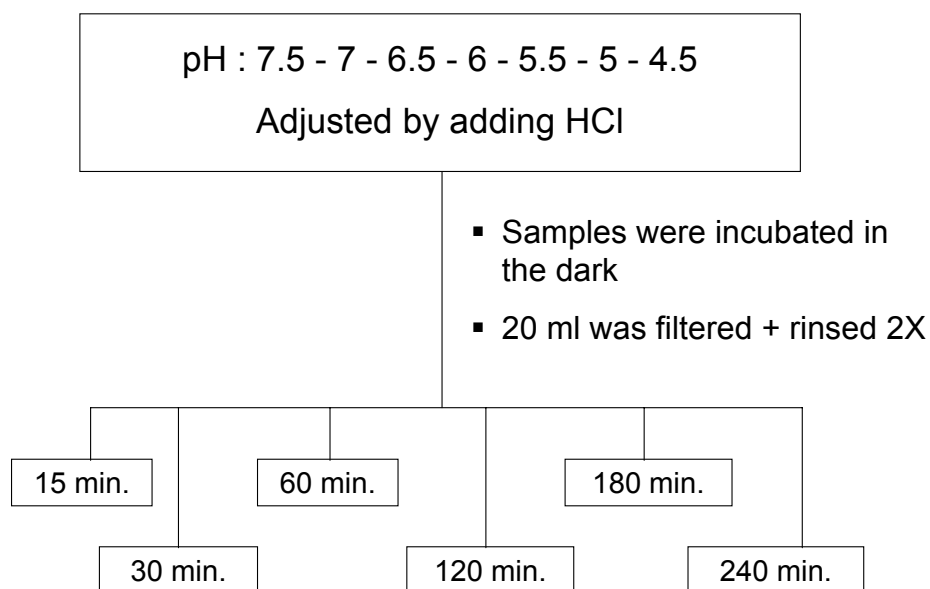
Figure 5. Setup of the dissolution experiments using Emiliania huxleyi cultures.

Solutions with *E. huxleyi* suspensions were incubated in the dark at room temperature and were sampled at various time intervals. The *E. huxleyi* particles collected were examined with SEM to observe dissolution features.

3.4   Field study area and sampling strategy

The shelf break is characterized by a marked topographic discontinuity which is particularly pronounced in the Gulf of Biscay (Figure 6) where frequent coccolithophore blooms have been observed since years.
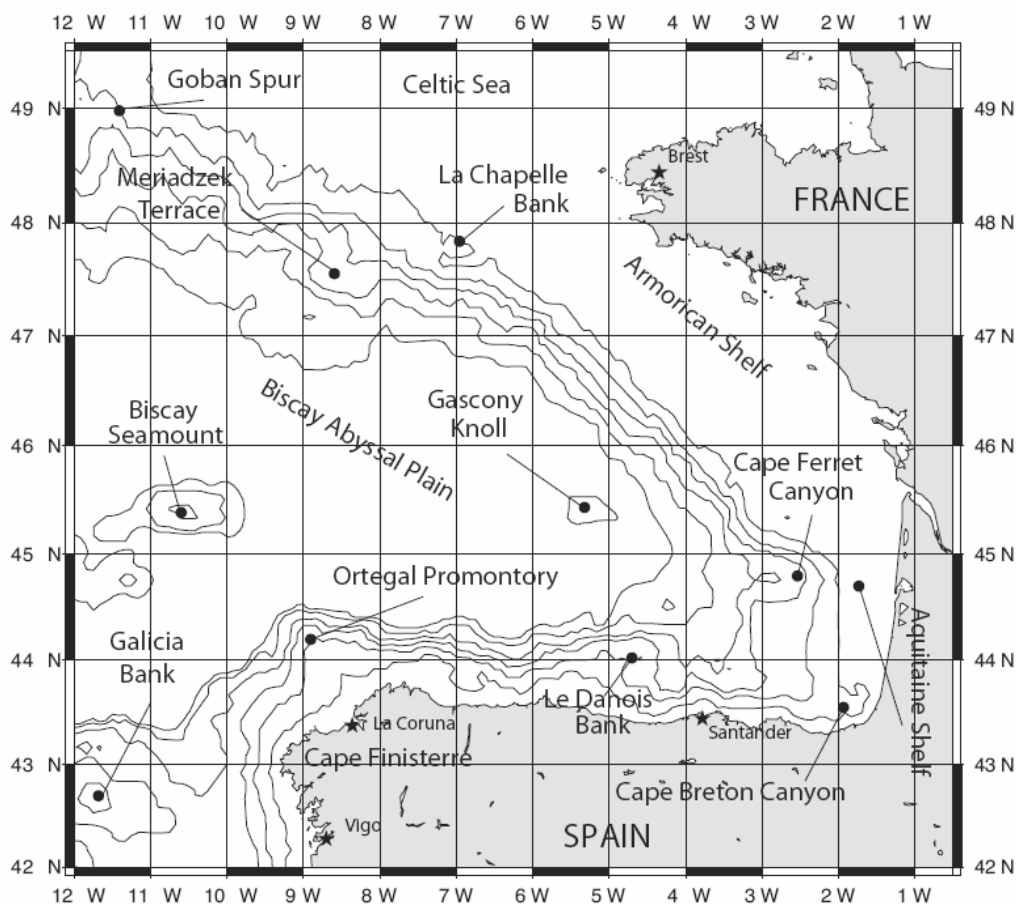
Figure 6. Map of the Biscay area. From Serpette *et al.*, 2006.

The bloom was located before and during the cruises, using daily remote sensing data (provided by the remote sensing group of the Plymouth Marine Laboratory) of the investigated area off Brittany, Northeast Atlantic. The sampling stations were located at the shelf and the shelf break of the continental shelf.

During the cruises, some stations were sampled in order to investigate processes (primary production, calcification) and parameters (vertical distribution of temperature, salinity, dissolved oxygen, pH, nutrients, suspended matter concentration and composition), which were named "process stations", and some others were sampled for parameters only, the "parameter stations".

Discrete samples were taken from a CTD Rosette sampler equipped with 10 l Niskin bottles. The samples were stored in the dark and treated shortly after sampling. Samples for oxygen concentration determination were fixed on the desk and were

kept in Winkler bottles until onboard analysis. Seawater for pH measurement was sampled in BOD 250 ml capped-bottles and stored at room temperature in the dark prior to analysis within 2 hours after the sampling.

3.5 Analytical methods for field surveys

3.5.1 Physico-chemical parameters

The **temperature** and **salinity** profiles were obtained with the Seabird CTD system that equips the Rosette sampler. The concentration of **dissolved oxygen** was measured on board by the classical Winkler method. Oxygen concentrations were converted to saturations taking into account *in situ* temperature, salinity and pressure. In parallel, vertical profiles of *in situ* **irradiance** were acquired.

3.5.2 Chlorophyll a

The concentration of **chlorophyll-a** (chl-a) was determined in one litre of seawater filtered on glass fibre filters (47 mm Whatman GF/F), wrapped in aluminum foil, stored in liquid nitrogen on board then deep-frozen at –40°C in the lab before analysis. For pigments extraction, filters were kept in 5 ml 90% acetone overnight at 4°C in the dark and centrifuged for 5 minutes at 5 000 rpm to clarify the solution. Chl-a concentration values were obtained fluorometrically, together with Phaeopigments concentration, according to Yentsch and Menzel (1963).

3.5.3 Nutrients

Seawater **Phosphate** concentration was measured spectrophotometrically according to the molybdate/ascorbic acid method. The determination was realized on frozen samples filtered onto 0.4 µm Nuclepore filters (Murphy and Riley, 1962). Seawater **Silicate** concentration was determined according the molybdate/ascorbic acid method (Grasshof *et al.*, 1983) onto acidified filtered samples kept at 4°C in plastic tubes.

3.5.4 pH and dissolved inorganic carbon

In parallel, discrete measures of **pH** were obtained at lab temperature using a Ross type combined electrode (ORION®) on the seawater scale (DOE, 1993), using a calibration with TRIS (2-amino-2-hydroxymethyl-1,3-propanediol) and AMP (2-aminopyridine) buffers in synthetic seawater of a salinity 35.5.

Total alkalinity (TA) was measured on board using a classical Gran potentiometric procedure on 100 ml GF/F filtered seawater (Gran, 1952).

The corrections for *in situ* temperature, salinity and pressure were based on the computation of the dissolved inorganic carbon system from pH and TA with the CO_2sys package (Lewis & Wallace, 1998). We used the carbonic acid constants of Roy *et al.* (1993) and the dissociation constant of boric acid from Dickson (1990).

The seawater partial pressure of carbon dioxide (**pCO$_2$**) was measured underway with an infrared gas analyser (Li-Cor©) coupled to an inflow seawater equilibrator. The seawater was taken from the non toxic seawater supply of the ship (3 meters depth). The temperature at the outlet of the equilibrator was monitored using a Metrohm platinum thermo-resistance. Data in ppmV unit were recorded automatically every 30 seconds and combined with the track of the cruise.

The *in situ* continuous pCO_2 values were normalized to a temperature constant representative to the area (15°C) using the Takahashi *et al.* (1993).

3.5.5 Suspended particulate matter (SPM) concentration

Two litres of seawater were filtered at low vacuum through preweighed Nuclepore (0.4µm, 47mm) filters and the filters were stored onboard at –20°C. The samples were oven-dried overnight at 50°C and reweighed after cooling to obtain the final dry weight. Suspended matter concentration is expressed in dry weight per litre unit.

3.5.6 Particulate organic and inorganic carbon concentration

Two litres of seawater were filtered after collection through GF/F precombusted (4 hours, 500°C) filters. The samples were stored onboard at –20°C. The filters were oven-dried overnight at 50°C. Total particulate carbon (**TPC**), particulate organic carbon (**POC**), and total particulate nitrogen (TPN) percentages of the SPM were determined sequentially with a Fison CHN micro-analyzer. The filtered area was stamped out with a calibrated punch. Triplicate stamps were kept in solvent-rinsed tin sample boats (TPC and TPN) while another triplicate was acidified overnight (POC) under HCl fumes at room temperature before being packed in solvent-rinsed tin sample boats for elemental analysis. Particulate inorganic carbon (**PIC**) percentage was estimated as the difference between averaged TPC and POC.

The CHN micro-analyzer was calibrated for each sample set using 4-5 standards (acetilanide) and 3-4 empty boat blanks to obtain a straight-line calibration as determined by the method of least-squares. The linearity of individual calibrations is excellent for both carbon and nitrogen.

Results are presented as the percentage of organic and inorganic carbon in the particulate matter.

Suspended matter analyses have been conducted on the suspended matter collected by **centrifugation** of large volumes (1500-3000 l) of surface seawater (3m depth). Inductively Coupled Plasma–Optical Emission Spectroscopy for total calcium concentration determination was carried out after complete digestion of the suspended matter by an acidic mixture (HNO_3 65%, HCl 30%, HF 40%; Suprapur Merck). Calcium carbonate concentration in surface waters and the $CaCO_3$ fraction of suspended matter (in %) are presented.

The same particulate matter was also analysed for elemental C and N composition with a Fison CHN micro-analyzer in order to compute the molar ratio of inorganic to organic carbon in the surface particulate matter (PIC:POC) and the molar ratio of organic carbon to organic nitrogen (POC:PN).

3.5.7 *Primary production and calcification by ^{14}C incorporation*

The rate of carbon fixation was estimated from the incorporation of ^{14}C-bicarbonate. Seawater was sampled at dawn with a CTD-Rosette equipped with 10 litres Niskin bottles, sieved onto 200µm mesh size, transferred into acid-cleaned carboys and then inoculated with $NaH^{14}CO_3$ (45 µCi/ml) to a final concentration of c.a. $20µCi.l^{-1}$. Five samples of 500 µl of labelled seawater were sampled from each carboy, mixed with the same volume of 0.1N NaOH in scintillation vials, frozen and used as standards.

At 3m depth fourteen sterile 250 ml culture flasks were filled with the labelled seawater and incubated for c.a. 6 hours in a linear flow-through incubator maintained at sea-surface temperature with sea surface water from the ship's continuous water supply. One flask was wrapped in aluminium foil and kept in the dark, another one was poisoned with 5% sodium azide ($3ml/l_{sw}$) and kept in the dark. The range of light received by the culture flasks ranged between 5 and 400 µmol $Photons.m^{-2}.s^{-1}$ and was calibrated daily.

In the meantime, eight other sterile culture flasks were filled and incubated under constant-light (180 µmol $Photons.m^{-2}.s^{-1}$) in a flow-through incubator maintained at sea-surface temperature with sea surface water from the ship's continuous water supply, for 2, 4, 8 and 12 hours. Two flasks were kept in the dark and two others were poisoned with 5% sodium azide ($3ml/l_{sw}$).

After the incubation period, 125ml of each sample were filtered at very low vacuum through the Nuclepore 0.4µm filters. Two filters were done for each flask. One was rinsed with 0.2µm-filtered seawater, the other one was treated with drops of 0.1N Acetic Acid and rinsed with 0.2µm-filtered seawater in order to remove particulate inorganic carbon. Both filters were dried and stored in 10ml-scintillation flasks then

frozen on board. Radioactivity was determined in the laboratory on land by liquid scintillation counting. Quenching corrections were made with an external standard.

Acidified filters were used to estimate the primary production. Daily production rates were calculated from hourly rates taking into account a daylight period (14.5 hours, incoming irradiance at noon of 1265 $\mu mol.m^{-2}.s^{-1}$) representative of both the geographic zone and the period of the year. Integration was performed over time (1 minute) and depth (0.1 m) for the water column. The photosynthetic parameters used to integrate the primary production were calculated according to Eilers & Peeters' model (1988) down to 100m and expressed in $gC.m^{-2}.d^{-1}$.

The calcification rate was estimated by difference between total ^{14}C incorporation non-treated filters (^{14}C incorporation in the total carbon pool) and primary production filters (acidified filters) down to 100m and expressed in $mgC.m^{-2}.d^{-1}$.

3.5.8 SEM and EPXMA analysis of suspended matter

The seawater samples were filtered immediately after collection to prevent interaction between dissolved and particulate phases in the storage bottles. Filtration was performed on 47 mm aerosol-grade 0.4 mm pore-size Nuclepore filters. In order to enhance the homogeneity of the particle distribution, a filter-holder was placed beneath the Nuclepore filter during filtration at low vacuum. A suitable particle density for single particle analysis was obtained by filtering 100 ml samples. To remove crystallised salts, all the filters were rinsed 3 times with 50 ml of the 0.05M NH_4HCO_3 buffer. The filters were placed in petri dishes, air dried and stored in a deep-freezer until preparation for SEM examination. During this preparation, part of the filter was cut with stainless steel scissors and mounted with double sided tape on a 25 mm plastic plate, which fits into the EPXMA sample holder. For every sample, two pieces were cut and put on a plate; the first was coated with 50 nm of carbon for automatic analysis, while the second was coated with gold to image collection. Determination of **coccospheres and coccoliths abundances** were realized by the use of automated single particle analysis by a Scanning Electron Microscope (JEOL JSM 6300), equipped for electron probe X-ray microanalysis. Computer controlled single particle analysis by EPXMA was performed to more than 200 samples, analyzing 400 particles, per sample resulting in approximately 80 thousand particles using an accelerating voltage of 20 kV and a beam current of 1 nA. X-ray spectra, collected for 20 seconds, provided information about the chemical composition of the individual particles. The magnification of 1000 times, used in the measurements, determined the minimum detectable diameter, which is about 0.7 micrometer. The size fraction analysed in each sample ranged from 0.7 µm to 10.0 µm including the size of coccoliths and Coccospheres. For analysis and interpretation, the data of each individual sample was subjected to hierarchical cluster analysis (Bondarenko *et al.*,

1996). The hierarchical results were then used as input for a non-hierarchical cluster analysis. The different particle groups present for each sample and their corresponding relative abundances were determined by the IDAS program as describe by Bondarenko *et al.* (1996). **Ca-rich particles** are characterised by a Ca-relative peak intensity higher than 90%. These particles can either be detrital or/and biogenic. *Ca-rich particles* were artificially subdivided into 2 classes based on their size fraction: coccoliths, smaller than 2.5 microns and coccolithophores ranging between 2.5 and 10 microns.

3.5.9 Transparent Exopolymer Particles concentration (2004 Cruise only)

TEP were determined spectrophotometrically according to the semiquantitative method described in Passow & Alldredge (1995). 250 ml of seawater were fixed with 1% formaline (final concentration) onboard. Within 3 months, 125ml were gently filtered through a 0.4µm polycarbonate Nuclepore membrane filter, stained with Alcian Blue (8GX) and washed with milliQ water. The concentration of TEP is expressed as gum xanthan equivalent ($\mu g.l^{-1}$).

3.5.10 Bacterial density (2004 Cruise only)

Five millilitres of seawater were fixed with 1% formaline (final concentration) and incubated for 2 hours in the dark, at room temperature. Microbes were stained with DAPI (4,6-diamidino-2-phenylindole, 0.5 $\mu g/ml_{SW}$). The sample was filtered through 0.2µm 25mm black polycarbonate Nuclepore membrane filters and quantified by immersion oil epifluorescence microscopy (at magnifications of 1,000).

3.5.11 Bacterial production (2004 Cruise only)

Bacterial production was estimated from [^{3}H]-leucine incorporation with the centrifugation method (Smith & Azam, 1992) during the 2004 cruise. A mixture of 15.6 ml of [^{14}C]-leucine (Amersham, 155 Ci mmole^{-1}) and cold leucine was added to achieve final concentrations of 16 nM and 4 nM, respectively in 5.1 ml samples. Two duplicates and one TCA-killed blank were incubated in 20 ml screw cap microcentrifuge tubes in the dark at the *in situ* temperature, for one hour. After incubation, 269 µl of 100% trichloroacteic acid (TCA) were added and the mixture was filtered after 30 minutes onto 0.2 µm 25 mm cellulose nitrate filters (Nuclepore). The filters were washed three times with 3 ml 5% TCA, dried in scintillation flasks and frozen. Radioactivity was determined in the lab by liquid scintillation counting. Quenching corrections were made with an external standard.

4.   RESULTS AND DISCUSSION

4.1   Laboratory chemostat experiments

The experiments described below aim at exploring the behaviour of coccolithophores grown under various pCO_2 concentrations. The experiments carried out by Sciandra *et al.* (2003) focuses on the calcifying stage of *E. huxleyi* in continuous nitrate-limited culture (chemostat). The experimental setup allows one to control the parameters (light, temperature, pCO_2, nutrients) of the cultured strain in order to interpret the results at the cellular level.

4.1.1 Cell density of E. huxleyi

Prior to start of the chemostat, the culture was prepared in batch conditions, corresponding to an increase in the cell number. In the first phase of the chemostat conditions, the dilution rate was increased in the reactor and 10 to 12 days was necessary to reach stable conditions for the experiment. Figure 7 shows the evolution of the cell density of *E. huxleyi* during the chemostat experiments.
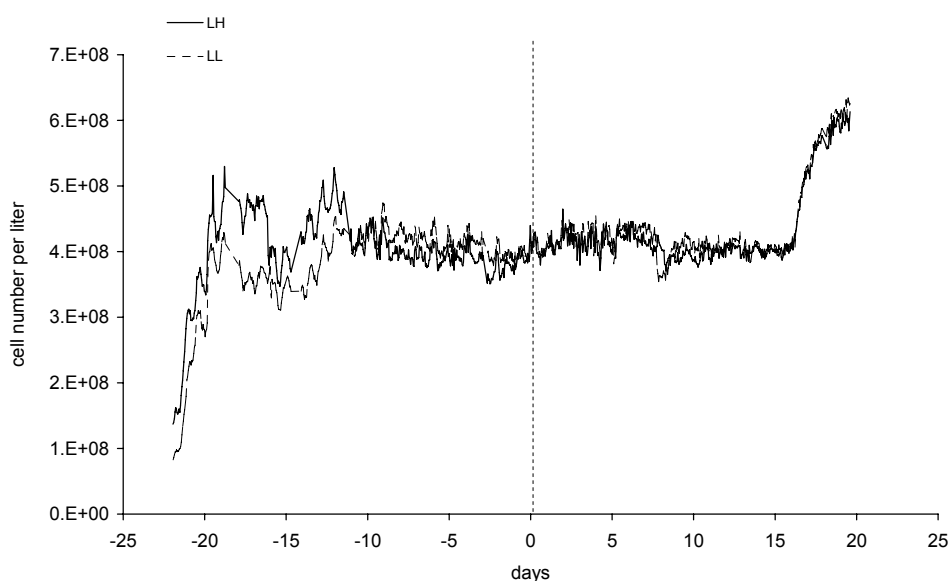

Figure 7. Cell density in chemostat LH (solid line) and LL (dashed line) during the experiment, including the pre-dilution phase (d23:d7), the pre-shift period (d7:d0), the post-shift period (d0:d15) and the return to batch culture (d15:d20)

The increase of pCO_2 had no noticeable effect on cell density (after day 0, solid line in Figure 7), compared to the control culture (dashed line in Figure 7). The cell density remained at around 4×10^8 cell l^{-1} during the experiment. The continuous record of the cell density displayed oscillations under nutrient limitation (mainly nitrate, Figure 7). These oscillations ceased after day 16, when the dilution was interrupted and the chemostat turned to batch cultures.

4.1.2 Particulate organic and inorganic carbon

The particulate organic and inorganic carbon (POC and PIC, respectively) concentrations were determined from the elemental analysis of carbon in particulate matter.

The organic carbon content per cell is in agreement with other reported values of Paasche (1998, 1999). Figure 8 shows its evolution during the experiment in the LL and LH cultures. Initial contents of organic carbon ranged between 5.09 ± 0.15 and 5.27 ± 0.10 pgC cell^{-1} in the LL and LH cultures, respectively before t_0. A slight but not significant increase was observed in the LL culture after the shift. A 14 % decrease was observed in the LH culture consecutively to the shift (4.37 ± 0.23 pgC cell^{-1}).
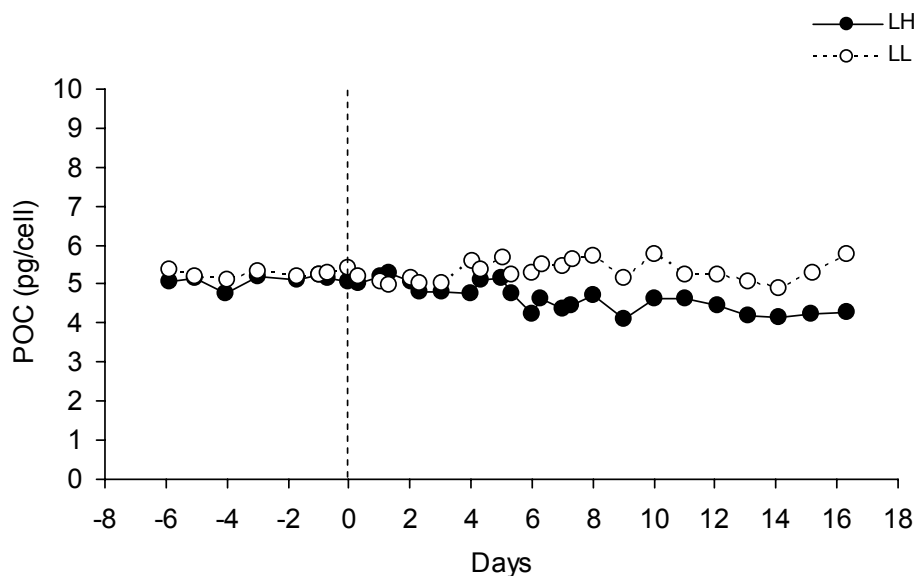
Figure 8. Evolution of particulate organic carbon content per cell in chemostat LH (solid circle) and LL (open circle) during the experiment (expressed in picograms of carbon per cell).

The properties of the chemostat allow one to convert concentrations into fluxes when the dilution rate (*D*) is known. The variation of the POC concentration within the experiment is given by the Eqn. (1).

$$\frac{dPOC}{dt} = Pn - DPOC \qquad (1)$$

At steady state, the values of POC and *n* (cell concentration) are sufficient to determine the net cellular production of organic carbon.

$$P = D\frac{POC}{n} \tag{2}$$

In response to higher pCO_2 conditions, the P remained stable in the control culture (LL) and decreased significantly in the LH culture by 15 % (Table 3). These data agree with the previous results of oxygen fluxes.

Table 3. Mean (SD) production of particulate organic carbon and calcification ($pgC.cell^{-1}.d^{-1}$) before and after t_0 in the LH and LL cultures

| Process		Before t_0	After t_0	
P	LH	2.55 (0.07)	2.17 (0.10)	$p < 0.0001$
	LL	2.63 (0.05)	2.65 (0.15)	$p > 0.04$
		$p > 0.03$	$p < 0.0001$	
C				
	LH	2.22 (0.13)	2.02 (0.06)	$p < 0.002$
	LL	2.30 (0.08)	2.38 (0.08)	$p > 0.03$
		$p > 0.08$	$p < 0.0001$	

The concentration of PIC (Figure 9) before the shift varied from 4.45 ± 0.27 to 4.60 ± 0.15 $pgC.cell^{-1}$ in the LL and LH cultures, respectively, and decreased significantly to 3.92 ± 0.36 $pgC.cell^{-1}$ in response to increasing pCO_2 during the experiment.

As suggested for POC, PIC concentrations can be converted to calcification C fluxes according to the Eqn. (3):

$$C = D\frac{PIC}{n} \tag{3}$$

In response to higher pCO_2 conditions, the C remained stable in the control culture (LL) and decreased significantly in the LH culture by 15 % (Table 3).

As a result of the changes in P and C under higher pCO_2 conditions, the calcification to organic production C:P ratio did not display significantly different values before and after t_0 (Figure 10).
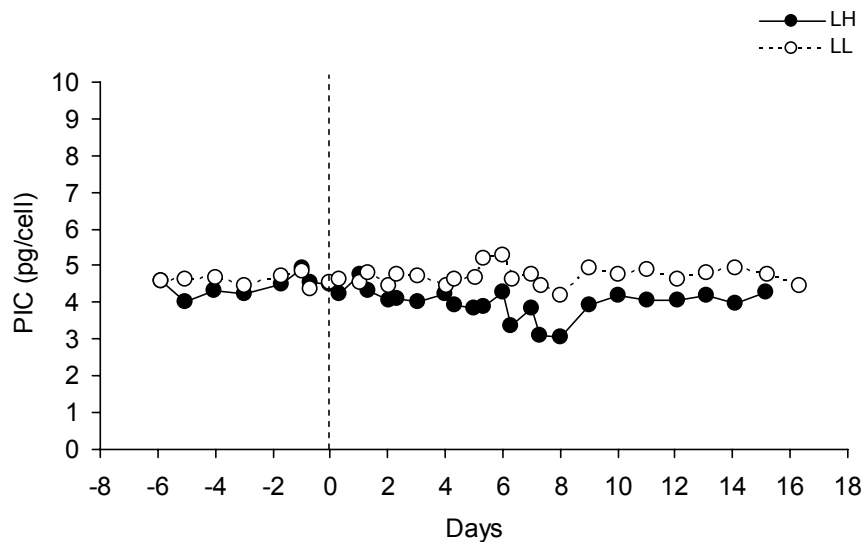
Figure 9. Particulate inorganic carbon in chemostat LH (solid circles) and LL (open circles) during the experiment (expressed in picograms of carbon per cell).
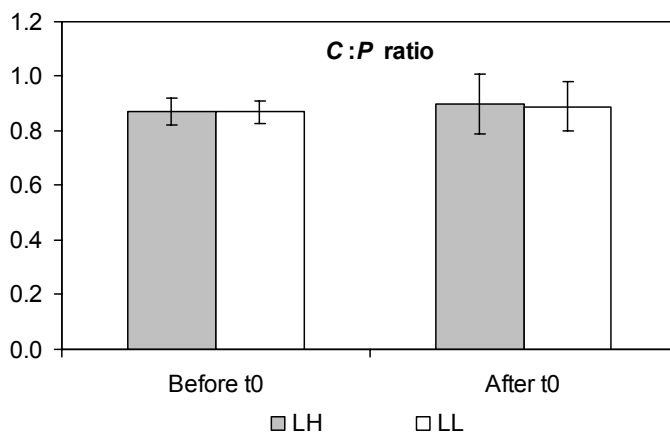

Figure 10. Mean molar ratios of inorganic to organic carbon production (C:P) in the LH (grey bars) and LL (white bars) cultures before and after the shift of pCO_2.

4.1.3 Total alkalinity and calcification

Total alkalinity was very stable in the enrichment medium (reservoir) and its variations in the cultures were essentially related to the magnitude of calcification within the *E. huxleyi* community.

The evolution of TA during the experiment is shown in Figure 11. Prior to t0, a very small difference was observed in TA between the two cultures. This difference disappeared completely by the time of the shift, suggesting that the conditions were very similar in the two cultures. Following the shift of pCO_2, the TA increased significantly in the LH culture, compared to the control (LL) one.
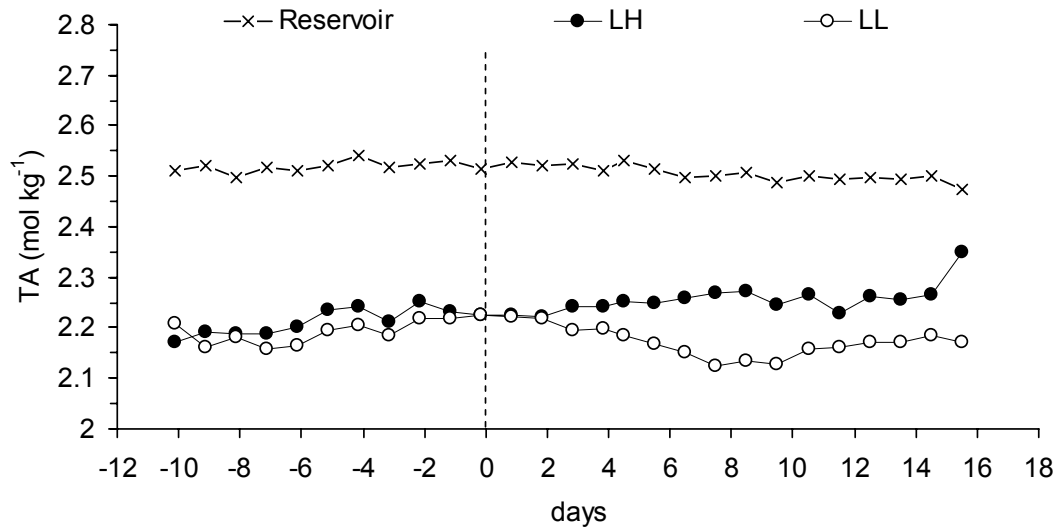
Figure 11. Total alkalinity (mmol.kg^{-1} of seawater) in the reservoir (crosses) and chemostats (LH, solid circles; LL, open circles) during the experiment.

According to Eqn. (4), the fluxes of TA may vary as a function of (1) the input of TA$_i$ from the reservoir (and are then dependant on the dilution rate D) and (2) the calcification rate of the community Cn (where C is the cellular calcification rate and n the cell abundance).

$$\frac{dTA}{dt} = D(TA_i - TA) - Cn \tag{4}$$

Rearranging the equation (4) leads to the expression of the mean cell calcification rate:

$$C = \frac{1}{n}\left\{ D(TA_i - TA) - \frac{dTA}{dt} \right\} \tag{5}$$

The discretized expression of Eqn. (5) allows the calculation of the net cellular calcification rate $\overline{C}$.

$$\overline{C} = \frac{1}{n_{(0)}}\left\{ D(TA_i - TA_{(0)}) - \frac{\Delta TA}{\Delta t} \right\} \tag{6}$$

Eqn. (6) is valid under the assumption that the process is linear during the time interval Δt. Under this condition, $\overline{C}$ can be considered as a good approximation of C.

ΔTA is the variation of TA during the time interval Δt and the $n_{(0)}$ and $TA_{(0)}$ are the cell abundance and the TA at the beginning of the time interval. The magnitude of

calcification is hence given by the difference between the TA of the renewal medium (reservoir) and the TA of the culture.

Figure 12 shows that the decrease of calcification in the LH culture was significant (Student's t-test, p is the probability of H_0) compared to initial conditions ($p < 0.0002$) and compared to the control culture ($p < 0.0001$). In contrast, no significant difference was observed in the control culture before and after t_0. The average rates of net calcification calculated from TA budgets agree reasonably with the ones calculated from PIC measurements. The consistency of these results validates the use of the total alkalinity anomaly for following and estimating the net rate of calcification in continuous cultures, as described in Sciandra *et al.* (2003).
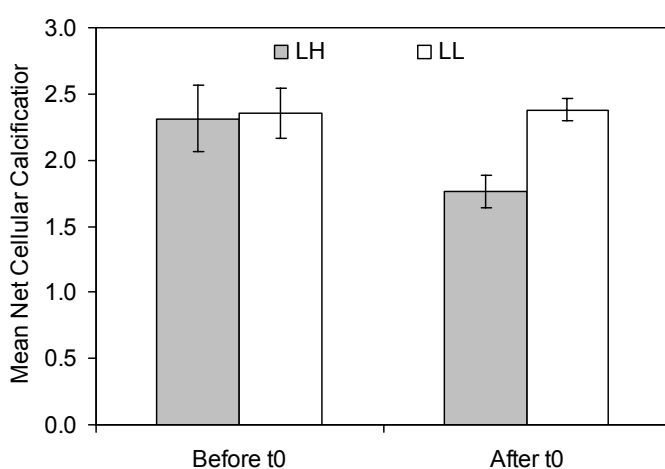

Figure 12. Mean net cellular calcification rate (pgC cell^{-1} d^{-1}) in the LL (grey bars) and the LH (white bars) cultures before and after t_0 (considering the steady-state from day 7 onward).

A 25 % decrease of the net calcification rate was observed in response to higher pCO_2 during the experiment, if one considers the last 8 days of the experiment as a steady-state situation (Figure 12). However, the decrease in C estimated from the PIC method was only 12 %. The detachment and subsequent release of coccoliths during the development of *E. huxleyi* and their accumulation in the culture medium may explain the difference between the two estimations (Fritz and Balch, 1996; Fritz, 1999). More credit should then be given to the estimation based on the total alkalinity anomaly, since calcium carbonate the in the form of released coccoliths could lead to overestimation of PIC when they accumulate in the medium. This is more important when the culture is aged because the mixing of the medium generally does not allow one to ensure a complete homogeneity of the suspension of particulate $CaCO_3$. This observation emphasizes the importance of coccolith detachment in the export of $CaCO_3$ material during *E. huxleyi* blooms.

Scanning electron microscopy (SEM) of individual cells shows the appearance of coccoliths in the control culture and in the high-pCO_2 one. The coccoliths, in the high-pCO_2 culture (Figure 13b) presented missing radii as shown by the white arrows.

Such features were not observed in the SEM pictures of the control culture (Figure 13a).
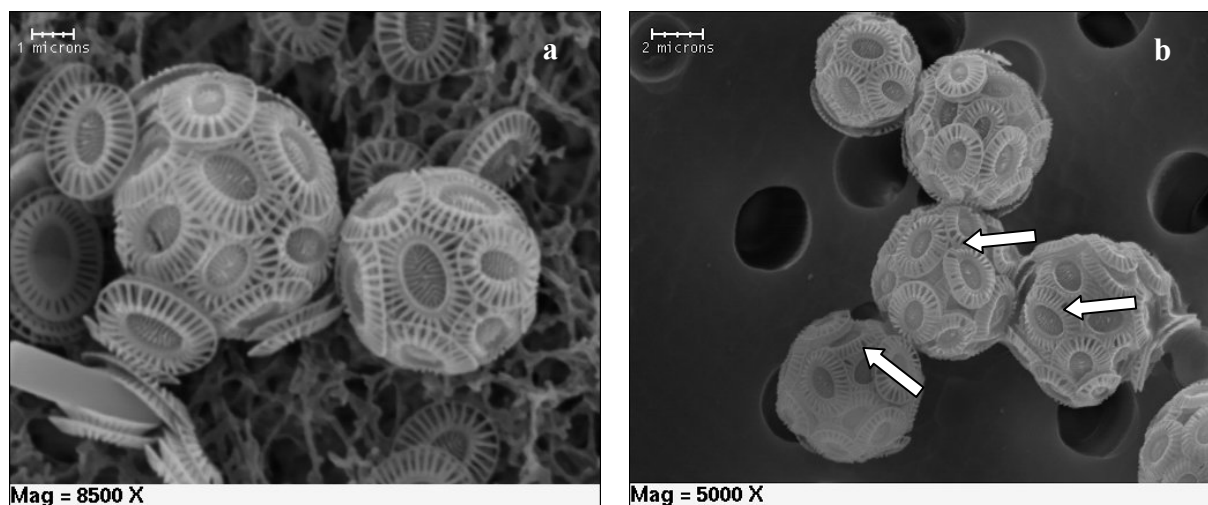
Figure 13. Scanning electron micrographs of *E. huxleyi* cells after t_0 (a) in the control culture and (b) in the high-pCO_2 culture

4.1.4 Concluding remarks on the chemostat experiments

The chemostat experiment is the first one to investigate the effect of increasing pCO_2 on cellular calcification of a N-limited culture of *E. huxleyi*. It also differs from previous studies by its regulation of pCO_2 based on the bubbling of gas mixtures that enables the use of total alkalinity anomaly to appreciate the changes in the rate of calcification.

This experiment provides experimental evidence that a sudden doubling in pCO_2 has a rapid effect on the cell physiology, leading to a decrease in cellular calcification rates by 25 %, which takes place within two generations. The magnitude of decrease in calcification rates in this work agrees with previous study of Zondervan *et al*. (2002) who found a 20 % decrease when pCO_2 was shifted from 100 to 750 µatm. In contrast to the results of Zondervan *et al*. (2002) in N-repleted cultures, the decrease of calcification rates in our study was not accompanied by a significant decrease in the PIC:POC ratio because the production of organic matter paralleled the decrease in calcium carbonate precipitation.

The major difference between the two experiments lies in the nutrient status and principally N-limitation if one considers that the pCO_2 control resulted in comparable changes in DIC (see §3.2). In nutrient-repleted conditions, Schippers *et al*. (2004) suggested, through modelling studies, that increasing pCO_2 would promote phytoplankton productivity. They argued that this effect could be larger than expected for Primnesiophytes such as *E. huxleyi*.

Even if high levels of NO_3 (>100 µM) has a potential impact on calcification (Nimer and Merrett, 1993), a minimum NO_3 is required for calcification (Merrett *et al.*, 1993). This simply indicates a coupling between organic matter production and calcification. Calcification has been shown to be a cost-effective mechanism for the cell (Anning *et al.*, 1996) and implies the synthesis of organic structures prior to coccolith extrusion. The time required to synthesize these structures depends on the efficiency of C and N uptake by the cells. Under N-limited conditions, Paasche (1998) found that the cellular organic carbon decreased and was accompanied by the decrease in the Ca-content of the cells and a decrease in coccolith size. These observations are consistent with ours, suggesting that the cells were significantly smaller after the dilution was turned on. After t0, the cell volume was smaller in the LH culture, compared to the control one, indicating that high-pCO_2 conditions reinforce the effect of nitrogen limitation on organic matter production. Nitrogen is the critical constituent of proteins that are involved in functional and structural components in the cells. It is also the main constituent of RUbisCO that may represent up to 10 % of the total nitrogen content in the cells. It is hypothesized here that the effect of N-limitation affects the uptake of C in the cultures. Changes in DIC availability coupled to N-limitation could be responsible for the observed decrease of organic carbon production in the LH culture.

It is very difficult to decouple the effect of pCO_2 on cellular calcification and on cell physiology, since calcification takes place internally and is consequently driven by the cell physiology. The sources of DIC for growth of calcifying strains of *E. huxleyi* are CO_2 and HCO_3^-. The exact species responsible for organic matter production is still under debate since CA activity (that catalyses the conversion of HCO_3^- to CO_2) was shown to happen both inside and outside the cells of some strains of *E. huxleyi* (Elzenga *et al.*, 2000; Rost *et al.*, 2003). The presence of CA activities is often associated with CCM activities that enable the use of the most abundant DIC species and make the species less sensitive to DIC variations (Israel and Hofy, 2002). However, Rost *et al.* (2003) emphasize the low affinity for DIC within this species as a general feature, compared to diatoms. This may be due to the presence of effective carbon concentration mechanism (Beardall *et al.*, 1998) and the ability to store nitrogen within the cells (Iglesias-Rodriguez *et al.*, 2002) in the latter species, in contrast to *E. huxleyi*. As pCO_2 increases from 412 to 708 µatm, the bicarbonate increased by 9 %, the CO_2 by 42 %, the carbonate (and hence, the saturation state with respect to calcite) and the pH decreased by 31 % and 2.5 %, respectively. We hypothesize, here, that the less efficient carbon uptake under N-limited conditions could result in a redistribution of the potential carbon substrates for growth. This hypothesis is speculative and would require further experiments with non-calcifying strains under the same conditions.

Besides carbon uptake, another possible cause for the decrease in the net production could be linked to the variation in pH linked to the pCO_2 shift. The cell membrane is a physical selective and active barrier that isolates the inner cell from the exterior environment. The inner medium concentration is actively regulated by cost-effective mechanisms that permit large ions to cross the membrane in exchange with protons. The use of bicarbonates for photosynthesis consumes protons while calcification has the opposite effect. A model of inner pH regulation by the interplay of both mechanisms has been presented by Anning *et al*. (1996) and further simplified by Buitenhuis *et al.* (1999). They suggest that, in response to external pH changes, the cell may adapt both processes in order to keep cytosolic pH to a relatively constant value. The inhibition of growth rate under high-pCO_2 conditions could, following their hypothesis, be related to the inability of *E. huxleyi* to generate sufficient OH^- (i.e. by photosynthesis) to counteract the acidification of the cytosol. This alternative hypothesis would also require further experiments on non-calcifying strains, using the "pH constant" pCO_2 regulation that allows the DIC to vary without changes in pH. The assembly of calcite crystal to produce the calcium carbonate phase is thermodynamically dependant on the oversaturation state with respect to this phase (Ω_{cal}) in the sense that higher Ω_{cal} is more favourable for fast growing $CaCO_3$ structures. Biogenic calcification responds positively to changes of Ω in seawater, as suggested by previous works on corals (Gattuso *et al.*, 1998). It is therefore intuitive to consider that decreases in calcification rates in response to increases of pCO_2 would be a general feature. The overall response of calcification mediated by organic matter growth is consequently difficult to assess when pCO_2 increases since, as we see in this study, the response of biology depends on various parameters such as, among others, environmental conditions (nutrient status, irradiance variations, seawater chemistry …) and genetic variability. This experiment could therefore be considered as a pioneer work in the understanding of the behaviour of *E. huxleyi* in the coming decades and should be completed by other aspects of cell biology, including experimental works and modelling effort.

4.2   Mesocosm experiments

At a higher integration level, the experiment carried out in mesocosms (Engel *et al.*, 2005) provides important information on the response of the coccolithophorid community under "pre-industrial", "present" and "year 2100" pCO_2 conditions. In contrast to the previous experiment using chemostat, the experimental setup of mesocosms experiments aims at being as close as possible to environmental conditions (natural light and light attenuation with depth, water column design with vertical mixing). Our approaches differ from previous studies on cultured strains or natural assemblages by two major points. Firstly, the pCO_2 has not been regulated by adding base or acid in order to respect the conservative aspect of total alkalinity in

the short-term perspective of the IPCC IS92a's scenario for "year 2100" atmospheric CO_2 concentration (Millero *et al.*, 1998). Secondly, the daily survey of the parameters makes possible using the total alkalinity anomaly to calculate the net calcification rate for each condition.

4.2.1 Dissolved inorganic carbon system

The partial pressure of CO_2 in seawater was determined with an equilibrating system coupled to an infrared gas analyser (Frankignoulle *et al.*, 2001) and total alkalinity was measured using the classical Gran potentiometric method (Gran, 1952). The measured pCO_2 was corrected for temperature and vapour pressure and TA was corrected for changes due to phytoplanktonic nutrient utilization during organic biosynthesis and normalized to a constant salinity of 31 (Delille *et al.*, 2005).

The speciation of dissolved inorganic carbon was determined through the daily measurements of pCO_2 (uncertainty of $\pm$ 3 ppmV) and TA (reproducibility $\pm$ 3 $\mu mol.kg^{-1}$).

The initial setup for seawater pCO_2 ranged between 190 $\pm$ 2.4 ppmV for the low-pCO_2 treatment (i.e.; "glacial", bags 7-9), 414 $\pm$ 11 ppmV for the actual pCO_2 treatment (i.e. "present", bags 4-6) and 713 $\pm$ 6.0 ppmV for the high-pCO_2 treatment (i.e. "year 2100", bags 1-3). After nutrient addition (d0), the air-space was kept to the initial pCO_2 while the underlying seawater was let to evolve with biological activity (Figure 14).

The onset of biological activity, enhanced by nutrient addition in the bags, has caused a decrease in seawater pCO_2 during the course of the experiment according to Eqn. (7). The magnitude of the changes in pCO_2 depended both on the magnitude of the primary production and the buffer capacity of seawater in each bag (Figure14).

$$106CO_2 + 16NO_3^- + H_2PO_4^- + 17H^+ + 122H_2O \rightarrow (CH_2O)_{106}(NH_3)_{16}(H_3PO_4) + 138O_2 \qquad \textbf{(7)}$$
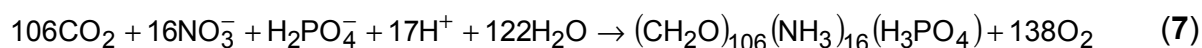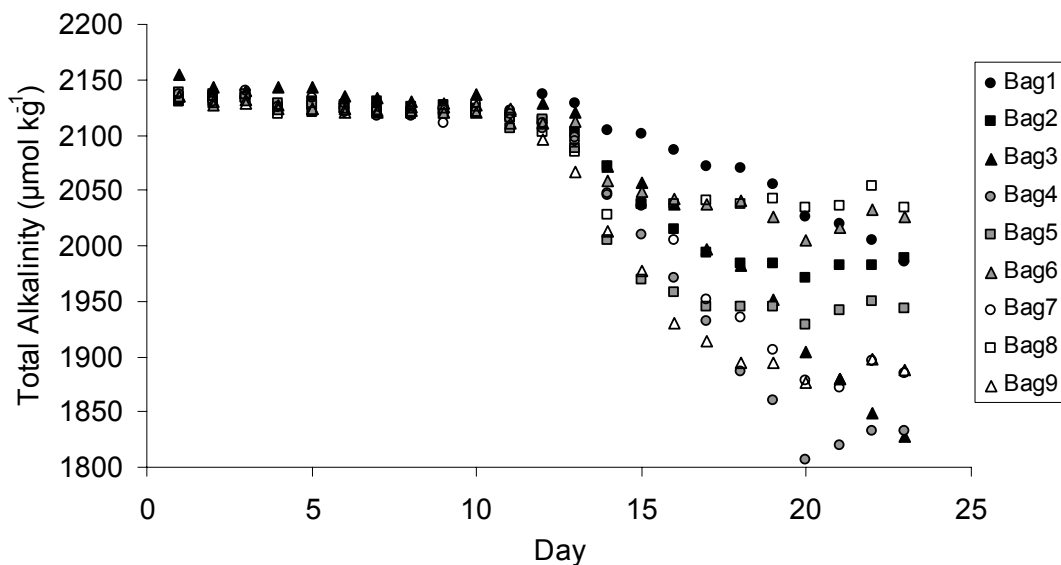
Total alkalinity decreased after d10 (Figure 15), as a result of enhanced calcification during the coccolithophore bloom according to the following equation:

$$2HCO_3^- + Ca^{2+} \rightarrow CaCO_3 + CO_2 + H_2O \qquad \textbf{(8)}$$
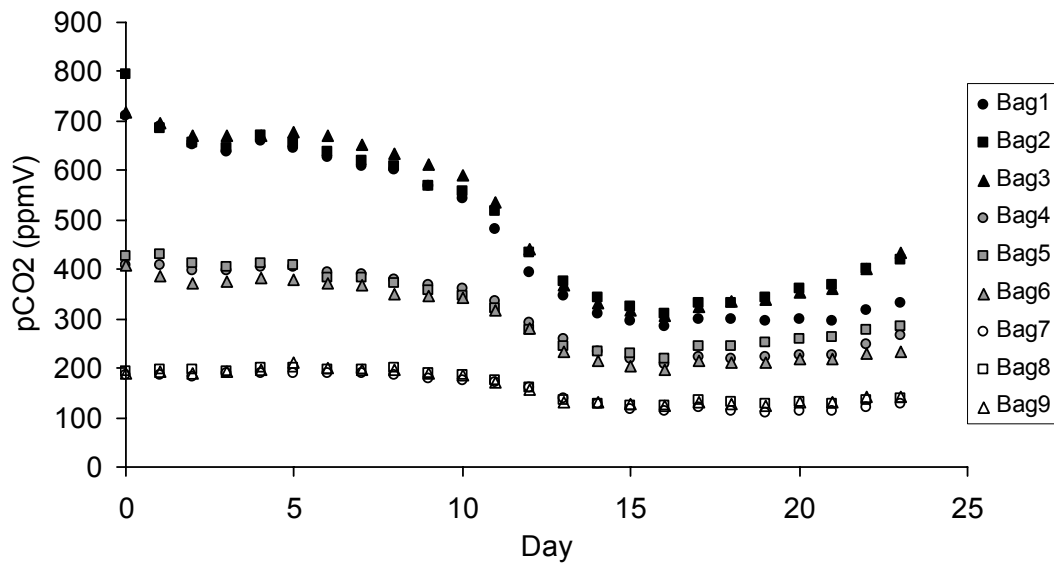
Figure 14. Seawater pCO$_2$ (ppmV) in enclosures for "year 2100" (black symbols), "present" (grey symbols) and "glacial" (open symbols). From Delille et al. (2005) and Engel et al. (2005).
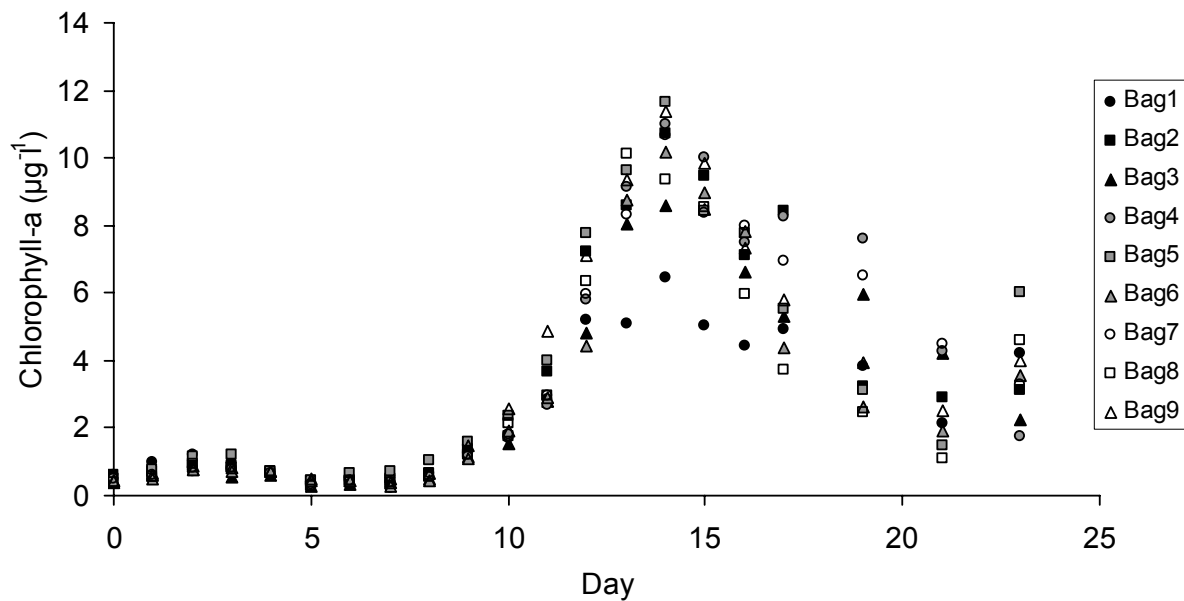

Figure 15. Total alkalinity (μmol.kg^{-1}) in enclosures for "year 2100" (black symbols), "present" (grey symbols) and "glacial" (open symbols). From Delille et al. (2005) and Engel et al. (2005).

4.2.2 *Chlorophyll-a and phytoplankton dynamics*

A net growth of the phytoplanktonic community, as represented by chlorophyll-a (Chl-a) concentrations was detectable after day 5 for all the bags (Figure 16). Within 10 days, Chl-a concentrations has increased from pre-bloom concentration of 1 μg.l^{-1} to values between 6.5 (bag 1) and 12 μg.l^{-1} (bag 5) at the height of the bloom on

day 14. The dynamics of Chl-a concentrations after day 14 (post-bloom situation) became more variable between mesocosms.

Figure 16. Chlorophyll-a ($\mu g.l^{-1}$) in enclosures for "year 2100" (black symbols), "present" (grey symbols) and "glacial" (open symbols). From Engel et al. (2005).

Within the 10 first days of the experiment, during the pre-bloom situation with respect to *E. huxleyi*, the phytoplankton community was dominated by picocyanobacteria (*Synechococcus spp.*) and other autotrophic microflagellate (of which *Micromonas spp.* was dominant) species (Figures 17 and 18). Both species did not show any response to pCO_2 (Engel *et al.*, 2005). However abundant in terms of cell density, they did not contribute significantly to the increase in biomass, compared to *E. huxleyi*.

The abundance of *E. huxleyi*, detectable after 5 days, increased and became the dominant species during the exponential growth phase (Figure 19). Maximum cell abundance was reached on days 17 and 18 (up to $6 \cdot 10^4$ cell.ml^{-1} in bag 4) in the mesocosms and was followed by a net decrease. The net specific growth rate (μ), calculated as the average daily growth rates until the peak of the bloom on d14 (Engel *et al.*, 2005) for each treatment, ranged between 0.50 ± 0.26 d^{-1} in the low-pCO_2 treatment and 0.43 ± 0.19 d^{-1} in the high pCO_2 treatment. The average growth rates in the low-pCO_2 treatment was significantly higher than in the high-pCO_2 treatment (Engel *et al.,* 2005), although no systematic difference was observed between each of the three treatments.
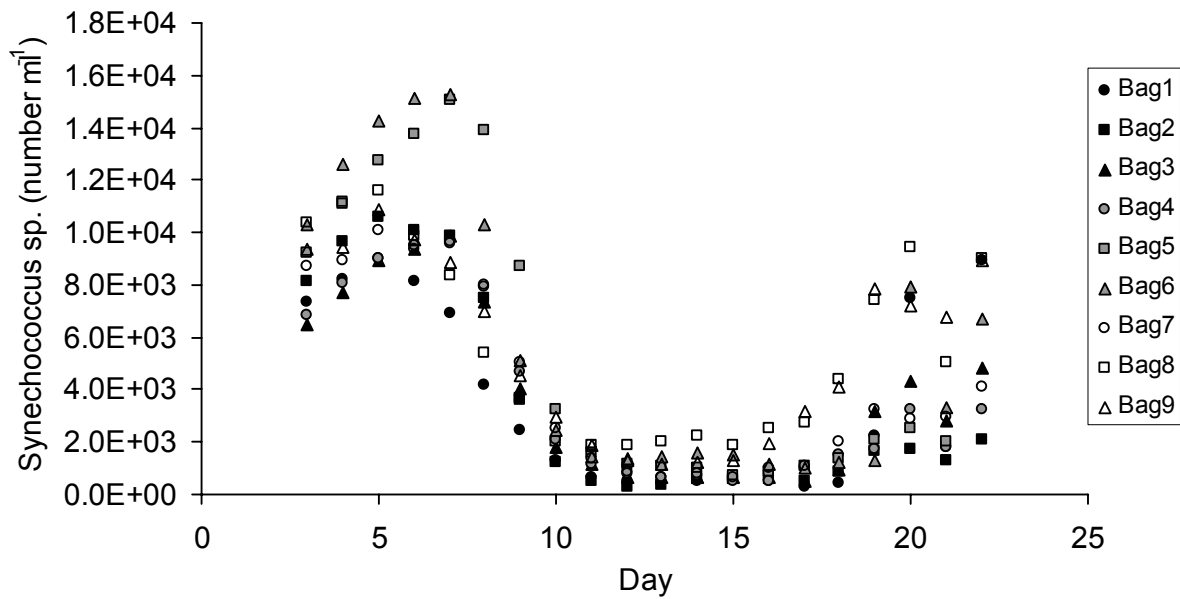
Figure 17. Abundance of *Synechococcus sp.* (number ml^{-1}) in enclosures for "year 2100" (black symbols), "present" (grey symbols) and "glacial" (open symbols). Modified after Engel et al. (2005).
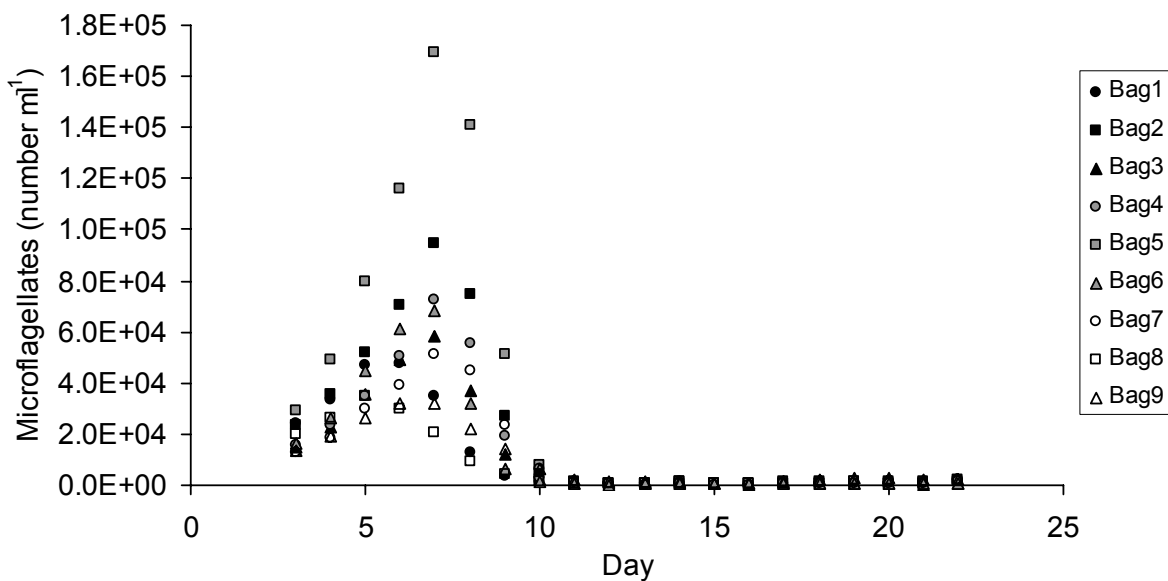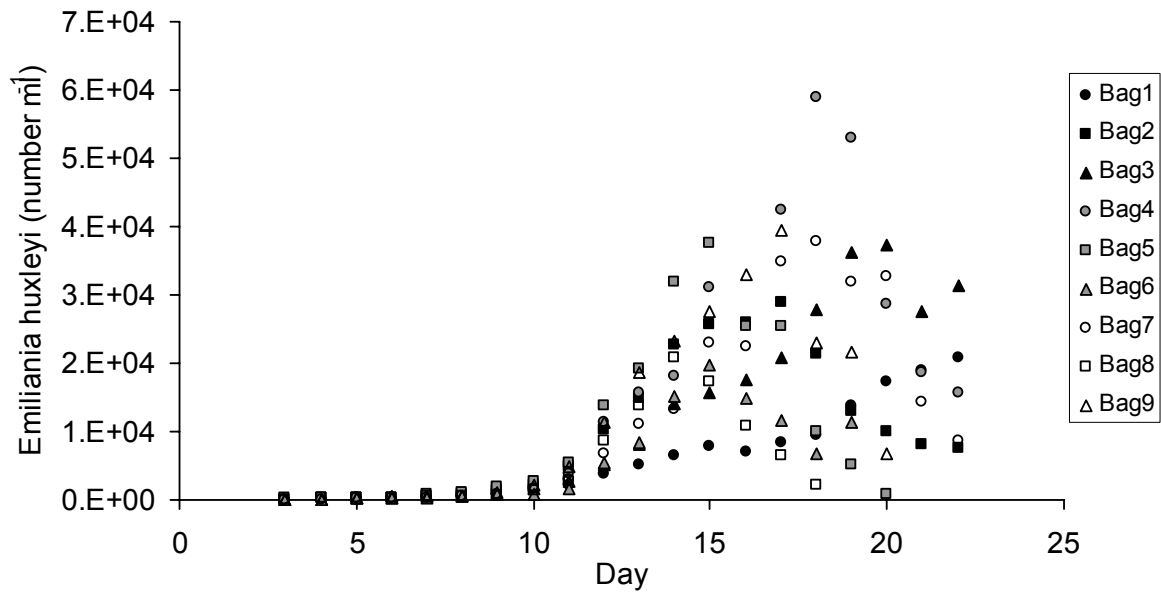

Figure 18. Abundance of microflagellates including *Micromonas sp.* (number ml^{-1}) in enclosures for "year 2100" (black symbols), "present" (grey symbols) and "glacial" (open symbols). Modified after Engel et al. (2005).

Figure 19. Abundance of *E. huxleyi* (number ml⁻¹) in enclosures for "year 2100" (black symbols), "present" (grey symbols) and "glacial" (open symbols).

The peak of *E. huxleyi* (d17-d18) was reached after the peak of Chl-a (before d15) as shown in Figure 19.

The declining phase showed the recovery of the *Synechococcus* that increased again until the end of the experiment (Figure 17). Such a succession of cyanobacteria, microflagellates and coccolithophores was already documented in other mesocosm experiments (e.g. Catsberg *et al.*, 2001).

The *E. huxleyi* grown under various pCO_2 conditions were examined for their size (Figure 20) and morphology (Figure 21) using the Automated Electron Probe Micro Analysis (EPMA). Figure 20 shows the variation in sizes at various initial pCO_2. It indicates that *E. huxleyi* grown at 200 ppmV CO_2 corresponding to glacial conditions has a larger size.
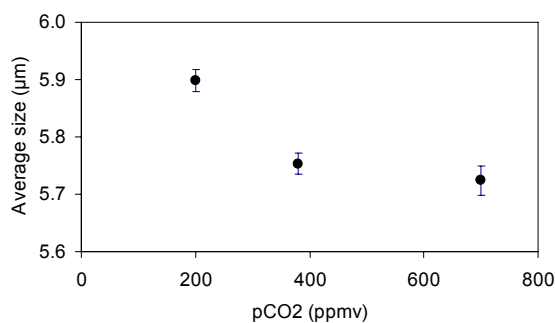

Figure 20. Size of *E. huxleyi* grown under different pCO_2 conditions.

| 200 ppmV | 380 ppmV | 700 ppmV |
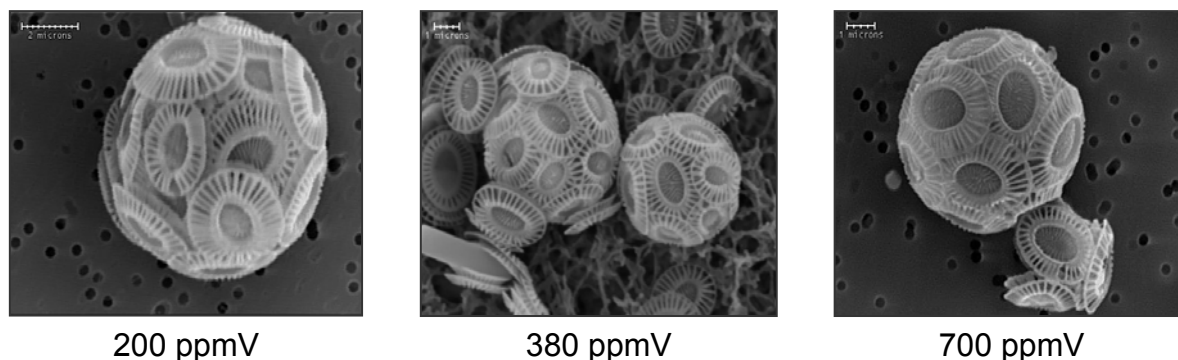
Figure 21. Scanning electron micrographs of *E. huxleyi* grown under various pCO_2 conditions.

Viral abundance was very low ($< 10^6$ particles ml^{-1}) at the beginning of the experiment and subsequently increased after d14, characterizing the post-bloom situation (Figure 22). *EhV* were undetectable in Bags 1 and 3. The interactions between viruses and their hosts are complex and depend on their densities, respectively. Both densities increase until a maximum capacity is reached, until which cell lysis occurs, resulting in the collapse of the bloom. This was particularly visible in bags 4 to 9 (i.e. low-pCO_2 and present-pCO_2 treatments), where higher cell densities were reached.
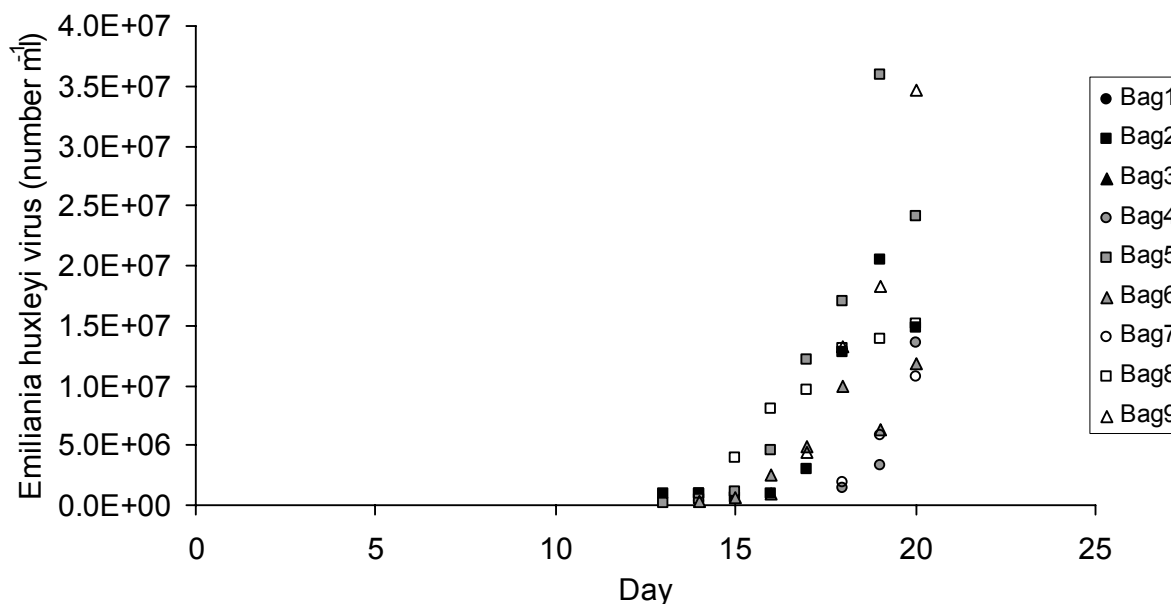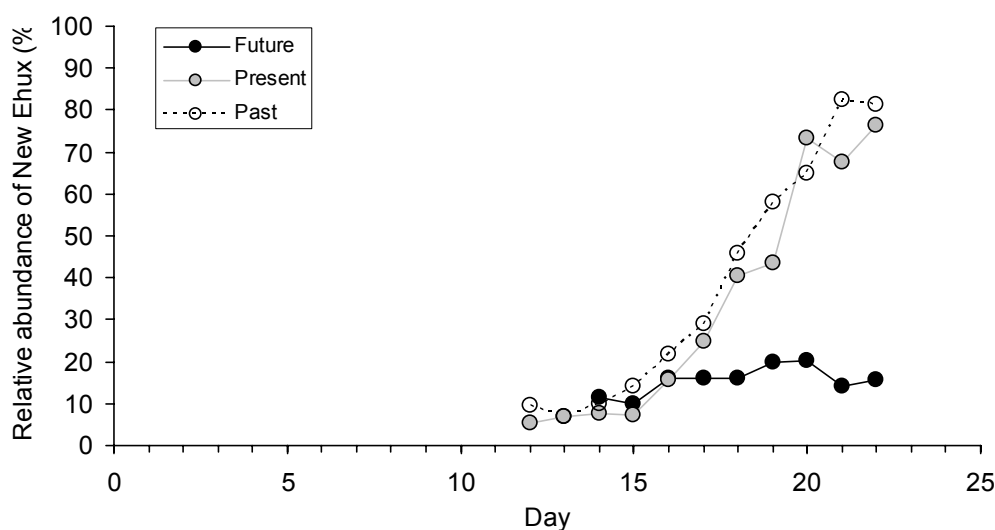

Figure 22. Abundance of *E. huxleyi* viruses (*Eh*V in number ml^{-1}) in enclosures for "year 2100" (black symbols), "present" (grey symbols) and "glacial" (open symbols). Data of S. Jacquet.

The singular behaviour of the *E. huxleyi* population in bag 1 was paralleled by lower viral density that did not reach the critical value needed for the phytoplanktonic bloom

to collapse. Viruses have already been observed in similar mesocosm conditions (Catsberg *et al.*, 2001, Jacquet *et al.*, 2002) and were known to actively participate in the specific collapse of *E. huxleyi* blooms by viral lysis.

A new type of *E. huxleyi* appeared, concomitantly with the decrease of the original one, mainly at the end of the exponential phase (Figure 23). Its relative contribution to the pool of coccolithophores could represent 80% in particular cases (bags 8 and 6) but was kept low in bags 1 and 3, where no viruses were detectable. This new type was characterized by a decrease of the scattering properties by flux cytometry. Such changes could be attributed to changes in the coccolith-bearing quality/quantity (number, size and weight) and/or the alteration of chlorophyllian pigments quality/quantity. Only the optical properties have been investigated, here, no genetic study has been carried out to investigate genetic diversity among coccolithophores.
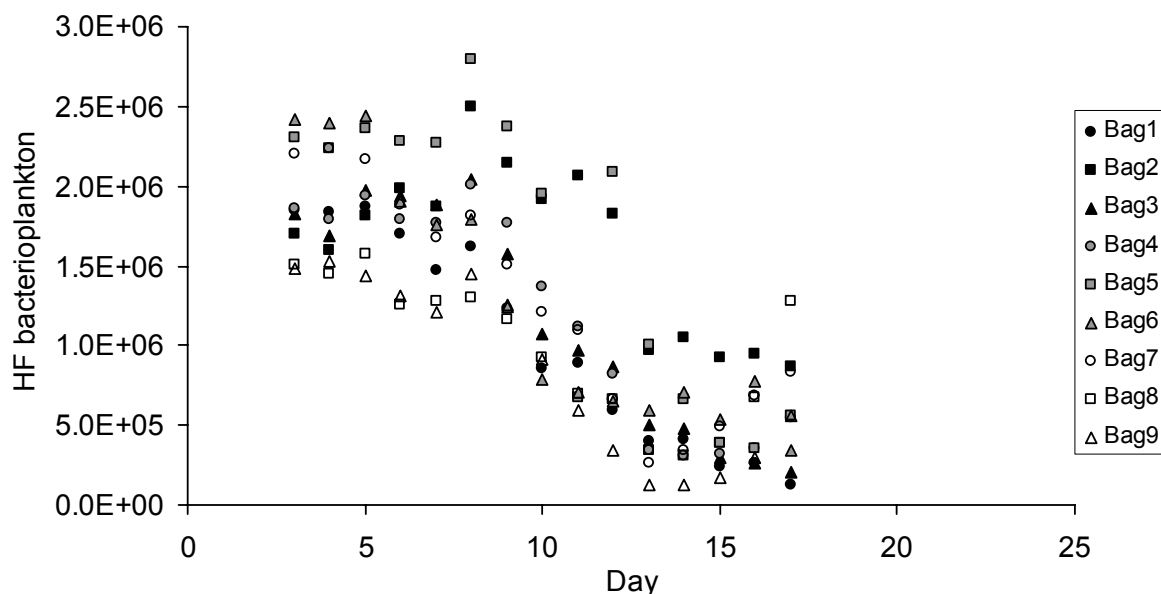

Figure 23. Relative abundance of a new type of *E. huxleyi* (in %) in the enclosures for "year 2100" (black symbols), "present" (grey symbols) and "glacial" (open symbols). This new type displays decreased scattering properties in flow cytometry, which could be attributed to viral infection. Data of S. Jacquet.

The succession of various morphotypes with different tolerance and/or requirements within this species needs to be understood. Since various morphotypes have been described in the field (Iglesias-Rodriguez *et al.*, 2002), it remains possible that what we defined as a new type, was, in fact, a morphotype.

The abundance of the high DNA bacterial group was initially high (1-2 10^6 cells $.ml^{-1}$) and began to decrease to a final value of c.a. 5 10^5 cells $.ml^{-1}$ (Figure 24). Such a decrease during the exponential growth of *E. huxleyi* could be explained by their inability to compete this species for available resources. After d15, when viral lysis occurred in most of the bags, their concentration seemed to increase again (bags 5, 6, 8 and 9). The same tendency was also observed in the low DNA bacterial group

(not shown). The triggering of a new secondary production after viral lysis has already been observed in coccolithophore mesocosm experiments (Catsberg *et al.*, 2001) and is also documented for *Phaeocystis pouchetii* cultures (Bratbak *et al.*, 1998) as well as during natural blooms (van Boekel *et al.*, 1992). This could be attributed to the selection of a genetic pool of bacteria that is different from the original one. Their rapid turnover and their higher genetic diversity within natural seawater make them good competitors in changing environments.

Figure 24. Abundance of high fluorescent DNA bacterioplankton (number ml^{-1}) in enclosures for "year 2100" (black symbols), "present" (grey symbols) and "glacial" (open symbols). This group may be representative of the active part of bacterioplankton. Data of S. Jacquet.

4.2.3 Nutrient dynamics

Nitrate concentration was adjusted to c.a. 15 µM at the beginning of the experiment.

Nitrate dynamics during the experiment started with a slow decrease from d0 to d10, probably due to the uptake by the minor species that developed before *E. huxleyi* (Figure 25). At the onset of the coccolithophore bloom, the decrease was more pronounced and led to the complete exhaustion of nitrates within 5 days (d14-d15) in correlation with the development of the coccolithophore bloom.
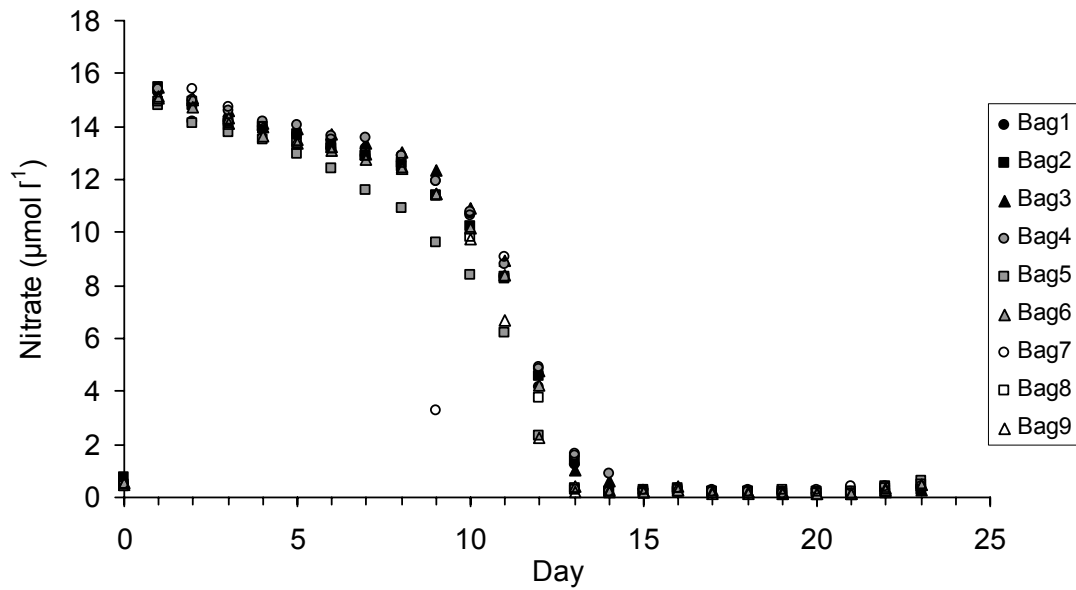
Figure 25. Nitrate concentration in enclosures (in µmol.l⁻¹) for "year 2100" (black symbols), "present" (grey symbols) and "glacial" (open symbols). From Engel *et al*. (2005).
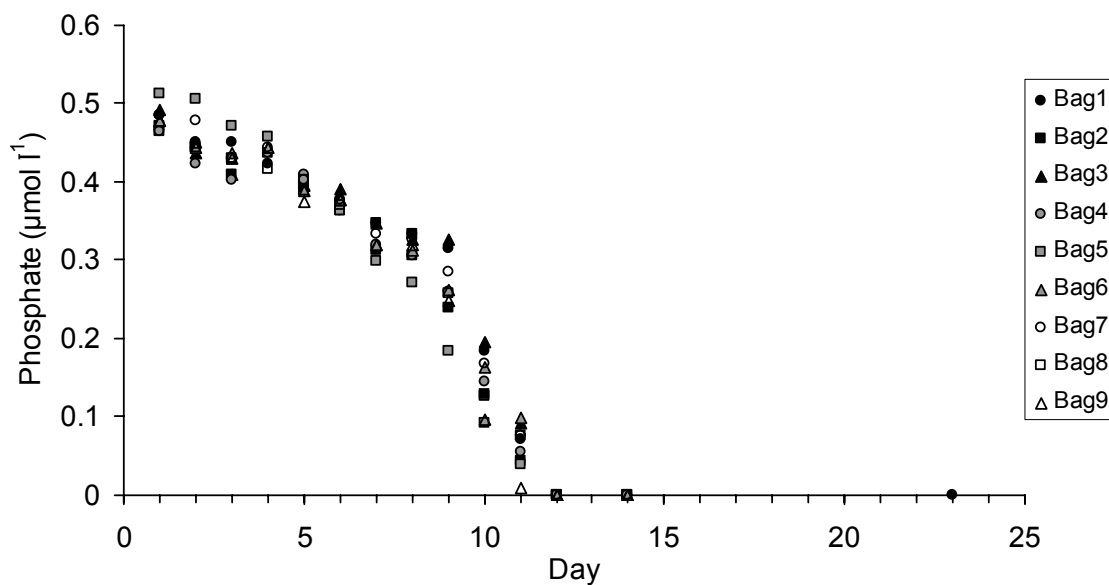
Figure 26. Phosphate concentration in enclosures (in µmol.l⁻¹) for "year 2100" (black symbols), "present" (grey symbols) and "glacial" (open symbols). From Engel *et al*. (2005).

Phosphorus concentration was adjusted to c.a. 0.5 µM at d0, giving a N:P ratio in mesocosms close to 32:1.

The dynamics of inorganic phosphorus decreased continuously during the 12 first days of the experiment, leading to a complete exhaustion on d12 (Figure 26). The timing between N and P exhaustion (a delay of 2 or 3 days) is sometimes observed (personal observations) during batch cultures. This may be due to the ability of coccolithophores to grow on organic phosphorus and nitrogen when inorganic

nutrients are scarce. The maximum concentration of Chl-a was observed on d15, when nutrients where exhausted.

No dissolved silica has been added at the beginning of the experiment and concentrations were low (data not shown). A rapid decrease was observed; concentrations rapidly fell to levels between 0 and 0.1 µM within 3 days and no dissolved silica was detectable after d10. Such low (< 0.4 µM) dissolved silica concentration cold be a limiting factor for diatom growth under favourable light and nutrient conditions.

4.2.4 Particulate organic matter and biogenic carbonate

The concentrations of particulate organic carbon (POC) ranged between 10 and 30 µM at the beginning of the experiment and globally increased during the exponential growth phase until 50 to 100 µM (Figure 27). Overall, the concentrations of POC continued to increase some days after nutrients were consumed (d12-d14) and the maximum Chl-a level was reached (d14). From this moment on, the increase on POC concentrations was not constrained by nutrient availability and the behaviour of the time-series became somewhat chaotic. They depended upon various processes, such as herbivorous and viral activities and export to depth, and could not be quantified with our sampling procedure.
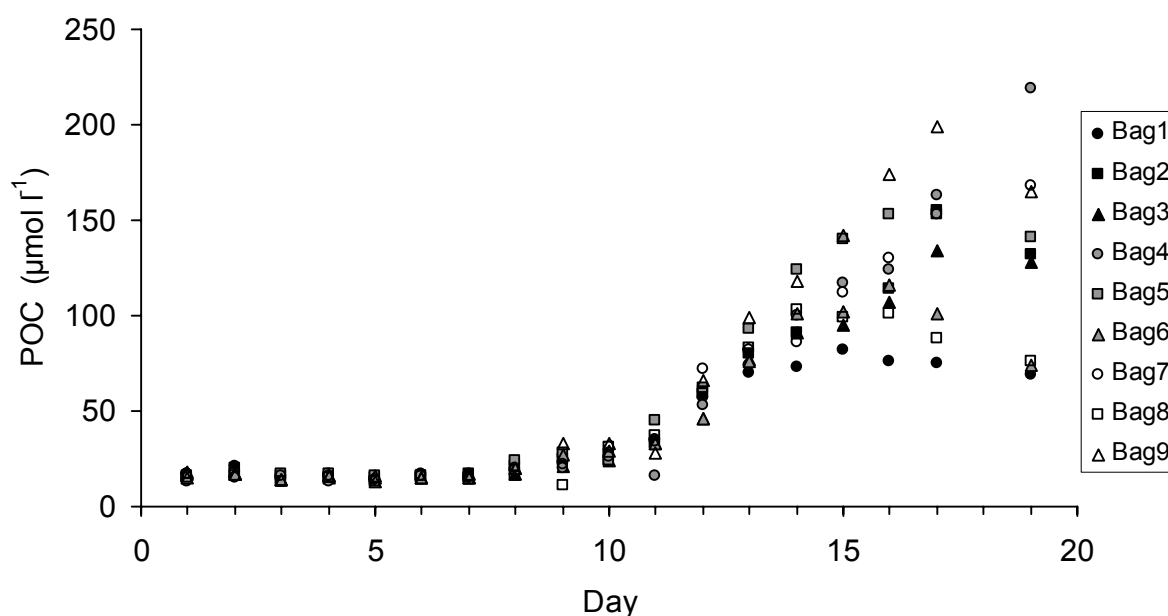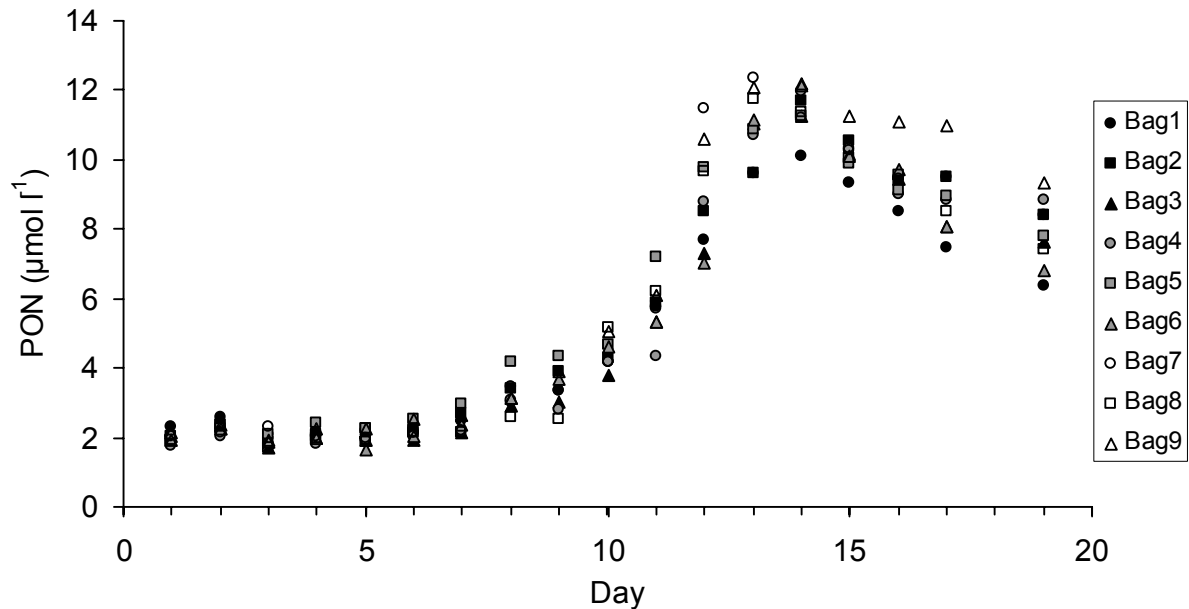

Figure 27. Particulate organic carbon (POC) concentration in enclosures (in µmol.l^{-1}) for "year 2100" (black symbols), "present" (grey symbols) and "glacial" (open symbols). From Engel *et al.* (2005)

The exhaustion of phosphates coincided more or less with the onset of calcification, as featured by the increase in particulate inorganic carbon (PIC) concentration after d10 (Figure 28). The range of PIC produced by the end of the experiment varied from 17 µg.l^{-1} (bag 2) to more than 55 µg.l^{-1} (bag 9), depending on the history of the bloom (interaction with viruses) and the pCO$_2$ treatment.
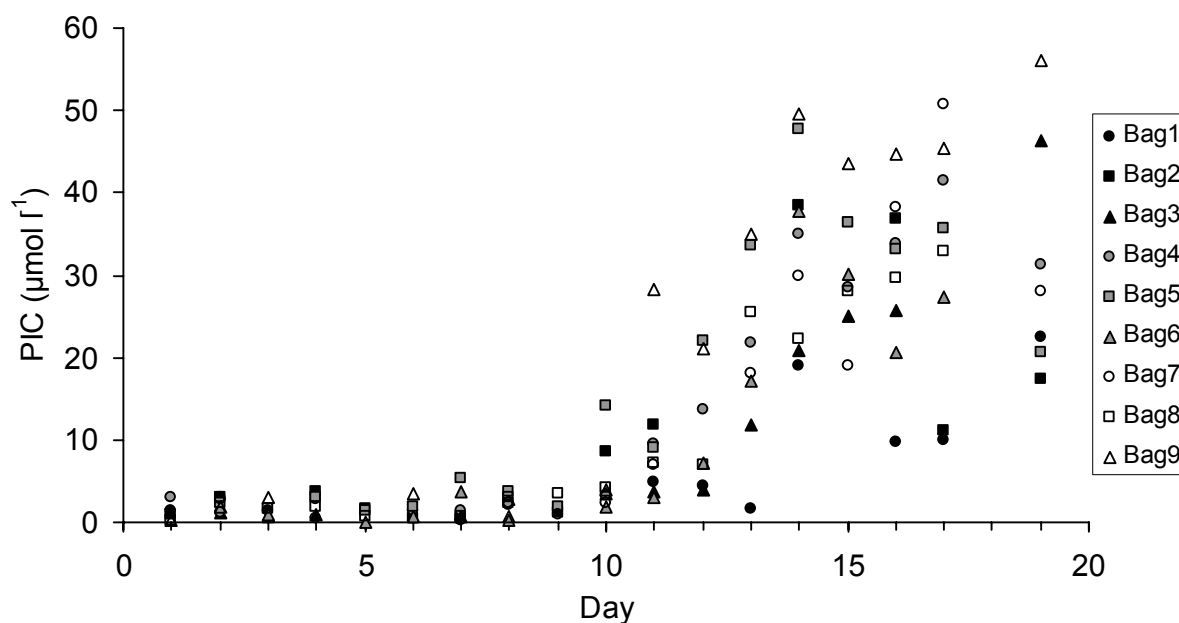
Figure 28. Particulate inorganic carbon (PIC) concentration in enclosures (in µmol.l^{-1}) for "year 2100" (black symbols), "present" (grey symbols) and "glacial" (open symbols). From Engel et al. (2005)

There is a significant scatter in the POC concentrations for mesocosms under the same treatment before the exponential growth phase (d0 to d10) and during the decay (from d20 onwards), as shown in Figure 27. The former probably originated from the growth of flagellates and cyanobacteria, while the latter was rather attributed to the interactions between the coccolithophores and the virus. Accordingly, a large scatter is also observed for PIC concentrations at the onset of calcification. This scatter may be linked not only to the one observed for organic carbon but also to the influence of pCO$_2$ on biomineralization.

The concentrations of particulate organic nitrogen (PON) ranged between 2 and 11.5 µM during the experiment (Figure 29). They increased until d13 during the exponential growth phase (as described for Chl-a) and the production of PON reflected the consumption of nitrate in the bags. The production ratio of *d*POC:*d*PON (6.46 ± 0.3) was comparable to the Redfield C:N ratio of 6.6 (Engel *et al.*, 2004).

The concentrations of PON apparently decreased during the decay phase (d14-d19), probably as a consequence of cell lysis and/or increased sedimentation. During this stage, the increase in the POC:PON ratio (Engel *et al.*, 2004) suggested a decoupling between POC and PON when nutrients were limiting the growth of phytoplankton.

Figure 29. Particulate organic nitrogen (PON) concentration in enclosures (in µmol.l^{-1}) for "year 2100" (black symbols), "present" (grey symbols) and "glacial" (open symbols).
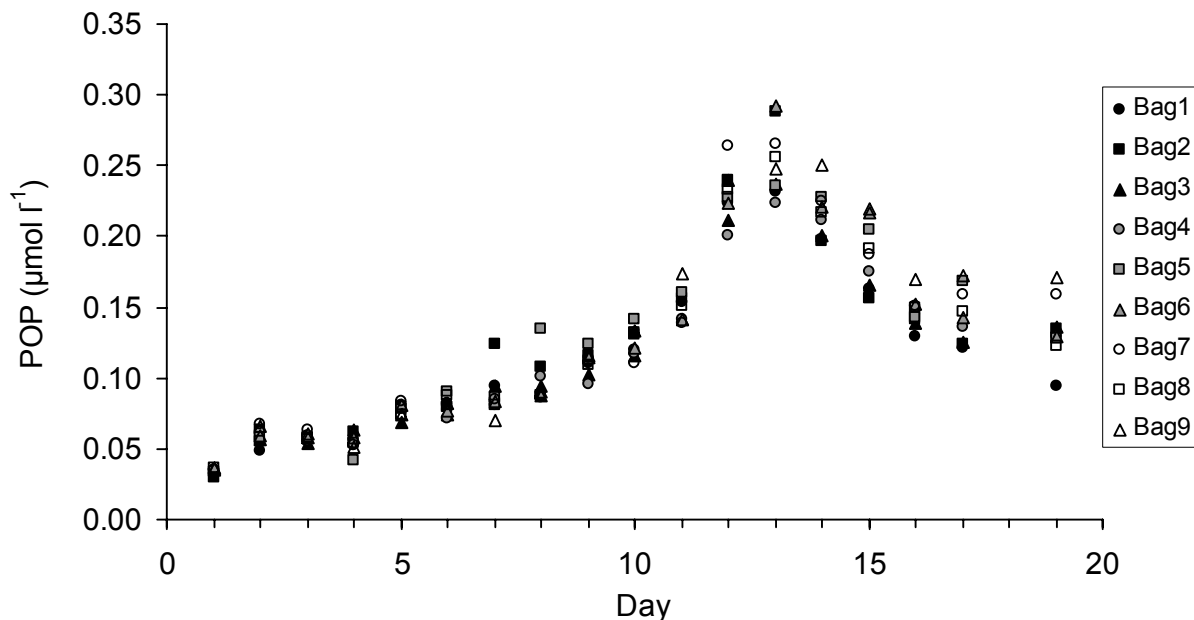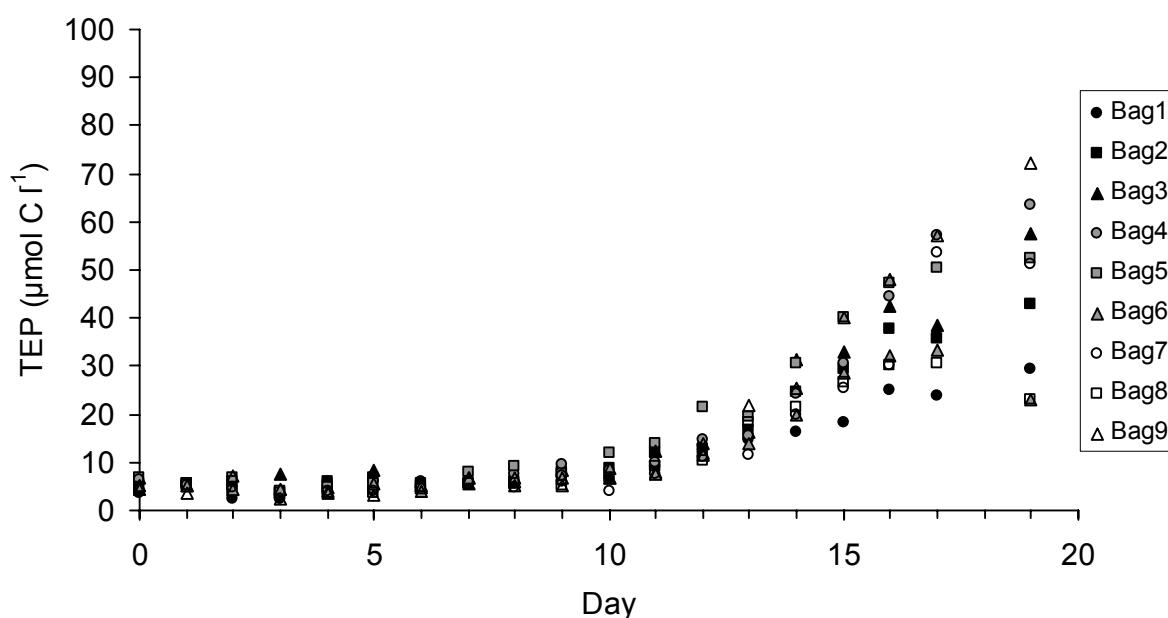

Figure 30. Particulate organic phosphorus (POP) concentration in enclosures (in µmol.l^{-1}) for "year 2100" (black symbols), "present" (grey symbols) "glacial" (open symbols).

The concentrations of particulate organic phosphorus (POP) ranged from 0.02 µmol .l^{-1} to 0.25 µmol .l^{-1} during the 13 first days of the experiment (Figure 30). The observed increase of POP was correlated with the increase of POC during the same period and the production ratio of dPOC:dPOP was equal to 338 ± 13 (Engel *et al.*, 2004). Such a high ratio, about twice as high as the Redfield C:P ratio (116), suggests the ability of *E. huxleyi* to grow on low inorganic phosphorus resource (Riegman *et al.*, 2000).

The concentrations of POP decreased after d13. The resulting increase of POC:POP ratio suggested, as observed for the POC:PON ratio, a strong decoupling between POC and POP during the decay (Engel *et al*, 2004), when nutrients were limiting the growth of phytoplankton.

4.2.5 *Transparent Exopolymer particles (TEP)*

Transparent exopolymer particles (TEP) concentration was measured colorimetrically (Passow & Alldredge, 1995) and converted into carbon units (TEP-C) according to a linear relationship between TEP and POC concentrations (Engel *et al.*, 2004), after tangential ultrafiltration of suspended particulate matter, according to the method described in Engel & Passow (2001).

Figure 31. Transparent exopolymer (TEP) concentration in enclosures (in µmolC.l^{-1}) for "year 2100" (black symbols), "present" (grey symbols) and "glacial" (open symbols).

TEP-C concentration increased from the average 5.5 ± 0.1 µmolC .l^{-1} value calculated for the 10 first days, until the end of the experiment (Figure 31). The increase was, at first sight, related to the cell abundance during the bloom of *E. huxleyi* (Engel *et al.*, 2004). However, TEP production normalized with respect to cell abundance was significantly and positively influenced by the pCO$_2$ increase in the "Year 2100" treatment, compared to the "Present" and "Glacial" ones.

The aggregation of marine particles, as followed by TEP formation in the bags could lead to the physical export of bacteria to the bottom. This constitutes is an alternative explanation for the observed decrease of free-living bacteria in the surface seawater. Such a theory is developed in Rochelle-Newal *et al.* (2004).

### 4.2.6 Primary production and calcification by ^{14}C incorporation

4.2.6.1 Incubations under constant light

The hourly rates of ^{14}C incorporation into the particulate matter reflect the ability of the phytoplanktonic community to uptake carbon under controlled environmental conditions.

Potential primary production displayed low hourly rates of ^{14}C incorporation in organic matter at the beginning of the experiment between the d0 to d7 (Figure 32). The same range, below 1 µmolC.l^{-1}.h^{-1}, was observed among pCO$_2$ treatment during this period (Bag 1-"year 2001", Bag 4-"Present", Bag 9-"glacial"), probably due to the other species that developed prior to *E. huxleyi*.

The exponential growth phase, from d5 to d15 was characterized by increasing rates of incorporation, corresponding to an increase in biomass, principally due to *E. huxleyi*. In "present" or in "glacial" conditions, similar increase was observed, reaching values above 3 µmolC.l^{-1}.h^{-1} (Figure 32). This increase was less pronounced in "year 2100" conditions (Bag 1), where the maximum uptake did not exceed 2 µmolC.l^{-1}.h^{-1}. The highest rates were obtained on d15, confirming the tendency observed earlier.

The bloom decline from d15 onwards, showed a three-fold reduction of incorporation rate of ^{14}C in the organic matter, concomitantly with a decrease of Chl-a concentration in the "glacial" and "present" conditions, probably linked to viral lysis after d15. In contrast, these rates were kept at comparable or slightly lower levels as during the exponential growth phase in the "year 2100" (around 1.5 µmolC.l^{-1}.h^{-1}).
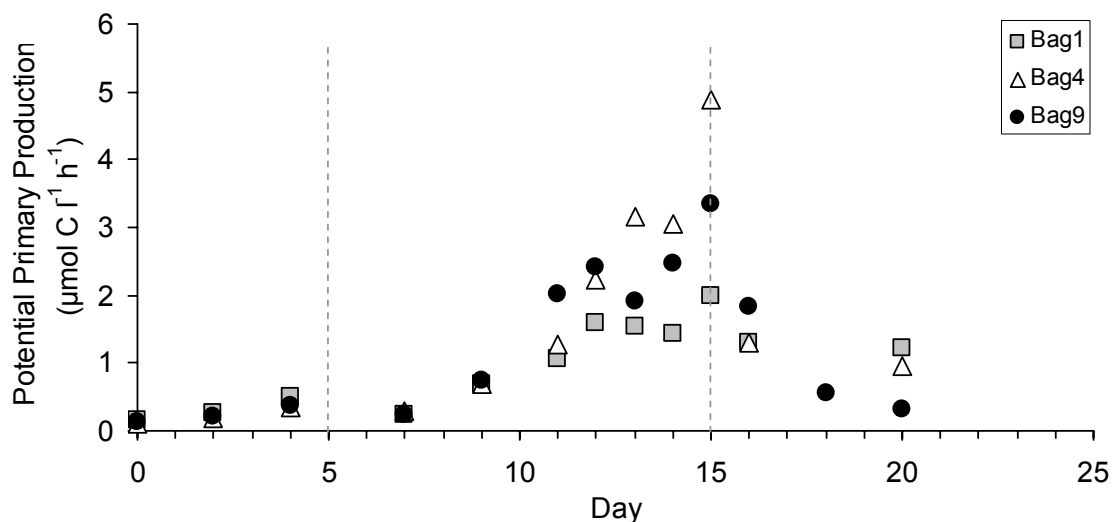
Figure 32. Potential net community incorporation of $H^{14}CO_3^-$ in organic matter (in $\mu molC.l^{-1}.h^{-1}$) in enclosures during constant illumination incubations (150 μmol Photons.$m^{-2}.s^{-1}$).
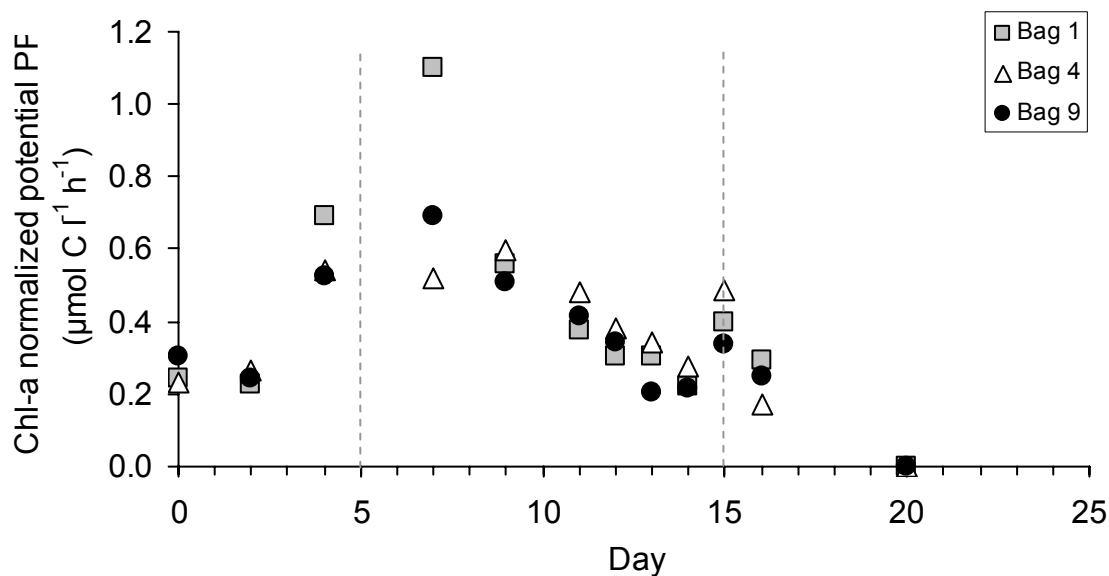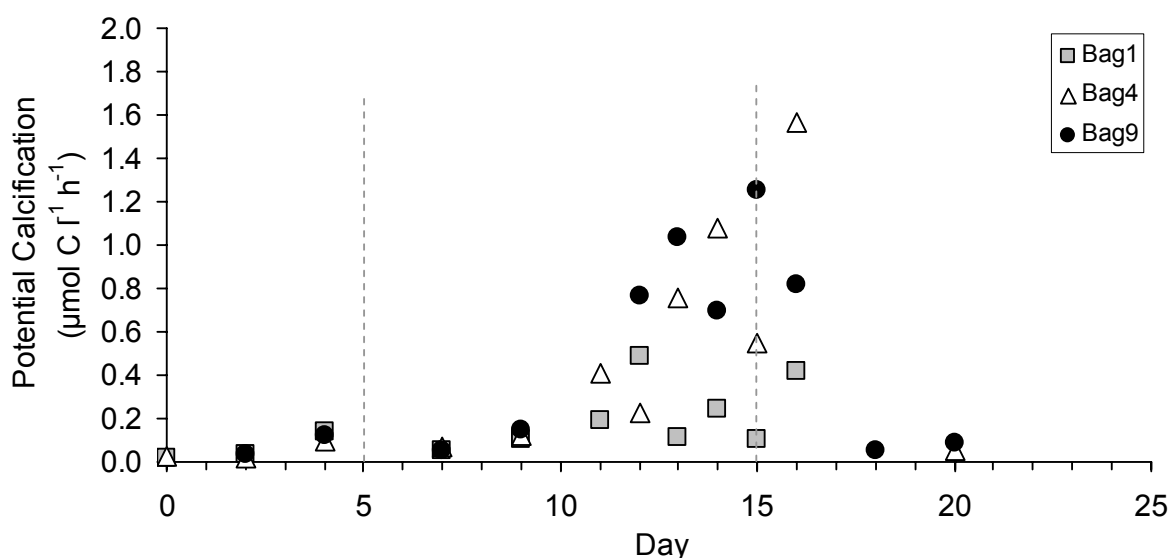

Figure 33. Potential net community incorporation of $H^{14}CO_3^-$ in organic matter normalized by Chl-a concentrations (in $\mu molC.\mu g$ Chl-a^{-1} .h^{-1}) in enclosures during constant illumination incubations (150 μmol Photons.$m^{-2}.s^{-1}$).

When normalized to Chl-a concentrations, potential primary productivity varied during the course of the bloom. Initial values, 0.26 ± 0.04 $\mu molC.(\mu gChl-a)^{-1}.h^{-1}$, increased rapidly at the onset of the exponential growth phase and were more scattered on day 7 (Figure 33). At this time, more PO^{14}C was produced by Chl-a unit in the "year 2100" treatment (1.1 $\mu molC.\mu g^{-1}.h^{-1}$) than in the "glacial" or "present" treatment (±0.6 $\mu molC.\mu g^{-1}.h^{-1}$). This pattern indicates that high pCO$_2$ concentrations enhanced POC

production at the onset of the growing phase, when the range between the three pCO_2 levels was the most pronounced in mesocosms (Delille *et al.*, 2005). Few days after, the differences in the uptake rates among the various pCO_2 treatments disappeared when pCO_2 decreased. A decrease was observed in the second part of the exponential growth phase followed by a slight recovery on d15. Finally, on d20, low Chl-a levels and low uptake rates of ^{14}C led to values close to zero.

During this experiment, calcification rates were only expected during the exponential growth phase of *E. huxleyi* since no other calcifying phytoplankton was found.

Similarly to the observations of potential primary production, potential calcification was low (below 0.2 $\mu molC.l^{-1}.h^{-1}$) during the pre-bloom situation in the three pCO_2 conditions (Figure 34). A rapid increase in potential calcification to a value >1.2 $\mu molC. l^{-1}.h^{-1}$ was observed in the "present" and "glacial" bags during the second part of the exponential growth phase, while the calcification rate stayed <1 $\mu molC. l^{-1}.h^{-1}$ in the "year 2100" treatment.

Figure 34. Net community incorporation of $H^{14}CO_3^-$ in calcium carbonate (in $\mu molC.l^{-1}.h^{-1}$) in enclosures during constant illumination incubations (150 μmol Photons.$m^{-2}.s^{-1}$).

The specific potential calcification (per 10^4 cells) did not display particular features with respect to the pCO_2 treatments (Figure 35). At the onset of the exponential growth phase, the rate of incorporation ranged between 0.88 $\mu molC.(10^4 cell)^{-1}.h^{-1}$ and 1.43 $\mu molC.(10^4 cell^{-1}).h^{-1}$, and decreased below 0.50 $\mu molC.(10^4 cell)^{-1}.h^{-1}$ towards the bloom decline. Because only one mesocosm was sampled for each treatment (Bags 1, 4 and 9), no information can be given on the variability of incorporation rates with the CO_2 treatments.
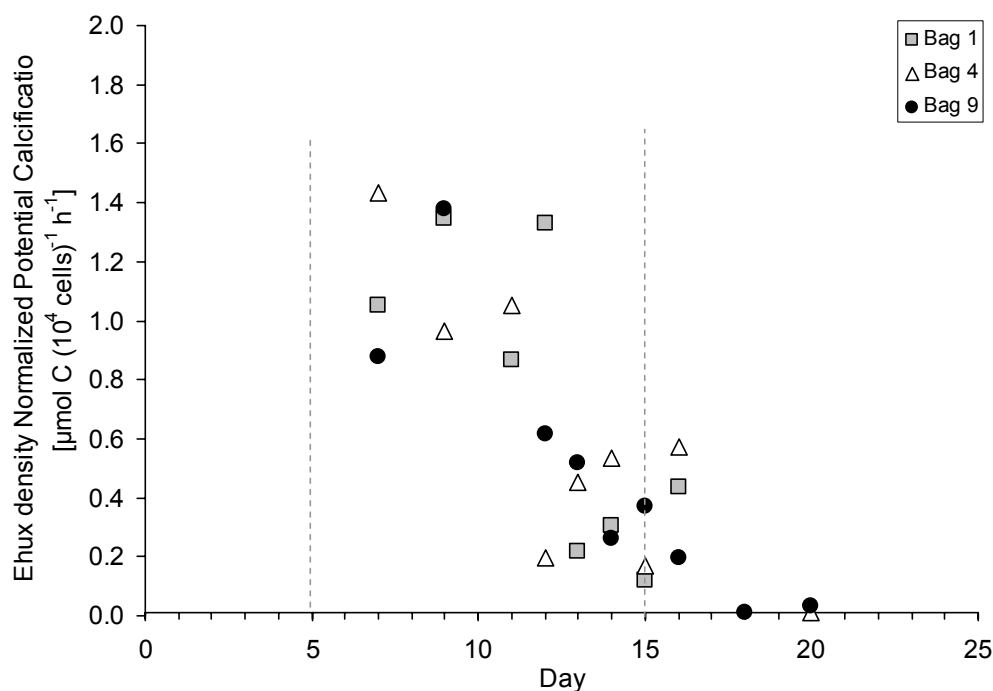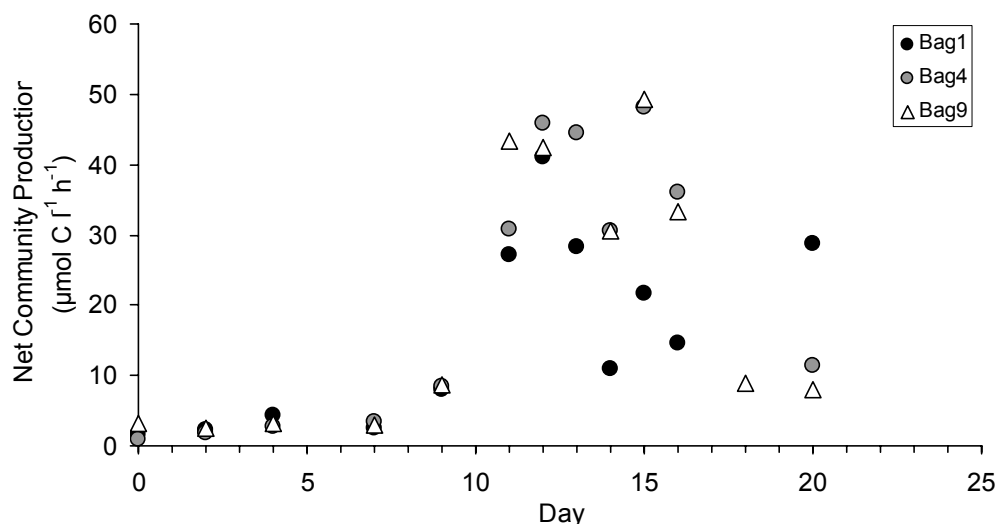
Figure 35. Net community incorporation of $H^{14}CO_3^-$ in calcium carbonate normalized to a 10^4 cells density of *E. huxleyi*, in $\mu molC.(10^4 \text{ cells})^{-1}.h^{-1}$, in enclosures during constant illumination incubations ($150 \mu mol \text{ Photons}.m^{-2}.s^{-1}$).
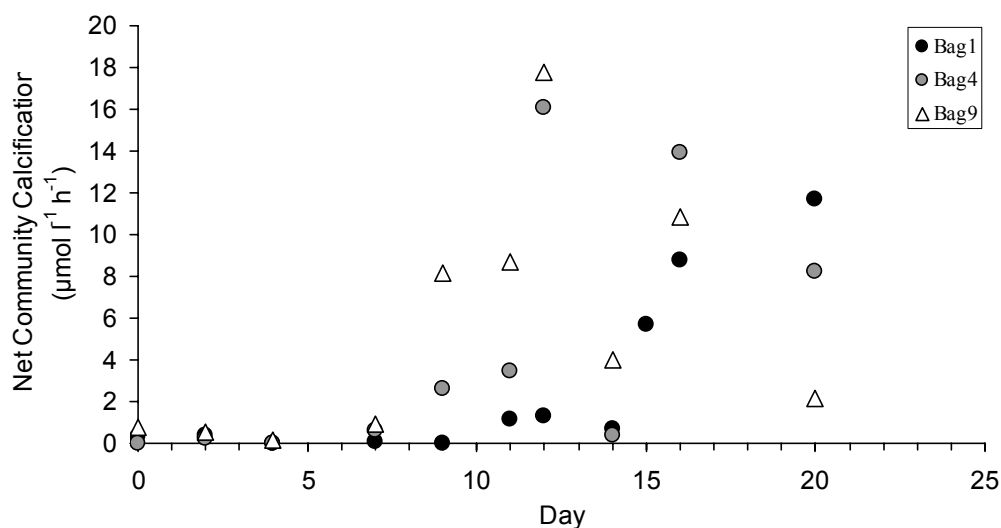
4.2.6.2   In situ incubations

The incorporation experiments carried out *in situ*, showed similar levels of production from d0 to d9 (Figure 36). A net increase was observed from d9 onwards, corresponding to the exponential growth phase of the coccolithophore bloom. During the second half of the exponential growth phase, increasing net community production (NCP) were observed in all the treatments, reaching 45 $\mu molC.l^{-1}.d^{-1}$ by d11 for "glacial" treatment and d12 for present" and "year 2100" treatments. The net community production reached values > 45 $\mu molC.l^{-1}.d^{-1}$ during this period. However, as hourly rates of net production were kept high until the end of the exponential growth phase in the past and present conditions, they decreased rapidly from d12 to d16 in the "year 2100" condition. A subsequent increase in the net community production was observed in "year 2100" that was not observed for the other bags.

This trend parallels the one observed in Chl-*a* and cell abundance patterns. The apparent decrease observed on day 14 in all treatments corresponds to a cloudy day during which the daily integrated photosynthetically active radiation was only 21% of the average value during the experiment (35 $\mu mol \text{ Photons}.m^{-2}.d^{-1}$).

Figure 36. Net Community incorporation of $H^{14}CO_3^-$ in organic matter (in $\mu molC.l^{-1}.d^{-1}$) in enclosures during *in situ* incubations.

Figure 37. Net Community incorporation of $H^{14}CO_3^-$ in calcium carbonate (in $\mu molC.l^{-1}.d^{-1}$) in enclosures during *in situ* incubations.

No calcification was observed during the first part of the bloom (d0 to d7). At the onset of the exponential growth phase, the net incorporation rates of ^{14}C in the inorganic matter within the community increased and were more important in Bag 9 and, to a lesser extent, in bag 4, compared to bag 1 (Figure 37). They remained low in Bag 1 until d14, when pCO_2 reached contemporary values (400 ppmV). Then, they started increasing to reach values close to the ones observed in the "present" and "past" conditions.

4.2.7 Net community production and calcification by DIC technique

An overview of the temporal evolution of net community production (NCP) relative to net community calcification (NCC), based on DIC measurements, is shown in Figure 38 where day-to-day estimates are connected. During the pre-bloom period, NCP_{DIC} increased steadily (upward displacement along the Y-axis), firstly due to the rising abundances of *Synechococcus* sp. and nano-flagellates, and subsequently to the onset of the bloom of *E. huxleyi*. The increase in NCP_{DIC} was greater from d11 onwards in all the conditions, concomitant with the beginning of the peak of the bloom period and led to maximum values of NCP_{DIC} on d12 and d13. By d15 when the nutrients were exhausted, NCP_{DIC} decreased markedly. NCC increased (displacement to the right along the X-axis) in a second phase, when the coccolithophorid bloom was well underway. NCC continued from d11 to d19 and remained at a high level while NCP_{DIC} decreased dramatically, which is consistent with observations in cultures of *E. huxleyi* (Dong *et al.*, 1993). The third phase was the collapse of the bloom with a dramatic decrease in both NCP_{DIC} and NCC. This phase corresponded to the period during which the coccolithovirus abundance passed over a threshold value estimated to be around 5.10^6 part ml^{-1} (dashed lines). At the end of the experiment, NCP_{DIC} and NCC showed negative values due to elevated respiration and $CaCO_3$ dissolution, as suggested by *Milliman et al.* (1999). This is consistent with the increase in both community respiration (CR) and bacterial abundance determined by flow cytometry (Jacquet, unpublished).

Under 'glacial' conditions (M7, M8 and M9), NCC started at the onset of the bloom (d10-d11) and then increased steadily in parallel to NCP_{DIC} leading to an almost simultaneous maximum (only 1d time lag). In contrast, in the 'year 2100' conditions (M1, M2 and M3), NCC began later (d12 to d13) and suddenly, while NCP_{DIC} had already reached its maximum. NCC subsequently increased very rapidly while NCP_{DIC} was decreasing. The 'present' conditions exhibited an intermediate behaviour between the 'year 2100' and 'glacial' conditions: the maximum level of NCP_{DIC} was reached when NCC was already substantial but had not reached its maximum value.

Thus, if the overall pattern of NCP_{DIC} prior to viral lysis were similar for all the conditions, the onset of NCC had occurred sooner in the 'glacial' and 'present' conditions than in the 'year 2100' conditions. This is consistent with the calcification rates measured with the ^{14}C *in situ* incubations. Furthermore, under 'glacial' conditions, NCC increased steadily from the very beginning of the bloom in parallel to the exponential rise of NCP_{DIC}, while in the 'year 2100' NCC occurred suddenly at the maximum of NCP_{DIC}.
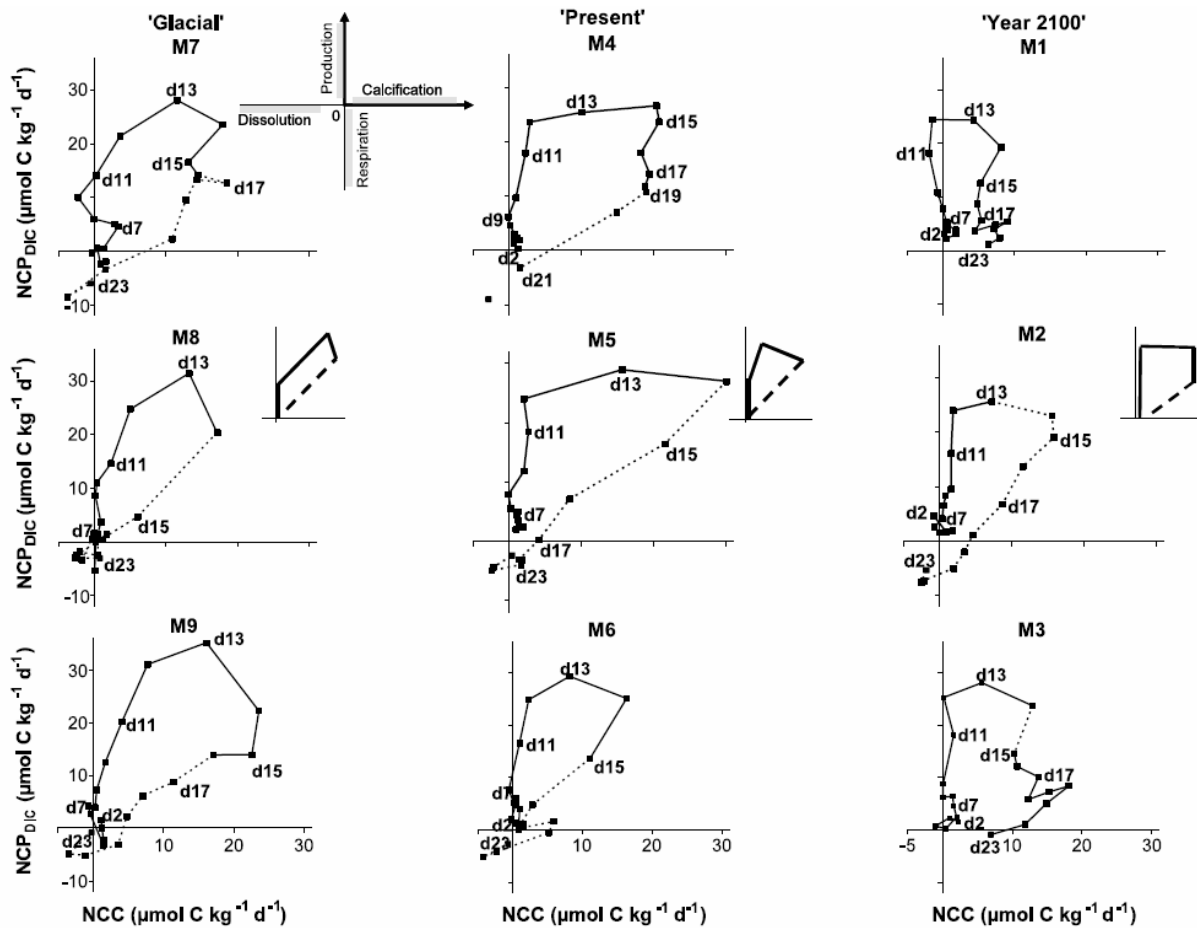
Figure 38. Hysteresis showing the net changes of net community production (positive, Y-axis) and net community calcification (positive, X-axis), based on daily measurements of total alkalinity and *in situ* pCO_2 in the enclosures.

4.3   Laboratory dissolution experiments of coccolithophores

Results of the dissolution experiments showed various degrees of dissolution features of coccoliths depending on the solution pH. At pH 7.5, most cells exhibited a good calcification, but some coccoliths showed signs of dissolution and malformation (Figure 39).

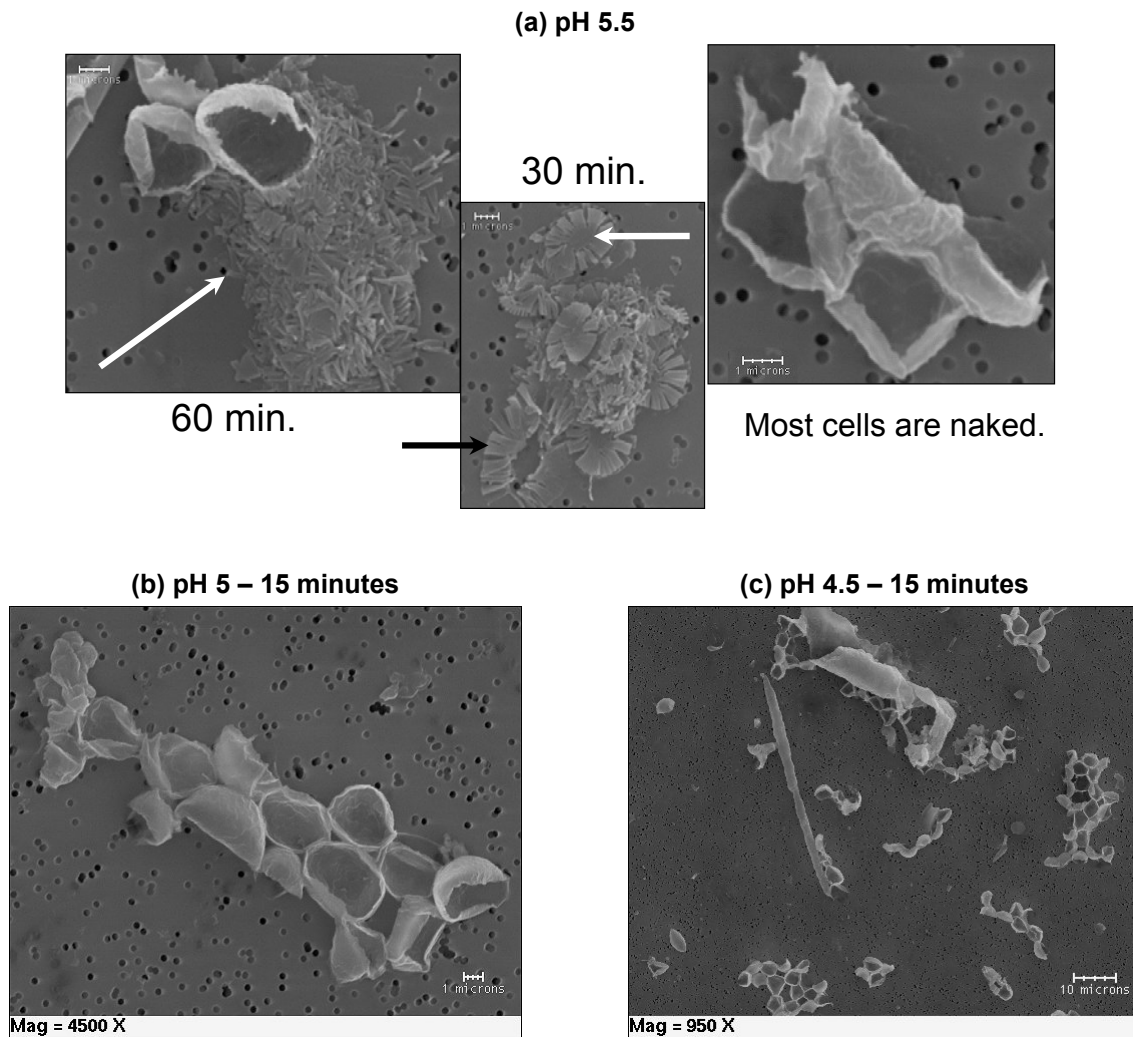**(a) pH 7.5 – 15 minutes**   **(b) pH 7.5 – 30 minutes**
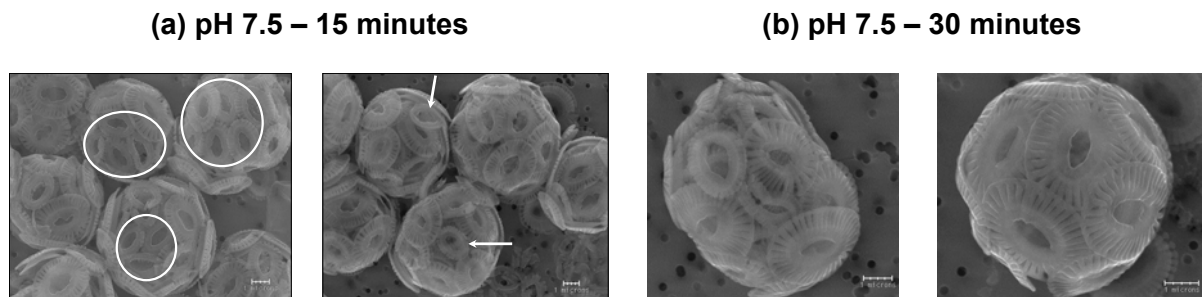
Figure 39. SEM micrographs of *E. huxleyi* after reacting in seawater at pH 7.5 for (a) 15 minutes and (b) 30 minutes.
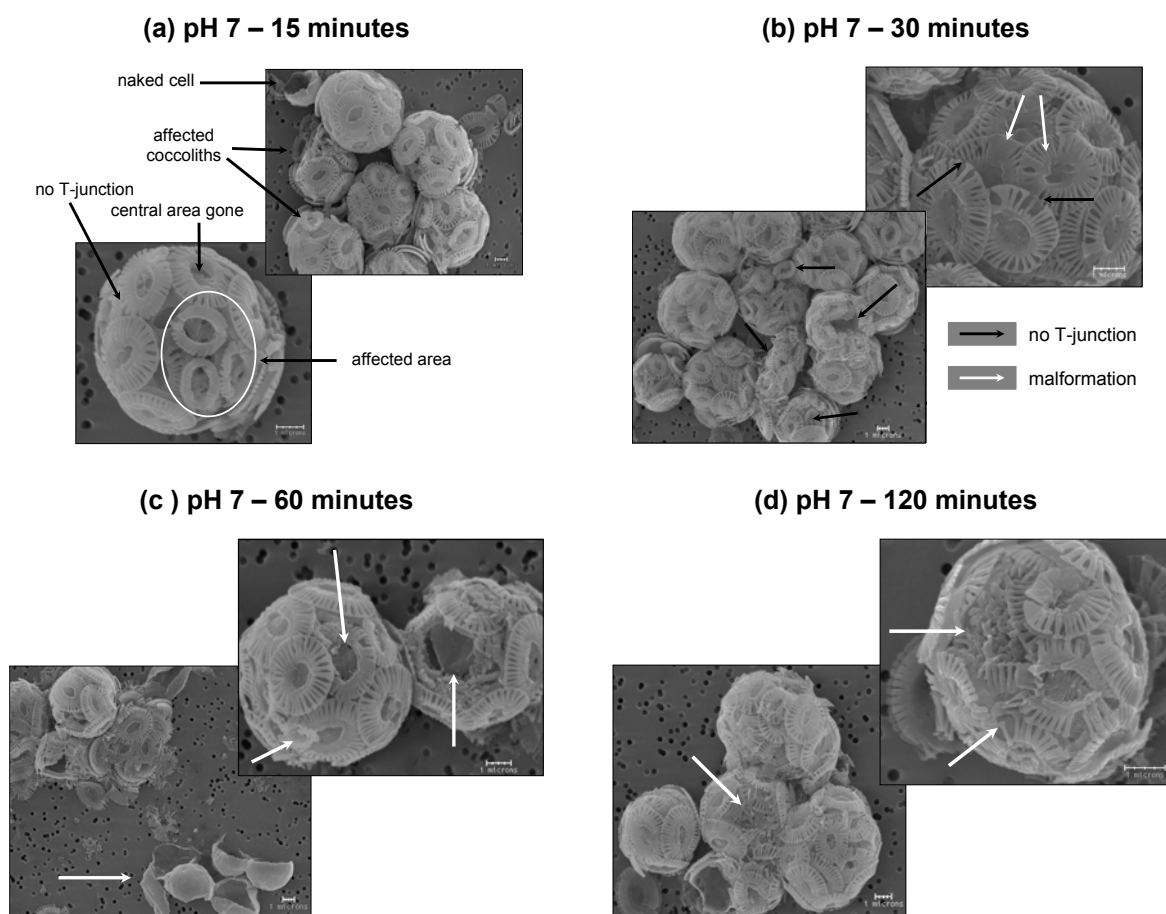
Figure 40. SEM micrographs of *E. huxleyi* after reacting in seawater at pH 7 for (a) 15 minutes, (b) 30 minutes, (c) 60 minutes and (d) longer than 120 minutes.

At the neutral pH 7, one observed dissolution features; naked cells could be found showing a complete dissolution of coccoliths after a long reaction time (Figure 40). It can be noted that it was the T-junction and the central area of the coccoliths that were most affected.

At slightly acidic pH, all coccoliths were dissolved and only broken and empty naked cells were observed (Figure 41).

(a) pH 5.5

30 min.

60 min.

Most cells are naked.

(b) pH 5 – 15 minutes

Mag = 4500 X

(c) pH 4.5 – 15 minutes

Mag = 950 X

Figure 41. SEM micrographs of Ehux after reacting in seawater at (a) pH 5.5, (b) pH 5 and (c) pH 4.

4.4 Field survey #1 (22 April – 11 May 2002)

The positions of the sampling locations during the Belgica cruise that took place from 22 April to 11 May 2002 in the Northern Gulf of Biscay are indicated in Figure 42. Remote sensing image taken on 9 May 2002 indicated the bloom of coccolithophore in the study area (Figure 43).
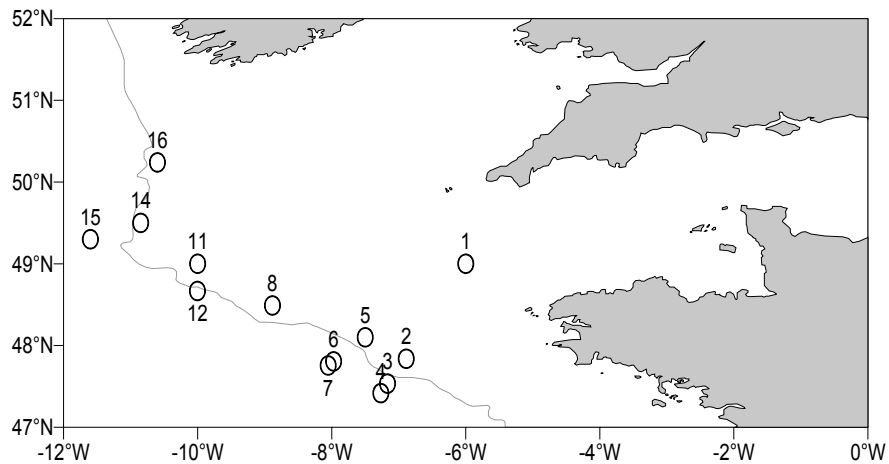
Figure 42. Sampling locations during the April-May 2002 *Belgica* cruise.
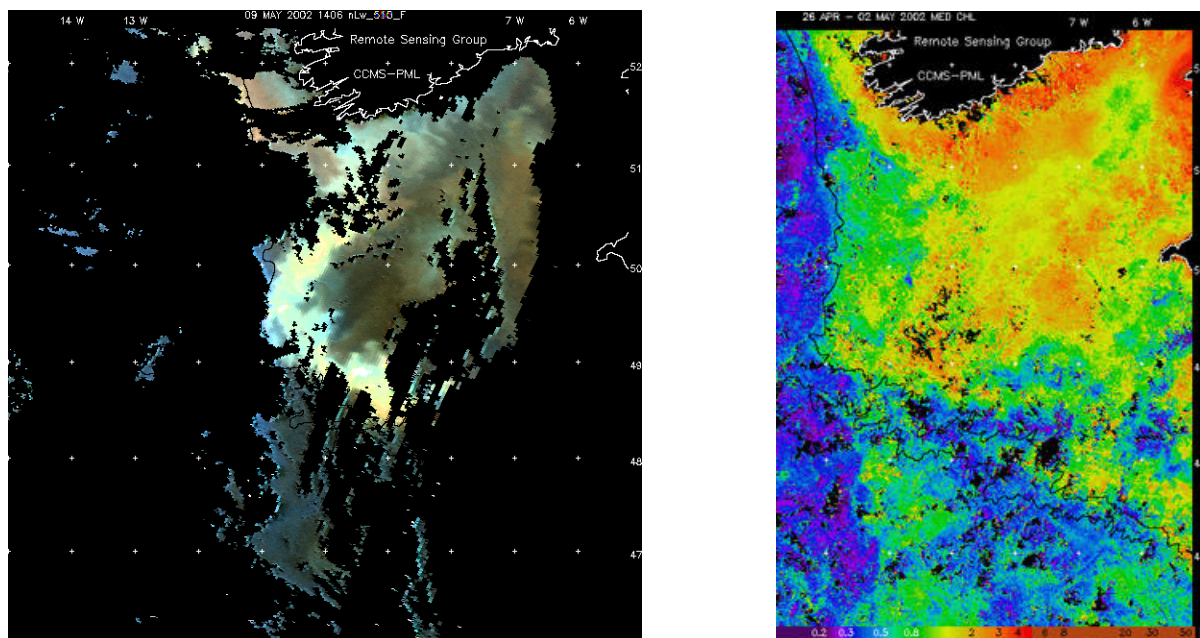
Figure 43. Satellite images showing the coccolithophorid bloom (left) and chlorophyll concentrations (right) in the Northern Bay of Biscay during the April-May 2002 campaign (NERC Dundee University Reveiving Station and processed by the Remote Sensing Group, Plymouth Marine Laboratory).

4.4.1 Vertical distributions of temperature, salinity and nutrients in the photic zone

Sea-surface **temperature** varied between 12°C and 13°C on the continental shelf. The southern stations were colder than the northern ones by 1 or 2 degrees (Figure 44). A slight thermocline in the first 20 meters of the water column was apparent on the continental shelf and was destructed on the slope, due to the strong vertical mixing.

Seawater had a rather constant temperature of 11-12°C below the thermocline down to 400-500 meters depth.

Salinity was constant in the photic zone, ranging between 35.5 and 35.6 on the continental shelf (Figure 44). It was slightly higher (between 35.6 and 35.7) on the continental slope and the western zone of study. Vertical profiles showed relatively constant salinity in the photic zone, suggesting an important vertical mixing with no marked halocline.

Station 1 was under the influence of the continental discharge of fresher waters, as indicated by the lower salinity.

Surface waters of the study area were globally depleted with both phosphate and dissolved silica, compared with their concentrations at 200 meters depth. Concentrations between 0 and 0.25 µmol.l^{-1} of **phosphate** were found in the first 30 meters of the photic zone on the continental shelf (Figure 45). They were associated with dissolved silica concentrations close to 1 µmol.l^{-1}, suggesting an active uptake by phytoplankton on the continental shelf.

Dissolved silica under the photic zone increased from 2.5 µmol.l^{-1} at 200 m to about 7.5 µmol.l^{-1} at 1400 m, as did dissolved phosphorus in the range of 0.5 - 1 µmol.l^{-1} between 200 m and 800 m (Figure 45).

On the continental rise and slope, phosphate concentrations were low, close to 0.25 µmol.l^{-1}, while dissolved silicate concentrations were more variables. Surface seawater was depleted in dissolved silicate at stations 12 and 7.
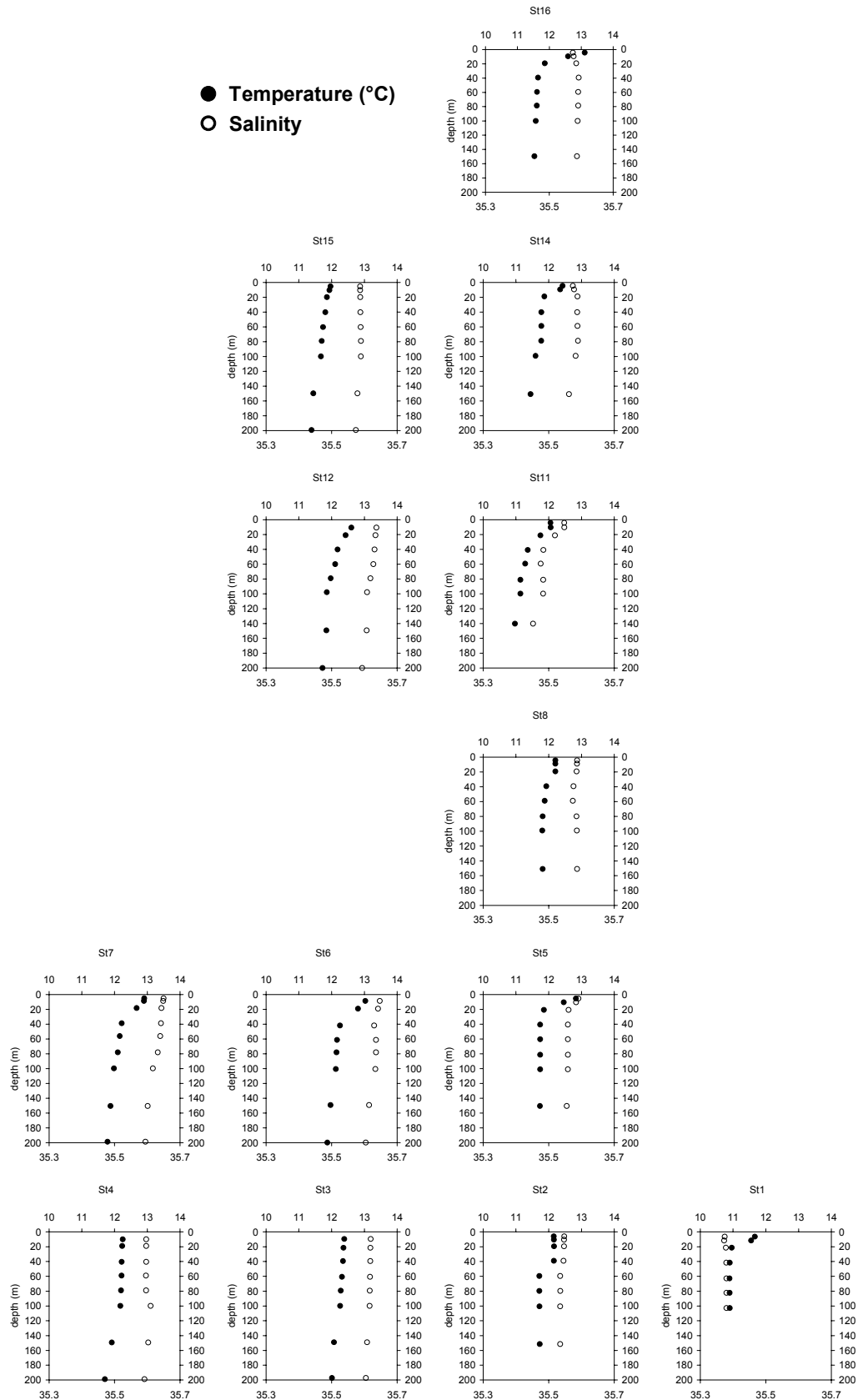
Figure 44. Vertical distributions of temperature (upper scale) and salinity (lower scale) in the photic zone during the April-May 2002 Belgica cruise.
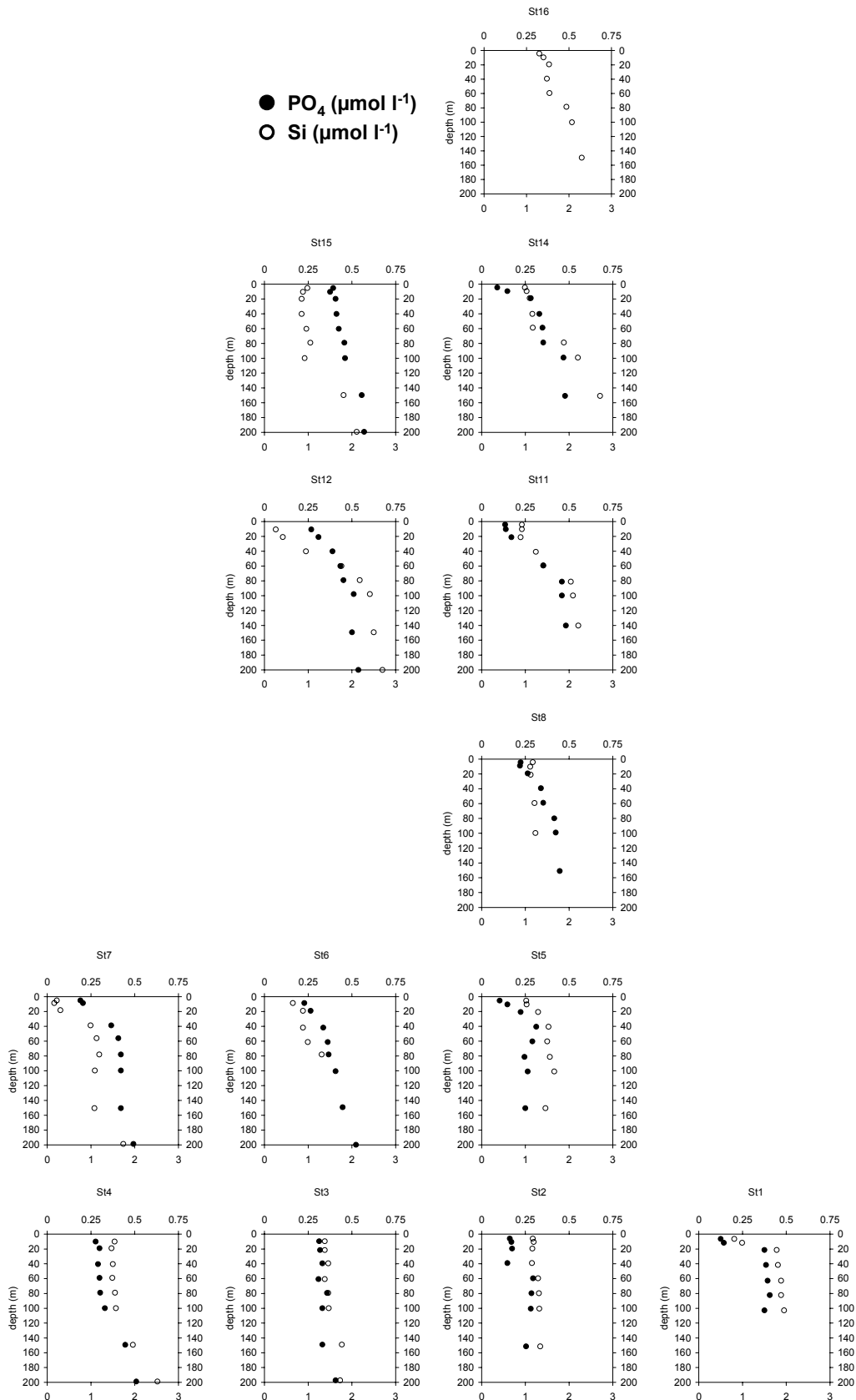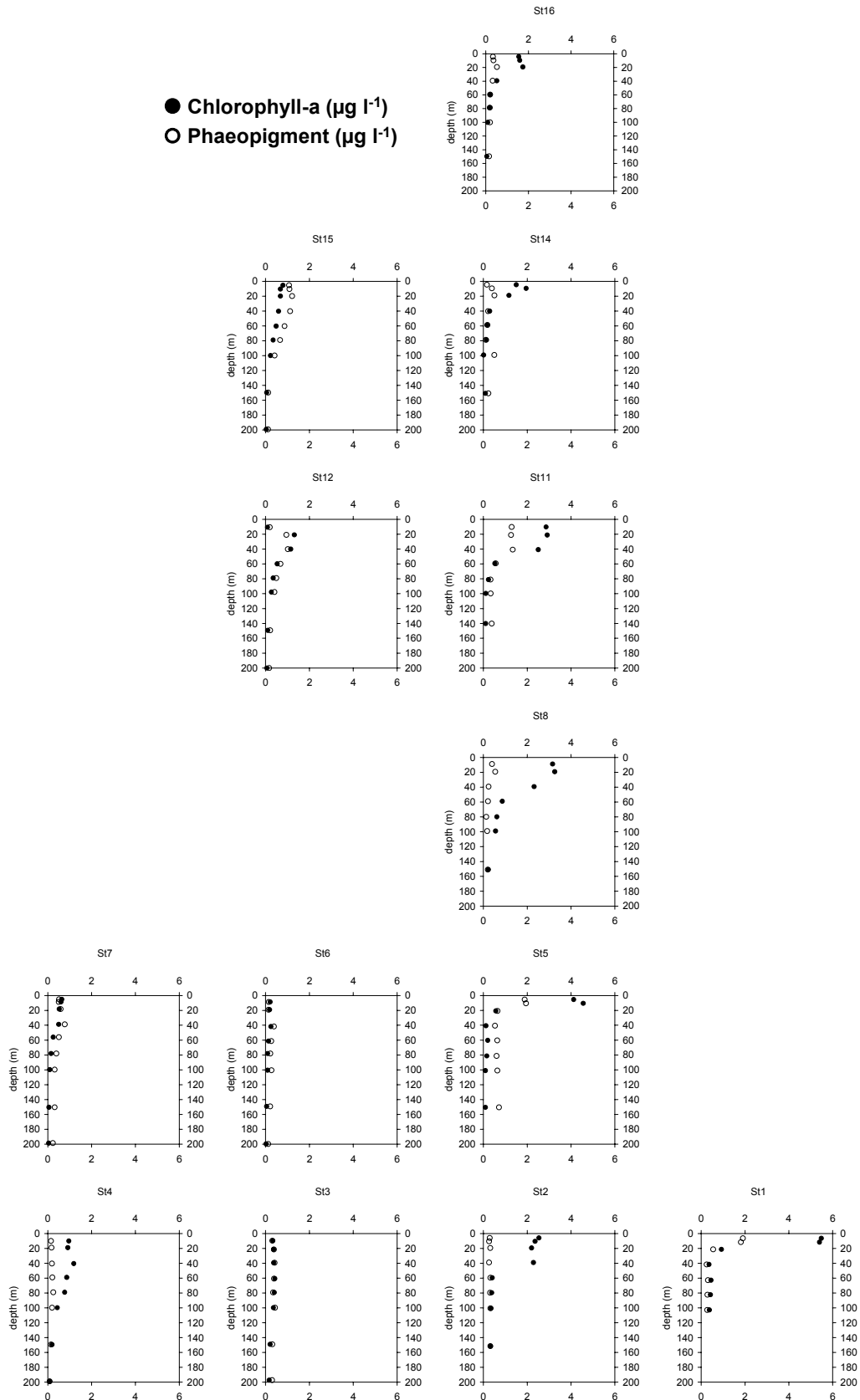
Figure 45. Vertical distributions of dissolved phosphate (upper scale) and silicate (lower scale) in the photic zone during the April-May 2002 Belgica cruise.

4.4.2 Photosynthetic pigments and dissolved oxygen

Chl-a concentrations in surface waters of the continental rise and slope were low, generally below 1 µg Chl-a.l^{-1} (Figure 46). They increased on the continental shelf to values higher than 2 or 3 µg Chl-a.l^{-1}, reaching a value of 5.5 µg Chl-a.l^{-1} at station 1 located near the Ushant front. The highest values of 3-4 µg Chl-a.l^{-1} were measured at stations 11, 8 and 5. The vertical profiles generally gave higher values in surface, where irradiance was higher. Chl-a concentration decreased with depth, down to 0 at around 40 m and 100 m, depending on the phytoplankton species requirements for light.

Higher **phaeopigment** concentrations were found in association with the highest Chl-a (Figure 46).

Surface seawaters were close to saturation with atmospheric **oxygen** but higher saturation was not always associated to higher Chl-a concentrations, depending on the intensity of the mixing with deep waters (Figure 47).

Figure 46. Vertical distributions of chl-a and phaeopigments in the photic zone during the April-May 2002 Belgica cruise.
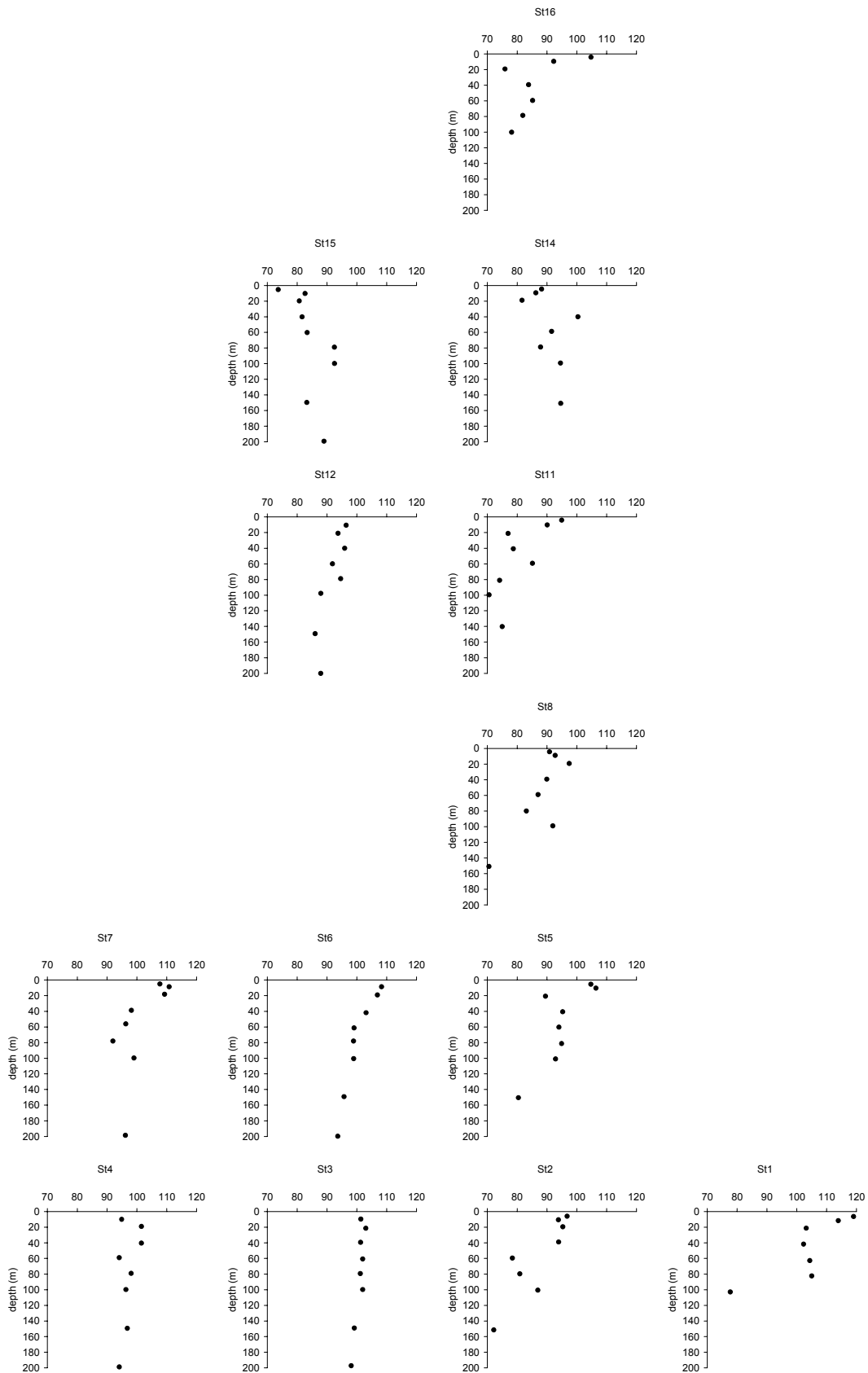
Figure 47. Vertical distributions of dissolved oxygen (% saturation) in the photic zone during the April-May 2002 Belgica cruise.

4.4.3 Inorganic carbon biogeochemistry

Seawater **pH$_{(SWS)}$** ranged between 8.1 and 8.2 in surface waters of the continental shelf break and decreased with depth to values around 8.000 under the photic zone (Figure 48).

Surface waters were in general under-saturated with respect to CO_2, compared to the atmosphere and underlying waters (Figure 49). During the campaign, the **pCO$_2$** of the upper photic zone never decreased below 300 ppmV and was rather constrained between 300 and 350 ppmV. Nevertheless, some stations were in quasi-equilibrium (station 1) with respect to atmospheric CO_2 (station 1) or even exceeded atmospheric CO_2 partial pressure (station 15 and 7).

Vertical profiles of **pCO$_2$** showed an increase from the surface, where the biological activity and air-sea exchange took place, towards the 200 m depth where seawater was supersaturated (around 500 ppmV) with respect to atmospheric pCO$_2$ (Figure 48).

The vertical profiles of **total alkalinity** normalized to salinity 35 showed a value of around 2340 µmol.kg^{-1} below the photic zone (value at 100 m depth) (Figure 50). Vertical profiles of relatively constant total alkalinity could be observed on the continental rise and the slope as well as in the southern part of the study zone. In contrast, vertical profile in the northern part of the zone displayed a decrease of alkalinity in surface waters (2320 µmol.kg^{-1}), suggesting the occurrence of calcification in the upper photic zone.

Surface seawater in the ocean was generally supersaturated with respect to calcite and aragonite. In this survey, the **saturation state** with respect to calcite (Ω_{cal}) exhibited values close to 4 in surface, which decreased with depth (Figure 50). The lowest value observed in this survey was 1.8 (St 4, 1500 m). Such a low value corresponded to a saturation state with respect to aragonite (Ω_{ar}) of 1.16.
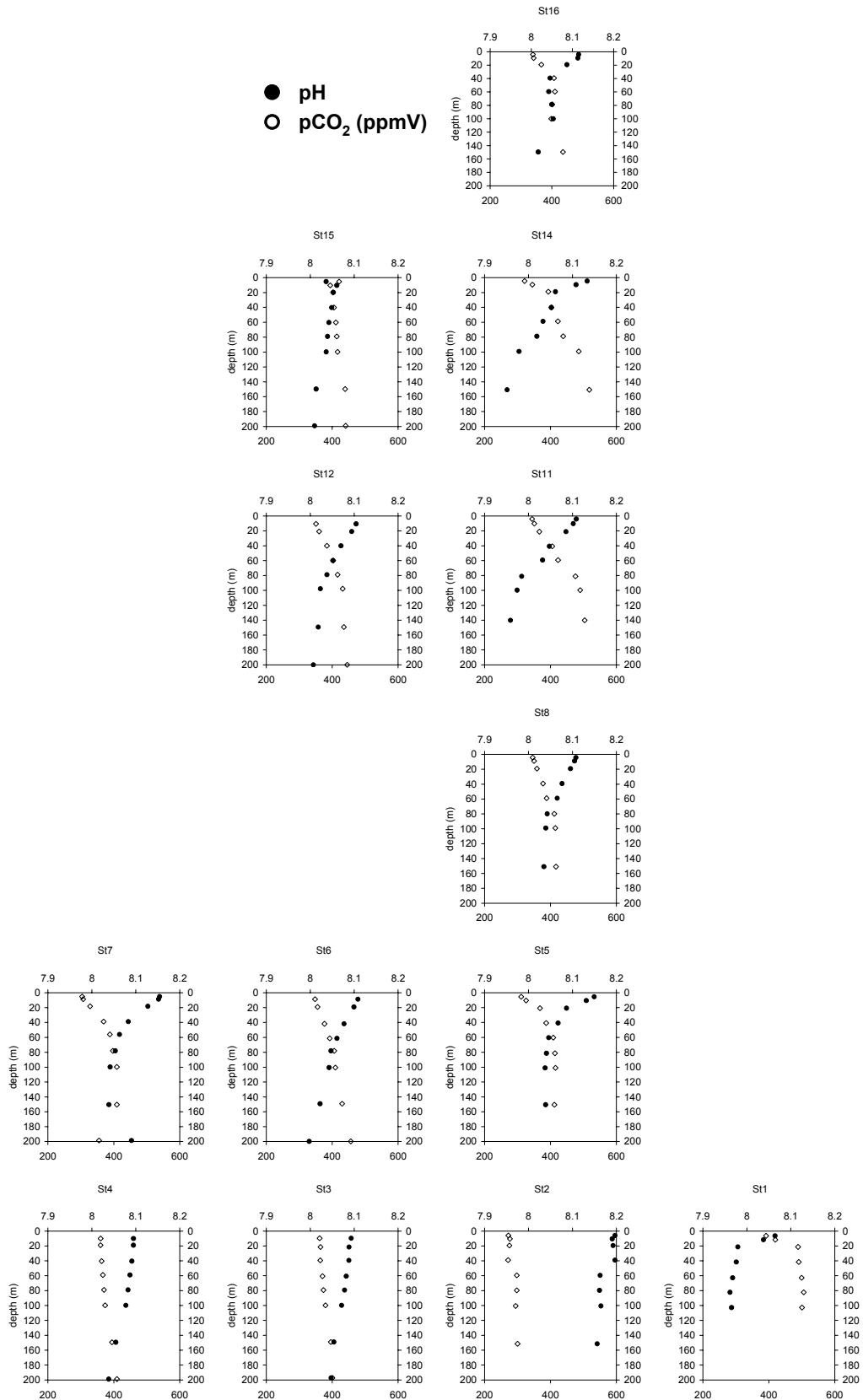
Figure 48. Vertical distribution of pH$_{(SWS)}$ (upper scale) and pCO$_2$ (lower scale) in the photic zone during the April-May 2002 Belgica cruise.
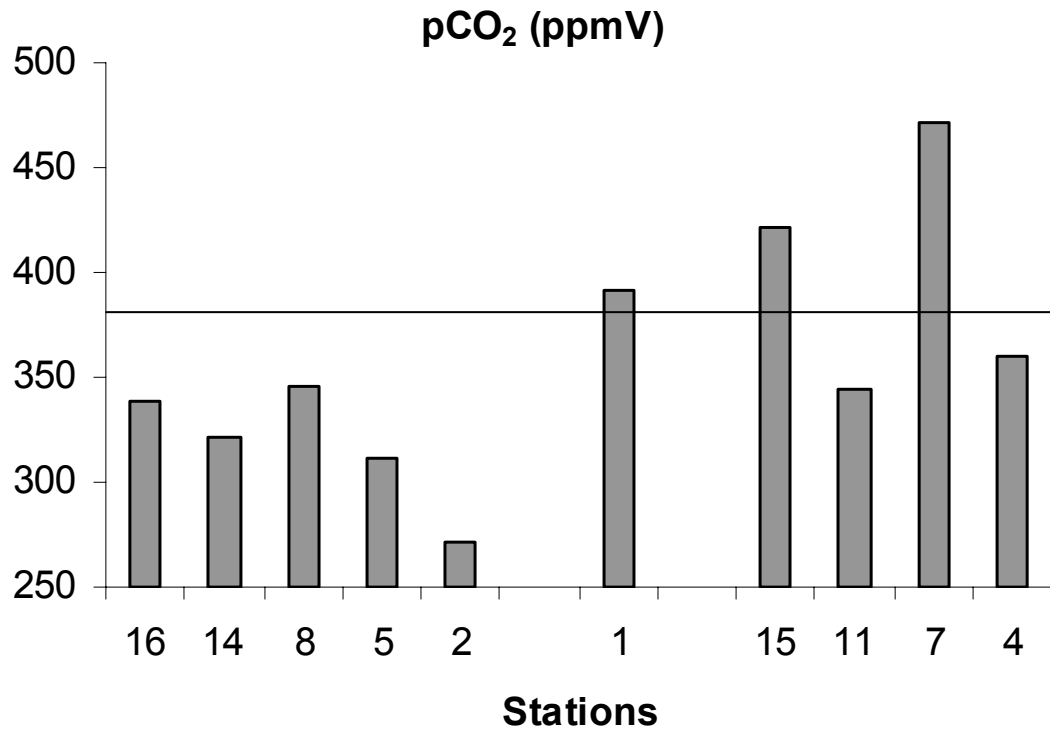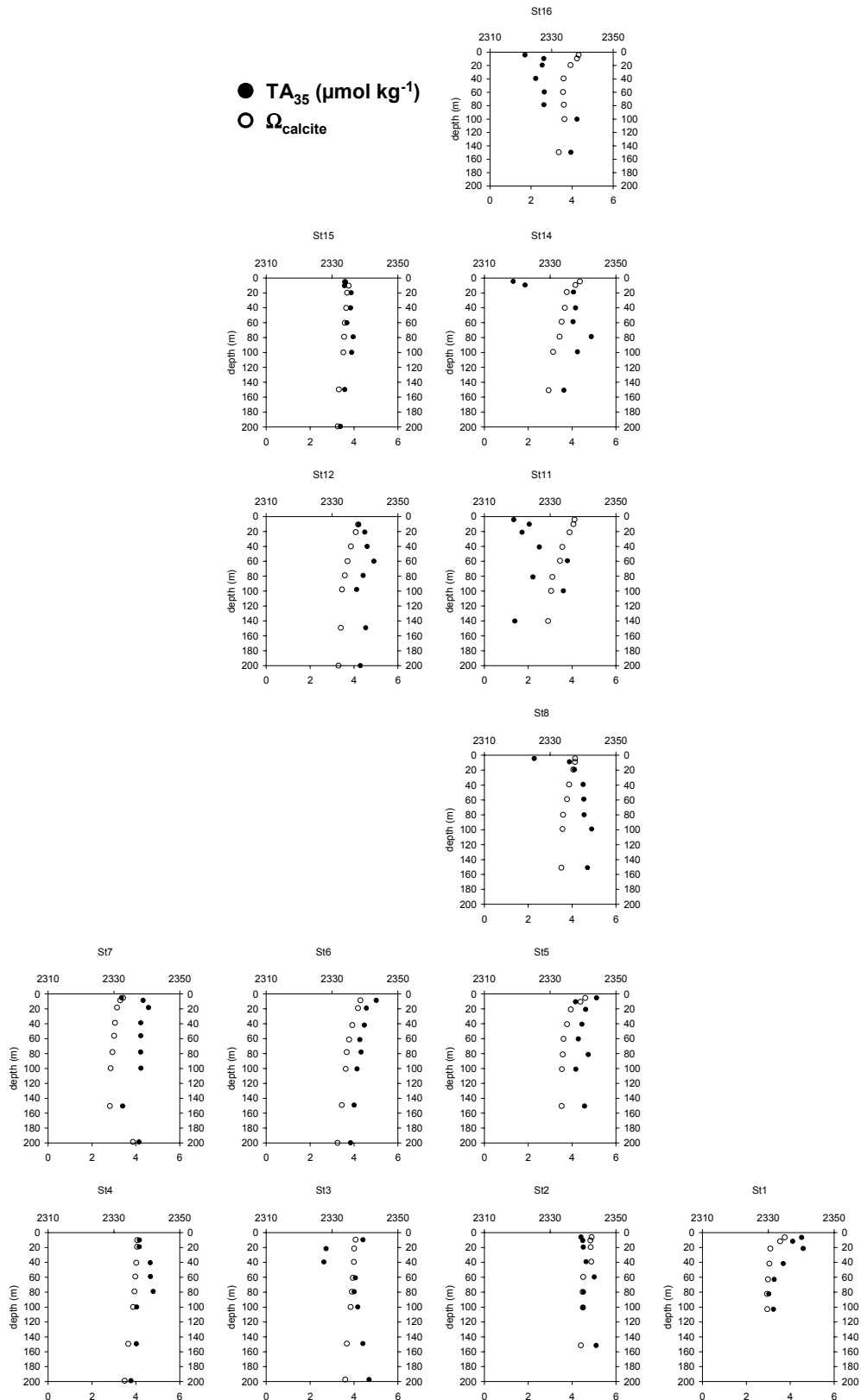
Figure 49. Surface distribution of pCO_2 (ppmV) along the 200 m isobath (continental shelf break, stations 16 to 2), on the continental shelf (station 1) and on the slope (stations 15 to 4) during the April-May 2002 Belgica cruise. Straight line represented atmospheric saturation with respect to CO_2.

Figure 50. Vertical profiles of total alkalinity normalized to salinity 35 (TA$_{35}$, upper scale) and saturation state with respect to calcite (Ω_{cal}, lower scale) in the photic zone during the April-May 2002 Belgica cruise.

4.4.4 Particulate matter distribution, composition and PIC:POC ratios

Suspended matter was quantitatively more important on the continental shelf with values ranging from 0.5 to 1 mg.l^{-1} in surface, compared to the slope stations where surface concentrations were smaller than 0.4 mg.l^{-1} (Figure 51).
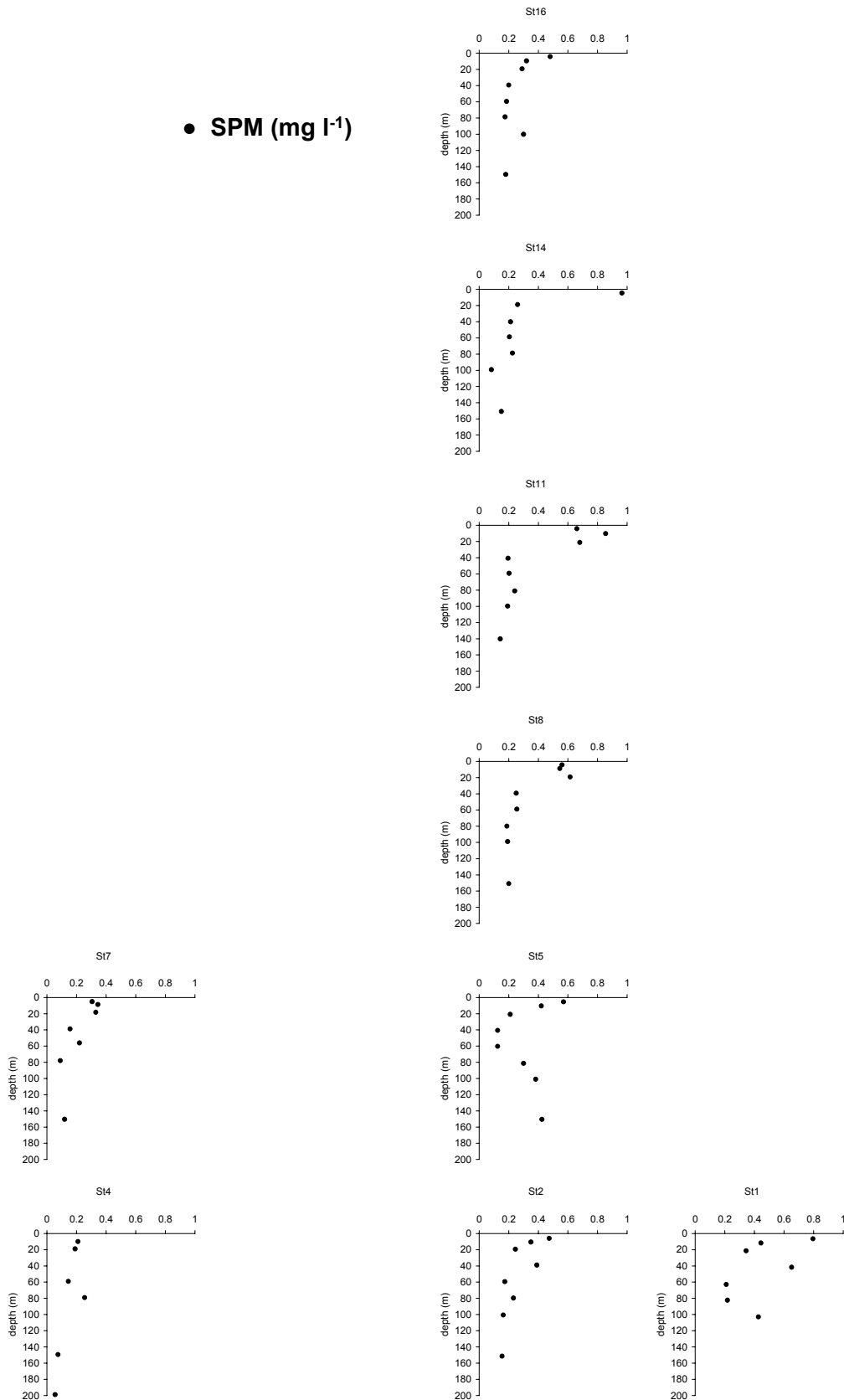
Vertical distribution of suspended matter concentrations seemed to be bimodal on the shelf with a first maximum at the base of the photic zone (100 m depth) and a second more important one in the upper photic zone (subsurface to surface).

Particulate organic carbon (POC) concentrations in the surface waters of the study zone ranged between 0.1 and 0.24 mg.l^{-1} on the continental shelf and were below 0.05 mg.l^{-1} on the slope (Figure 52). Most of the organic carbon was located in the upper photic zone, between 40 m depth and the sea-surface. Station 1 displayed the highest concentrations at the surface, which decreased to 0.03 mg.l^{-1} at depth.

The seawater concentrations of **particulate inorganic carbon (PIC)**, were in the range of 0.05 to 0.1 mg.l^{-1} on the continental shelf and below 0.05 mg.l^{-1} on the slope (Figure 52). The vertical profiles showed higher values in surface.

The **ratios of PIC:POC** in particulate matter were below unity in the water column. Values close or greater than 0.8 were found in surface waters on the continental shelf for stations 11, 8 and 5, as well as for station 7 on the slope. This ratio was higher in surface and generally decreased with depth (Figure 53). An increase to 0.5 was observed sometimes between 60 m and 100 m, which could be attributed to vertical mixing allowing inputs of fine carbonated sediments from below.
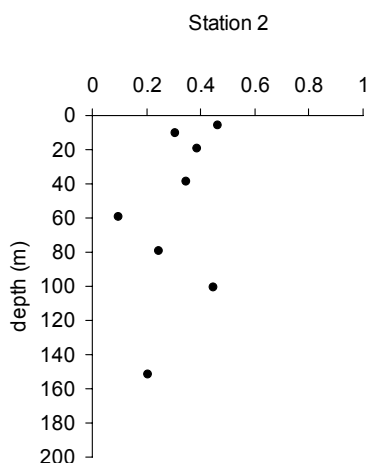
Figure 51. Vertical distribution of suspended particulate matter in the photic zone during the April-May 2002 Belgica cruise.
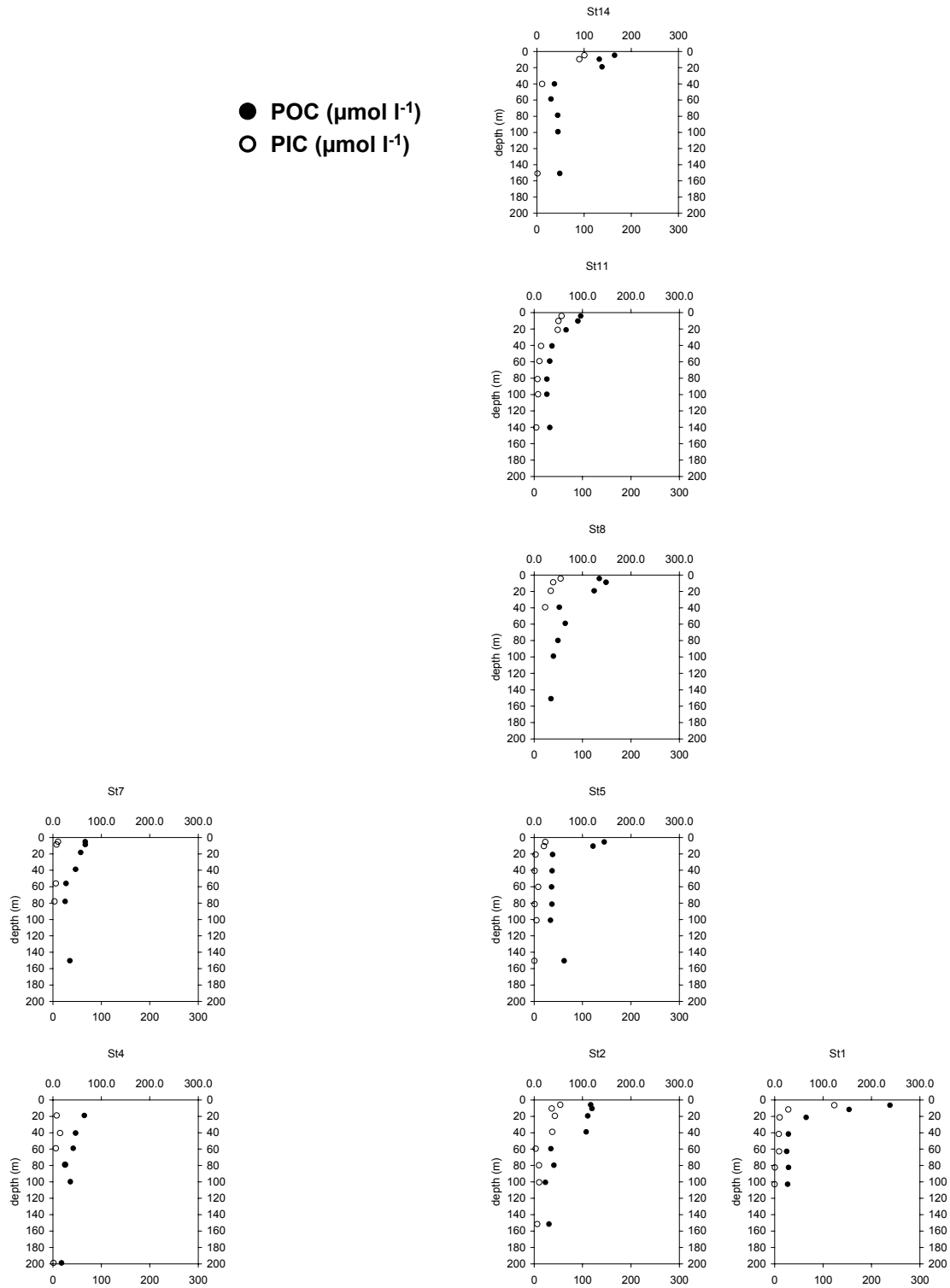
Figure 52. Vertical distribution of particulate organic carbon (POC) and particulate inorganic carbon (PIC) in the photic zone during the April-May 2002 Belgica cruise.

Figure 53. PIC:POC ratios for station 2 on the shelf break during the April-May 2002 Belgica cruise.

Based on continuous centrifugation of surface waters in the zone, the contribution of carbon to particulate matter and the distinction between the organic and inorganic phases can be detailed more precisely. Carbon represented a significant fraction of the suspended matter. At stations 2, 5, 7 and 16, total carbon accounted for half of the weight of the suspended matter (Table 4). These high values contrasted with the 22-30 % found at stations 8, 11 and 14.

Table 4. Particulate carbon (organic and inorganic) and nitrogen contents in the suspended matter, expressed in % (wt/wt).

| Station	Ctot % MES	Corg % MES	Cinorg % MES	Ntot % MES
2	45.7	37.3	8.3	8.9
4	33.4	31.0	2.4	5.5
5	54.7	50.7	4.0	10.3
7	49.5	42.6	6.9	9.3
8	29.8	22.3	7.4	4.6
11	27.6	15.8	11.8	4.0
14	22.3	10.2	12.0	2.1
16	49.9	43.9	6.0	6.8

The POC content ranged between 10.2 % and 50.7 % of the suspended material. In surface waters at 3 m depth along the isobath 200 m, organic carbon represented a significant fraction of the total carbon (80-90 % of Ctot) at the stations 2, 5 and 16, compared to stations 8, 11 and 14. In contrast, the PIC fraction in the suspended matter of surface waters was maximal at the stations 11 and 14 (11.8 % and 12.0 % of the total mass of suspended matter, respectively), and was lower than 10 % at other stations. On the slope, particulate carbon in the suspended matter represented

one third to half of the total weight and most of this carbon was organic (more than 85 % of Ctot). Consequently, the ratios of PIC:POC were quite variable.

Total particulate nitrogen followed the trend of organic carbon with a POC:PN ratio of 4.94 $\pm$ 0.79 in this study (average $\pm$ standard deviation, r^2 = 0.87, n = 8).

4.4.5 Particle characterisation

Automated Electron Probe Micro Analysis (EPMA) was used to characterise the individual particles for their composition, morphology and size. Based on the data set obtained, the particles were further classified using hierarchical cluster analysis (HCA). The calculations were done using the statistical software package IDAS. Figure 54 shows that at Station 14 in the Goban Spur area the particles rich in calcium carbonate were most abundant while at station 2 in the southern part of the study area near La Chapelle Bank particles rich in silica could be equally abundant. SEM micrographs reveal the presence of *E. huxleyi* at station 14 and of diatoms at station 2; the herbivorous copepods were also present (Figure 55).

Station 14   Station 2
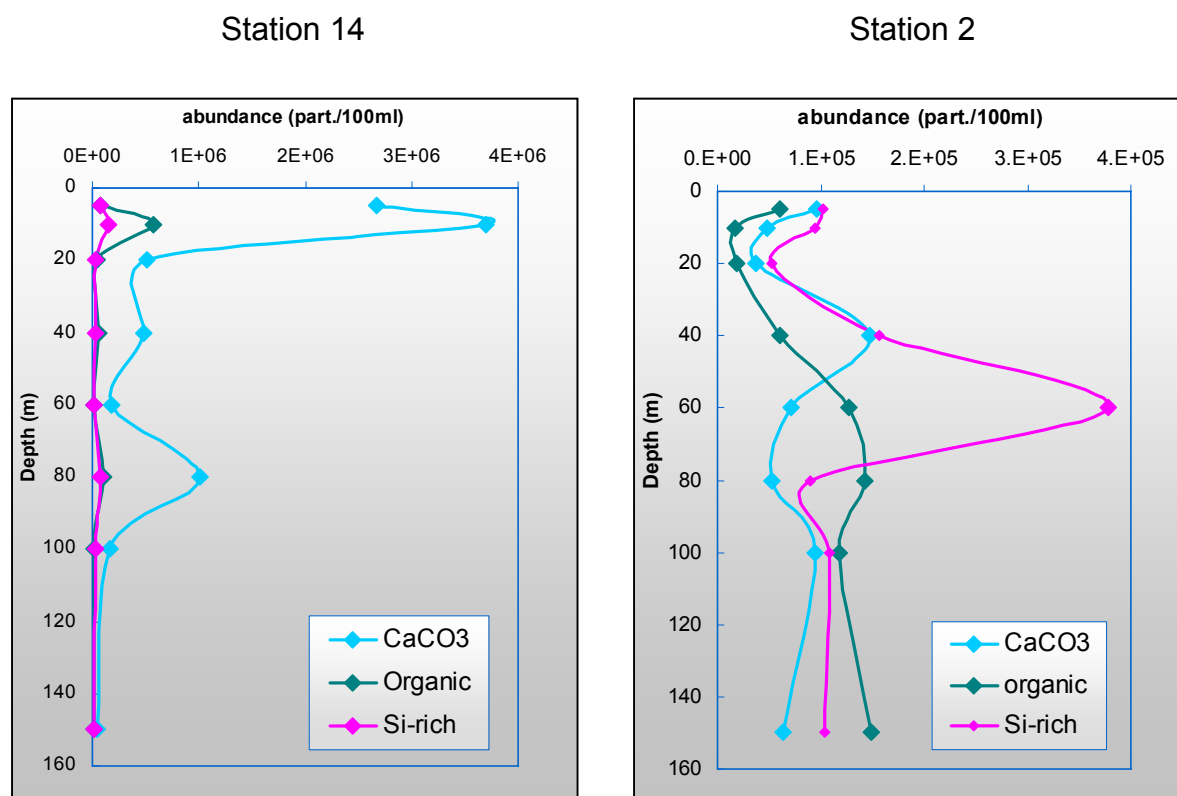

Figure 54. Vertical distribution of the relative abundance of different types of particles present at station 14 and at station 2 in the photic zone during the April-May 2002 cruise.
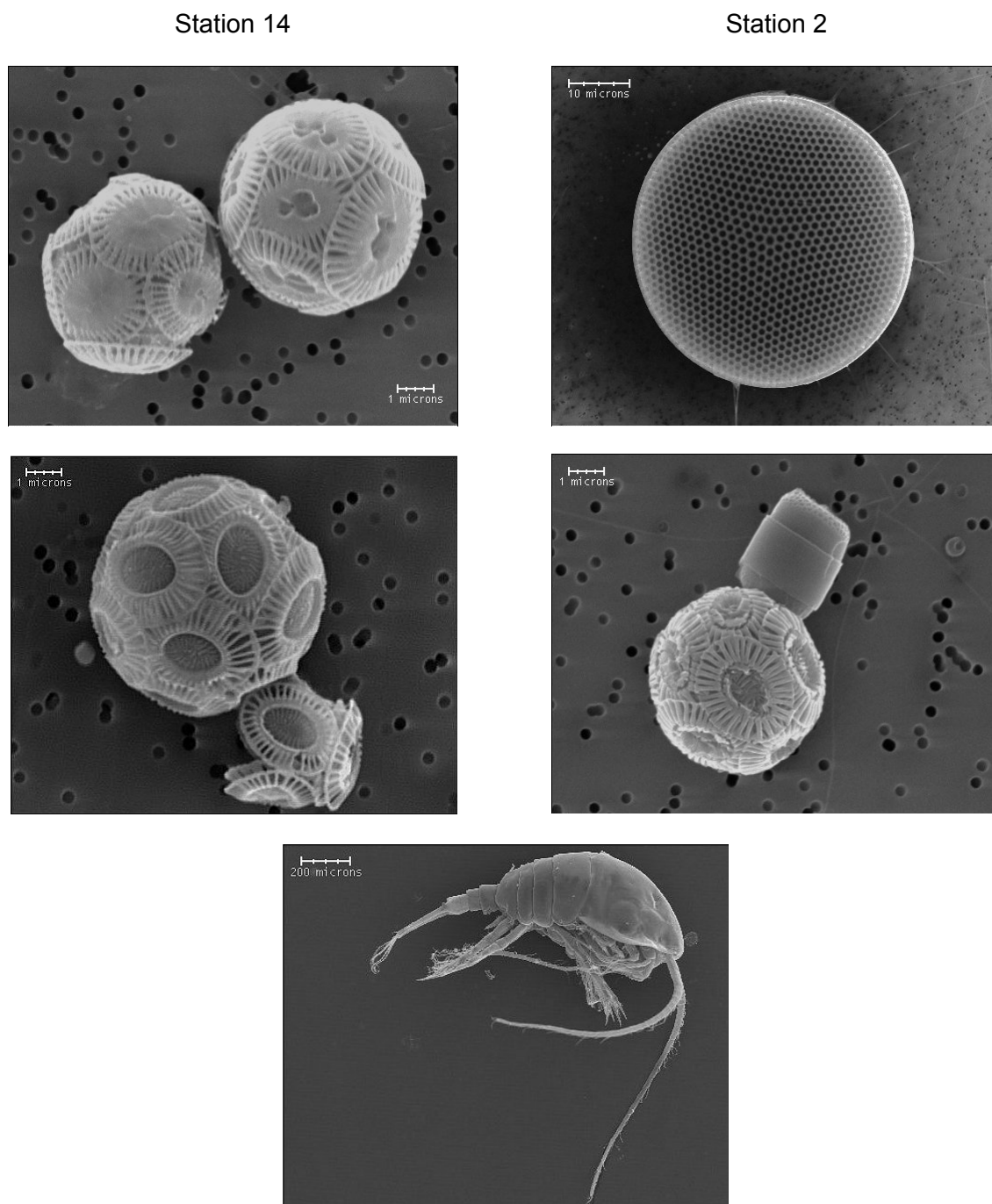
Figure 55. SEM micrographs showing the presence of *E. huxleyi* at station 14 and of diatoms at station 12 during the April-May 2002 Belgica cruise. The presence of copepods was also detected.

The absolute abundances of particles for all samples collected during the April-May 2002 Belgica cruise are shown in Figure 56. The very high number of particles observed in the upper layer at stations 1, 11 and 14 was an indication for a bloom.
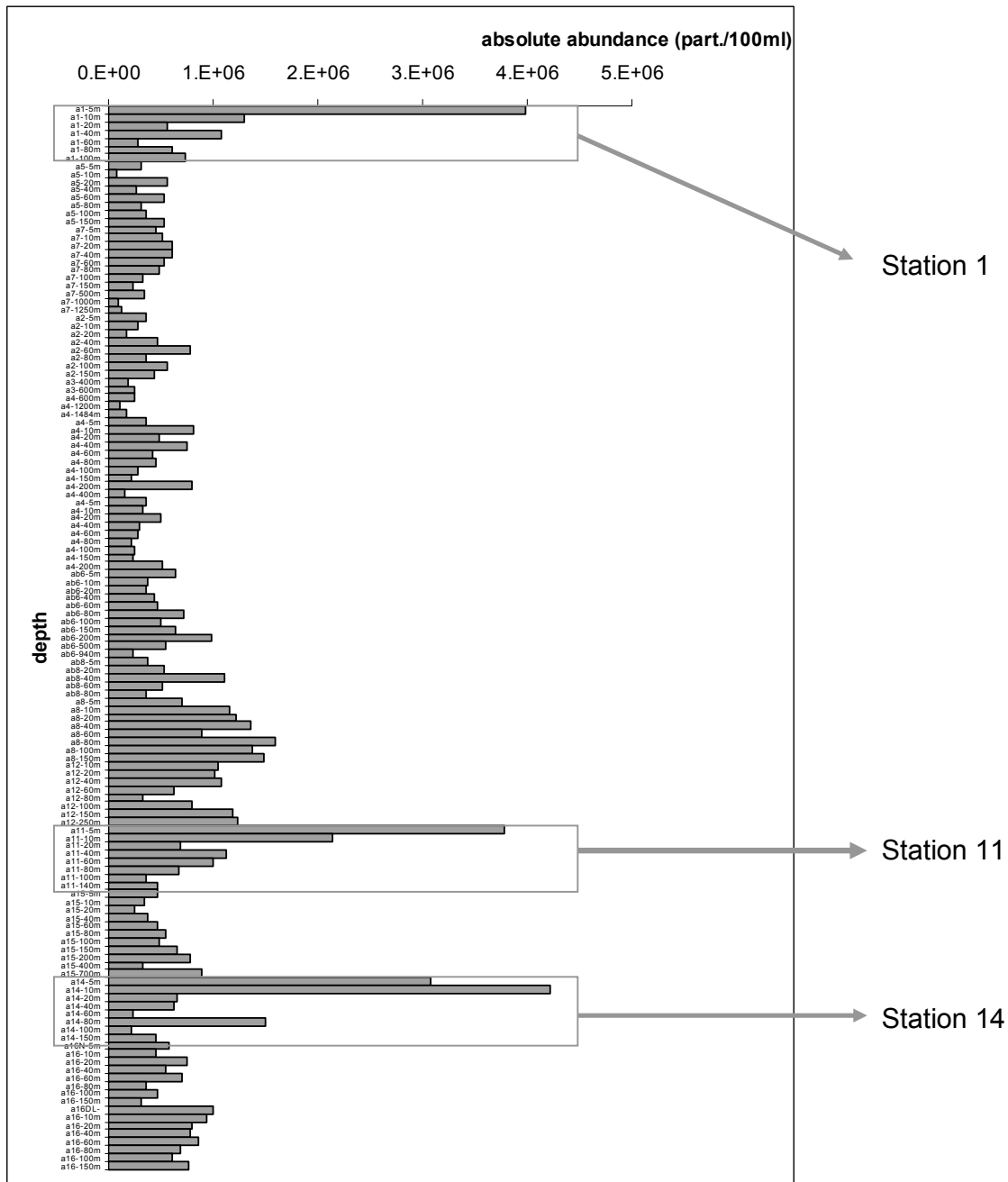

Figure 56. Absolute abundances of particles for samples collected at various stations and depths during the April-May 2002 Belgica cruise.

4.4.6 kinetics of ^{14}C incorporation

^{14}C incorporation in the organic matter exhibited generally linear kinetics during the first 18 hours of illumination. During the last 6 hours of illumination, the total amount of ^{14}C decreased as a result of reduced incorporation in the inorganic matter (Figure 57).

The rate of incorporation of ^{14}C in organic matter ranged from 0.2 (station 2) to more than 0.5 $\mu molC.l^{-1}.h^{-1}$ on the shelf break and exceeded 1 $\mu molC.l^{-1}.h^{-1}$ at station 1 (shelf). Lower values were observed on the slope (0.13 to 0.26 $\mu molC.l^{-1}.h^{-1}$ for stations 7 and 4, respectively).

^{14}C incorporation by heterotrophic processes was very low, compared to the autotrophic ones. Less than 1 % of carbon was taken up during dark processes.
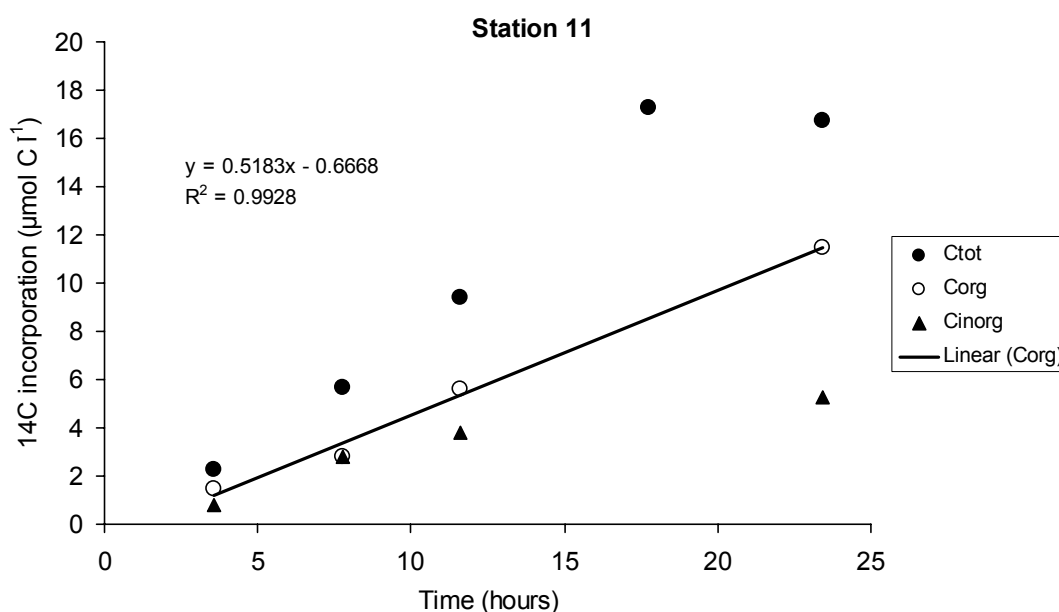
Figure 57. Kinetics of ^{14}C incorporation by the natural assemblages at station 11 (shelf break, in $\mu molC.l^{-1}$) under constant light (150 $\mu mol.m^{-2}.s^{-1}$) during the April-May 2002 Belgica cruise. Black dots represent the total incorporation of ^{14}C while open dots represent incorporation in the organic compartment. The difference between the two values is defined as the rate of calcification.

4.4.7 Integrated primary production and calcification

Primary production was in general higher on the continental shelf, up to 22 $gC.m^{-2}.d^{-1}$ at station 11 (Figure 58). At this station, calcification represented 11 $gC.m^{-2}.d^{-1}$, giving a calcification to primary production ratio close to 50 %. Most of the primary production took place in the Northern part of the survey (Stations 16 to 8) and calcification was higher at station 11 located inside the phytoplankton patch. A filament was observed (stations B8 and B6) across the shelf break, where primary production exceeded 30 $gC.m^{-2}.d^{-1}$ and calcification rates were close to 10 $gC.m^{-2}.d^{-1}$. Stations 4 and 7, on the continental slope, displayed lower rates of ^{14}C incorporation either in the organic (0.6 to 6.5 $gC.m^{-2}.d^{-1}$) or the inorganic (0.2 to 1.5 $gC.m^{-2}.d^{-1}$) fractions.

The integrated Chl-a concentration is indicative of the phytoplankton biomass responsible for primary production and calcification (Figure 58). Phytoplankton biomass, up to 121 $mgChl-a\ m^{-2}$ (station 2) was measured in the southern part of the survey and decreased generally towards the northern stations (stations 14 and 16), situated on the continental shelf.
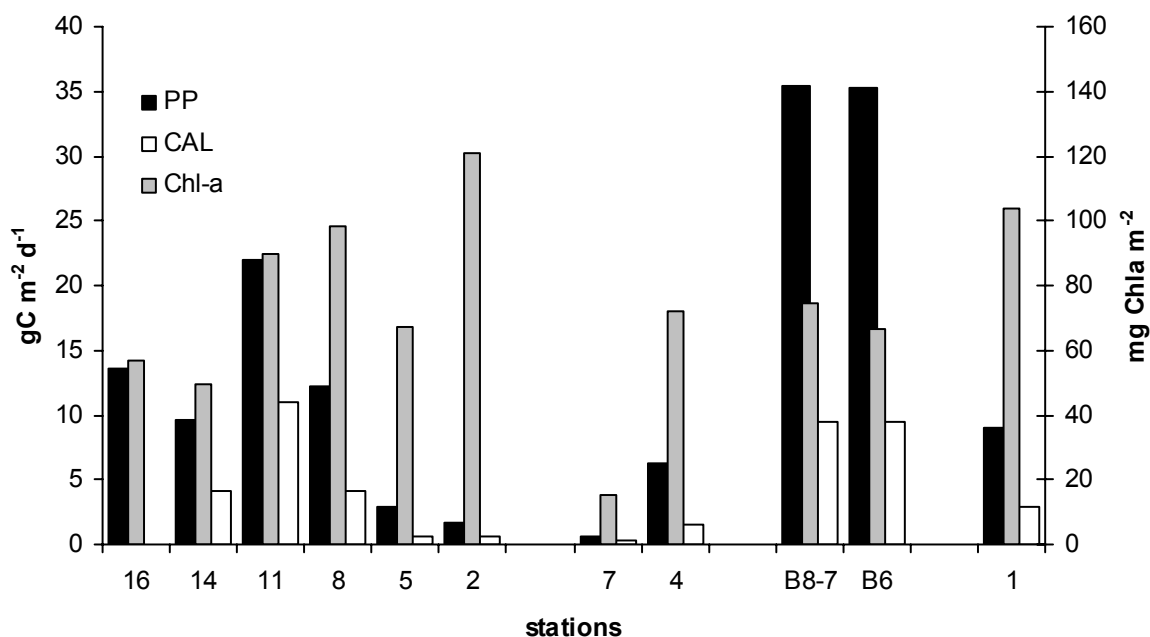
Figure 58. Primary production and calcification ($gC.m^{-2}.d^{-1}$) during the cruise (April 2002). Integrated Chl-a ($mg\ Chl-a.m^{-2}$) gives an indication of the amount of organic matter at the different stations.

## 4.5   Field survey #2 (28 April – 16 May 2003)

The positions of the sampling locations during the Belgica cruise that took place from 289 April to 16 May 2003 in the Northern Gulf of Biscay are indicated in Figure 59.
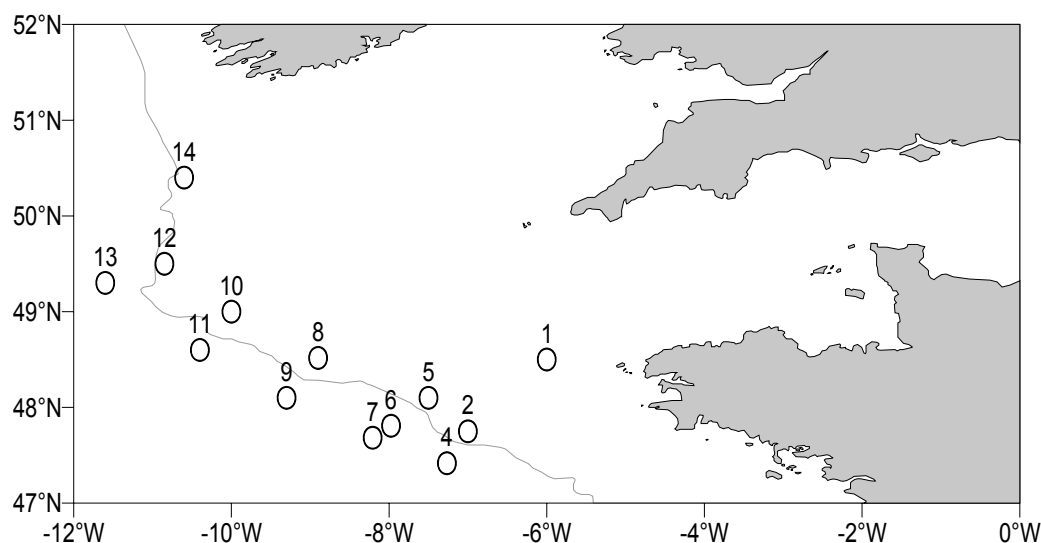
Figure 59. Sampling locations of the April-May 2003 *Belgica* cruise.

4.5.1   Temperature and salinity profiles in the photic zone

Sea-surface **temperature** was relatively constant, at about 12°C, in the study area. The vertical distribution of temperature was homogenous down to 40 m where a slight thermocline was observed between 40 m and 80 m depth in the northern part of the survey while it remained homogeneous in the south (Figure 60).
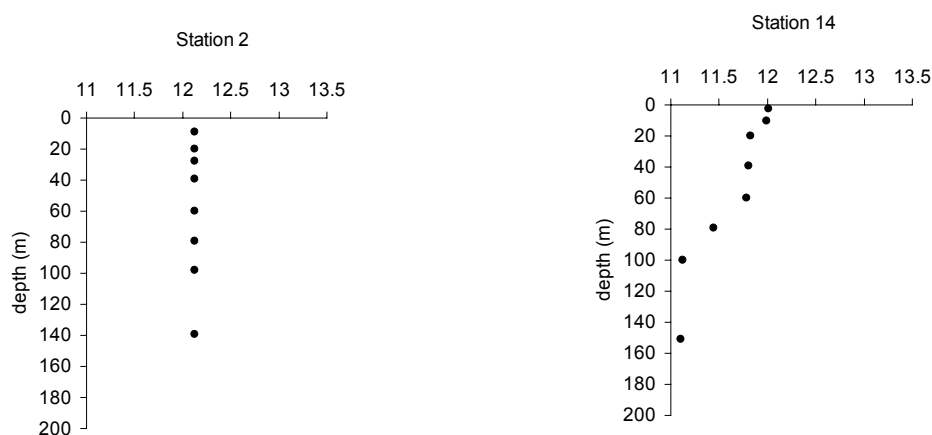
Figure 60. Temperature profiles on the shelf break at station 2 (south, shelf break) and station 14 (north, shelf break) during the April-May 2003 Belgica cruise.

Seawater **salinity** was in the range of 35.5 - 35.6; it was slightly lower at the station 1 located near the Ushant front and under the influence of freshwater discharge. Vertical profiles of salinity suggest an intense mixing in the photic zone for this parameter at the various stations visited during this survey (Figure 61).
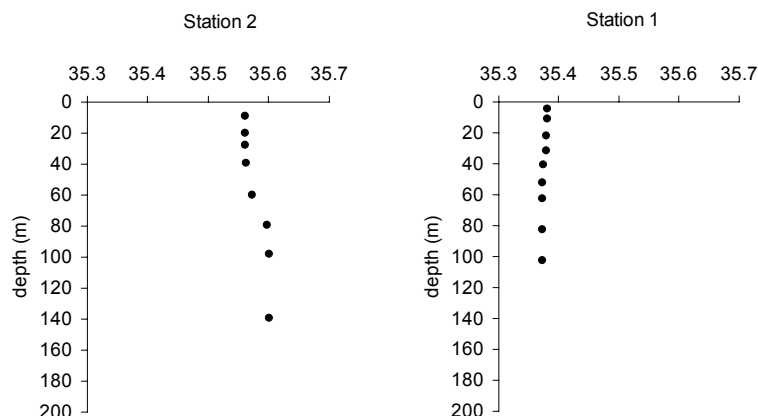
Figure 61. Salinity profiles at station 2 (shelf break) and station 1 (shelf) during the April-May 2003 Belgica cruise.

4.5.2 Nutrient profiles

Dissolved silica increased with depth from values around 2 µmol.l^{-1} at the top of the water column (Figure 62) to 11 µmol.l^{-1} at 1000m depth. The shape of the vertical distribution indicated a consumption of dissolved silica in the upper photic of 1 or 2 µmol.l^{-1}. A strong nutricline could be observed in some cases (for example at the stations 10, 12 and 14) from surface until a depth of 50 m to 80 m (data not shown). The general trend suggested that biological processes responsible for the consumption of dissolved silica in the upper photic zone were more pronounced in the northern part of the zone of study. No particular trend is observed in the vertical profiles that could be attributed to the bathymetry (i.e. rise, slope and continental shelf) or the depth of the water column within transects perpendicular to the isobath 200 m (data not shown).
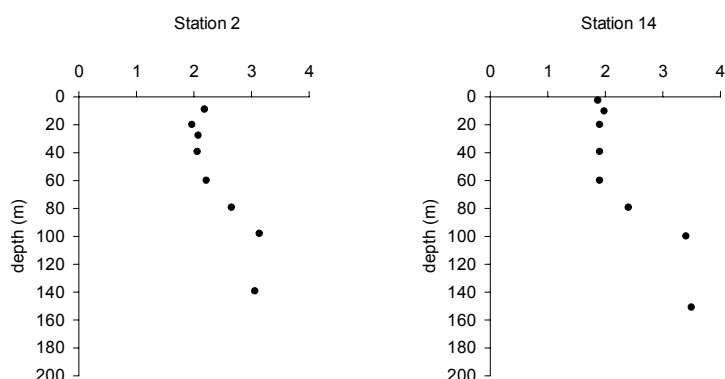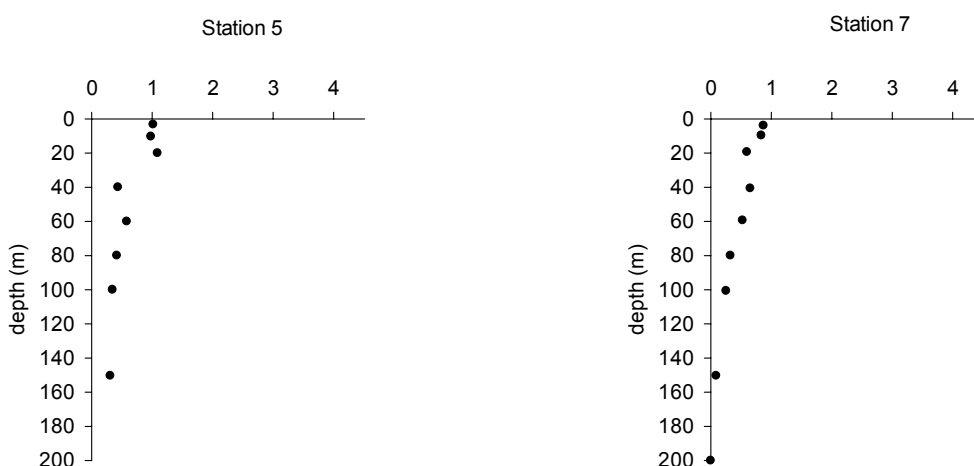

Figure 62. Vertical distribution of dissolved silica (µmol.l^{-1}) at station 2 (south) and station 14 (north) during the April-May 2003 Belgica cruise.

4.5.3 Photosynthetic pigments and dissolved oxygen

Sea surface concentrations of **Chl-a** varied between 1 and 2 $\mu g.l^{-1}$ in the study area. It was substantially higher (4 $\mu g.l^{-1}$) at station 1 that is a frontal one. The stations 5, 6, 8 and 10 represented a zone where Chl-a was the highest in our survey. Most of them were located on the continental shelf, except for station 8 (slope). The vertical profiles displayed higher values at the top of the water column down to 20-40 m depth, sometimes deeper (60 m at the stations 8 and 10) where the concentrations decreased drastically to 0 at around 100 m depth (Figure 63). A slight increase of Chl-a was observed on the slope (stations 7 and 4) from one leg to the other (10 days lag).
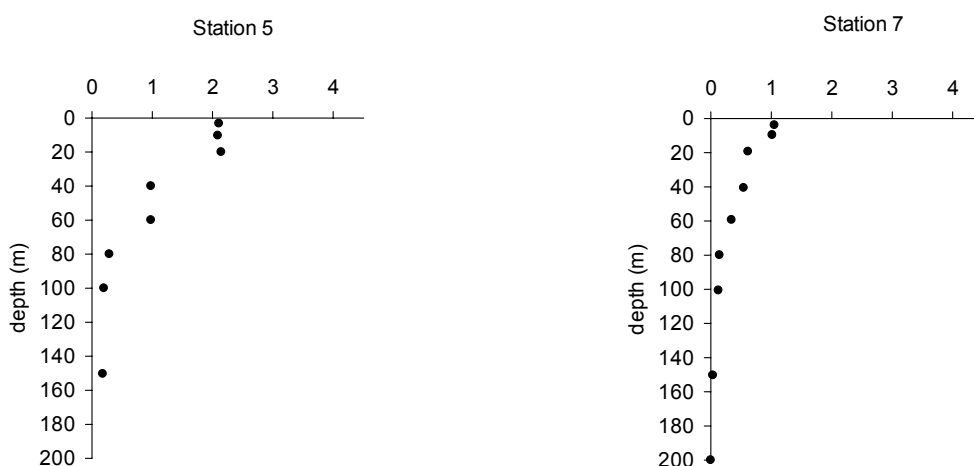
Figure 63. Vertical distribution of Chl-a ($\mu g.l^{-1}$) at station 5 (shelf break) and station 7 (slope) during the April-May 2003 Belgica cruise.


Figure 64. Vertical distribution of phaeopigments ($\mu g.l^{-1}$) at station 5 (shelf break) and station 7 (slope) during the April-May 2003 Belgica cruise.

The concentration of surface waters in **phaeopigments** was about 1 µg.l^{-1} and decreased with depth (Figure 64). No particular trend was observed between continental slope and shelf.

Most of the study zone appeared to be supersaturated with respect to atmospheric **oxygen** partial pressure (Figure 65).
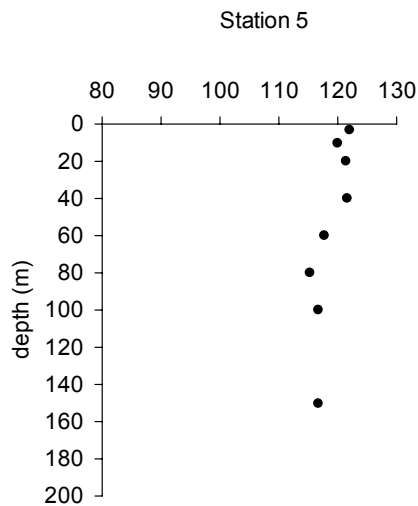
Figure 65. Vertical profile of dissolved oxygen (% saturation) at station 5 (shelf break) during the April-May 2003 Belgica cruise.

4.5.4 Inorganic carbon biogeochemistry

Seawater **pH$_{(SWS)}$** in surface waters averaged 8.10 during the survey. It decreased generally with depth to values below 7.90 (Figure 66).
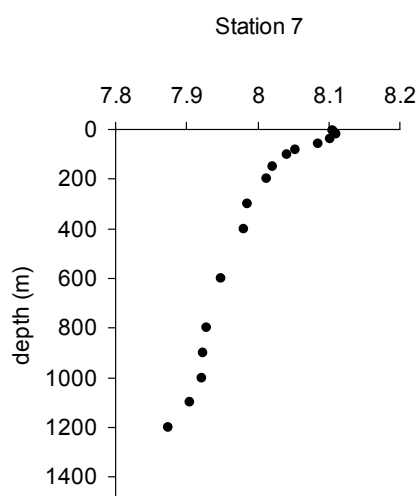
Figure 66. Vertical distribution of pH$_{(SWS)}$ at station 7 during the April-May 2003 Belgica cruise.

Partial pressure of CO_2 at depth was above 400 ppmV and decreased upwards when reaching the photic zone that became close to saturation with respect to the atmosphere (Figure 67). Undersaturation was more apparent during the second leg (stations Bis), compared to the first leg.

Figure 67. Surface distribution of pCO_2 (ppmV) along the 200 m isobath (continental shelf-break, stations 14 to 2), on the continental shelf (station 1) and on the slope (stations 11 to 4) during the April-May 2003 Belgica cruise. Straight line represented atmospheric saturation with respect to CO_2.
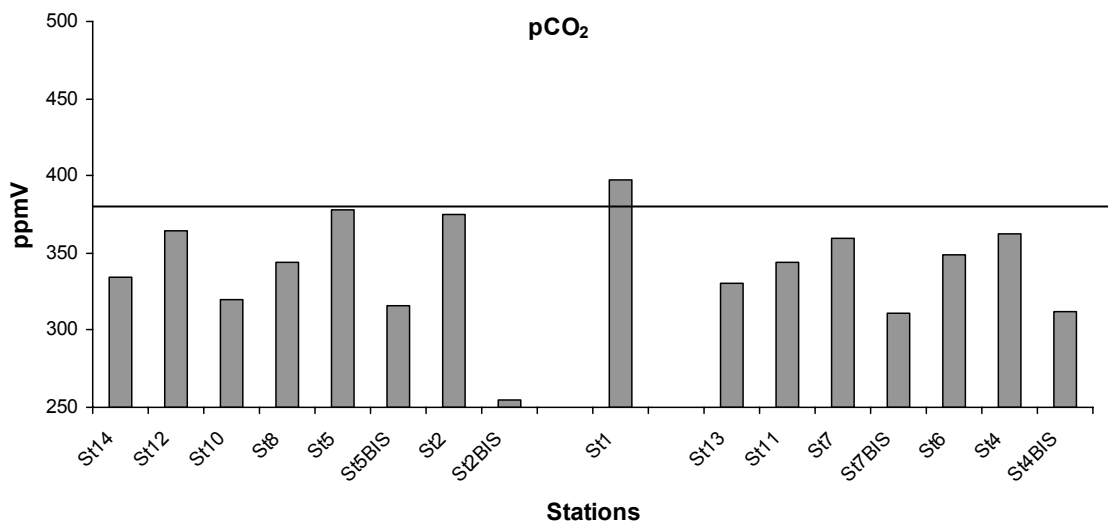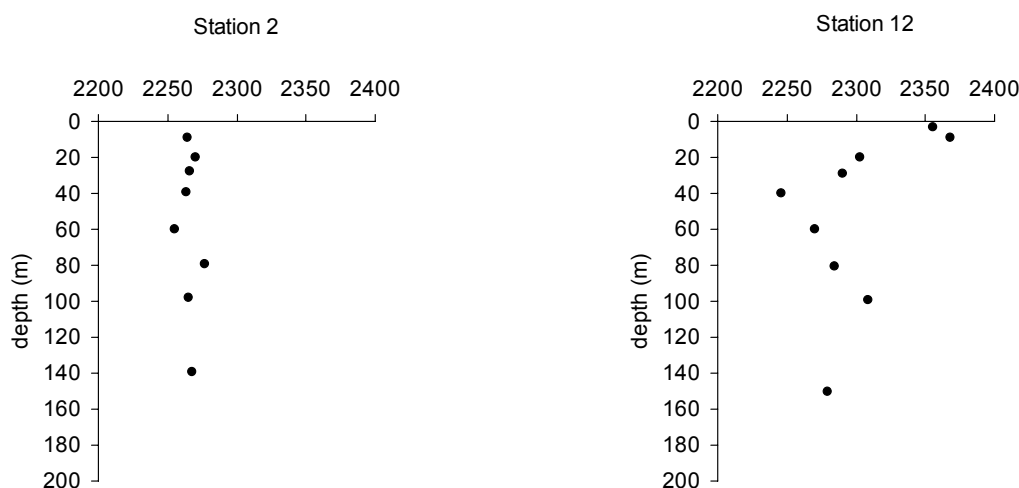
The distribution of **total alkalinity**, normalized to salinity 35, ranged between 2250 and 2350 $\mu mol.kg_{SW}^{-1}$. Values close to 2250 $\mu mol.kg^{-1}$ were observed, probably in relation with biogenic precipitation of calcium carbonate (Figure 68).

Figure 68. Vertical distribution of normalized (to salinity 35) total alkalinity ($\mu mol.kg_{SW}^{-1}$) at station 2 (south) and station 12 (north) showing a consumption by 15-20 $\mu mol.kg_{SW}^{-1}$ in the upper photic zone during the April-May 2003 Belgica cruise.

Surface seawater in the ocean is supersaturated with respect to calcite and aragonite. In this survey, the **saturation state** with respect to calcite (Ω_{cal}) was

around 4 in surface and decreased with depth (Figure 69).   The lowest value observed in this survey was 2 (St 4, 1400 m). Such a low value corresponded to a saturation state with respect to aragonite (Ω_{ar}) of 1.2.
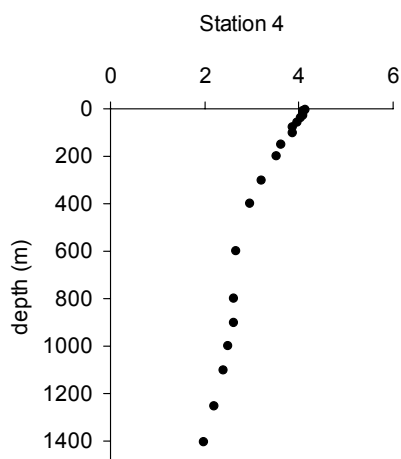
Figure 69. Vertical profile of saturation state with respect to calcite (Ω_{cal}) at station 4 in the water column during the April-May 2003 Belgica cruise.

4.5.5 Particulate matter distribution, composition and PIC:POC ratios

Total carbon concentration in the particulate matter was generally in the range of 150-180 µgl.l^{-1} in the upper water column (Figure 70). Most of it belonged to the **organic** fraction, except for stations 10 and 12 where the **inorganic** fraction was significantly higher than the organic one. At these stations, the molar ratio of PIC:POC exceeded unity and rose to 4-5, suggesting very high concentrations of calcium carbonate in the surface waters.
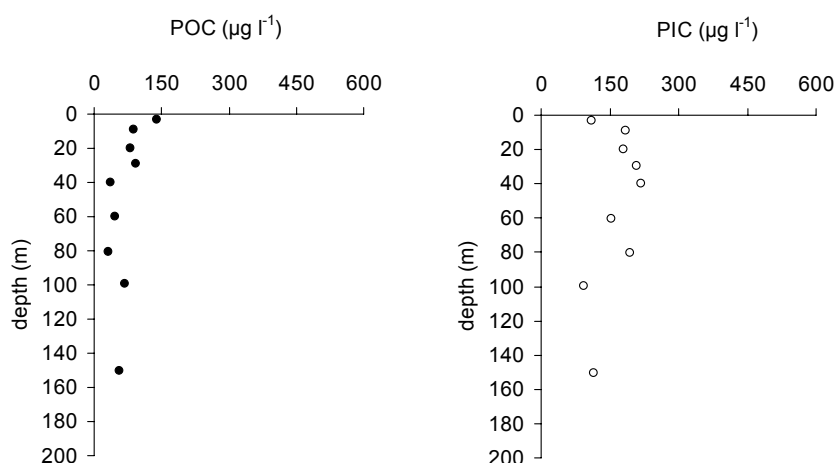
Figure 70. Organic (black dots, left) and inorganic (open dots, right) particulate carbon (in µg.l^{-1}) at station 12 (shelf break) during the April-May 2003 Belgica cruise.

Continuous centrifugation of surface waters during this cruise indicated that at least 50 % of particulate matter (by weight) was carbon, except for station 1 where it

contributed only to 21.9 % (Table 5). The organic fraction in Ctot decreased from south to north from 96.0 % at station 2 to 77.0 % at station 12. In contrast, the inorganic fraction that accounted for less than 10 % of the weight of suspended material in this survey increased from 4.0 % to 23.0 % of Ctot, while total nitrogen was rather constant around 10 %. The stations 4 and 7, located on the slope had been re-sampled after 10 days (4bis and 7bis), as well as station 5 (5bis) on the shelf. Their carbon content was in the range of that observed at stations on the shelf break. The decreasing trend from south to north was also observed as well as a decrease between the two legs. Total particulate nitrogen followed the same trend as POC with a POC: PN ratio of 5.03 ± 0.35 (average $\pm$ standard deviation, $r^2 = 0.90$, n = 11) in this study.

Table 5. Particulate carbon (organic and inorganic) and nitrogen contents in the suspended matter, expressed in % (wt/wt) for the April-May 2003 Belgica cruise.

Station	Ctot % MES	Corg % MES	Cinorg % MES	Ntot % MES	Corg/Ntot
1	21.91	18.70	3.22	3.56	5.25
2	48.83	46.88	1.96	9.68	4.84
5	51.26	45.64	5.62	9.37	4.87
5bis	39.56	37.38	2.18	6.68	5.60
8	51.20	43.76	7.44	9.44	4.64
10	47.28	40.80	6.49	8.27	4.93
12	50.23	38.66	11.57	8.86	4.36
4	54.62	50.38	4.23	9.83	5.13
4bis	48.55	42.19	6.35	8.07	5.23
7	52.87	48.55	4.32	8.99	5.40
7bis	50.82	45.71	5.11	9.06	5.05

The **inorganic** fraction of carbon in suspended matter increased as the organic fraction decrease (Table 5). This trend was observed in the case of the transect on the shelf as well as for the time evolution on the slope. The contribution of the inorganic carbon to the suspended matter did not exceed 10 % of the total weight, but its contribution to Ctot ranged between 4.0 % (station 2) and 23.0 % (station 12) on the shelf and between 7.8 % and 13.1 % on the slope. The PIC:POC ratio varied between 0.04 (station 2) and 0.3 (station 12).

4.5.6 Particle characterisation

Particles collected during the April-May 2003 cruise were analysed. The absolute abundances of particles are shown in Figure 71. The absolute abundances of particles were lower during 2003 campaign compared to the 2002 one. They were more or less the same at all stations except for station 11. Stations 9 and 10 could have been in the beginning state of an *E. huxleyi* bloom.
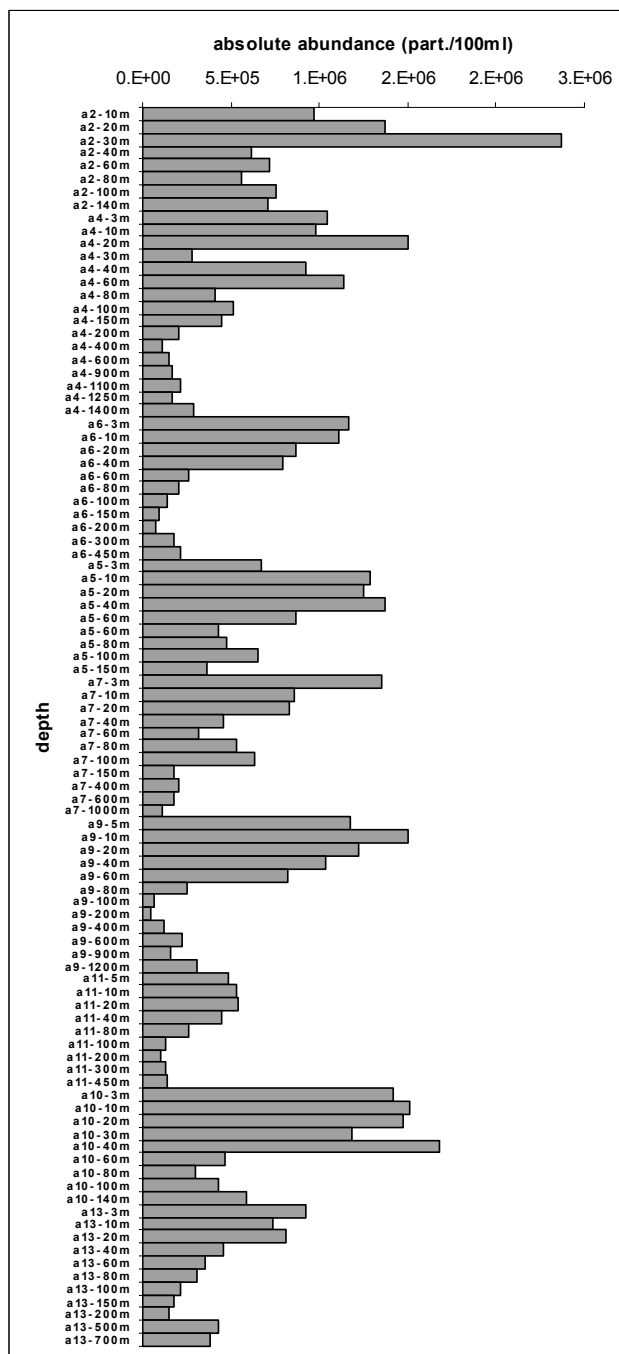
Figure 71. Absolute abundances of particles for samples collected at various stations and depths during the April-May 2003 Belgica cruise.

In all of the analyzed stations, several species of coccolithophorids were found: *E. huxleyi*, *Gephyrocapsa* sp., *Calcidiscus* sp., *Syracosphaera* sp.,

Meringospaera sp. and *Pleurochrysis* sp. (Figure 72). At stations 4, 5 and 6 many malformed E. huxleyi were observed (Figure 73).
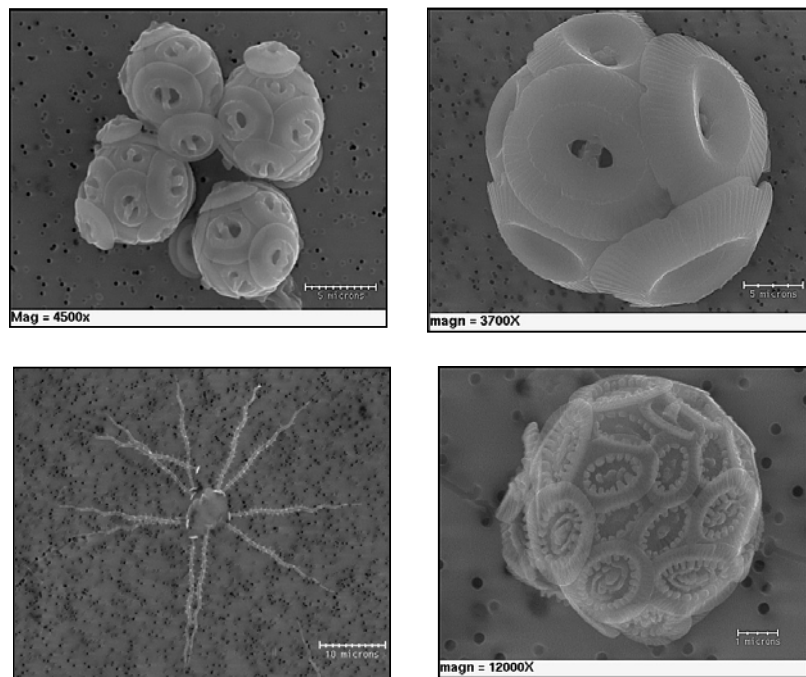
Figure 72. SEM micrographs of coccolithophores observed during the April-May 2003 Belgica cruise.
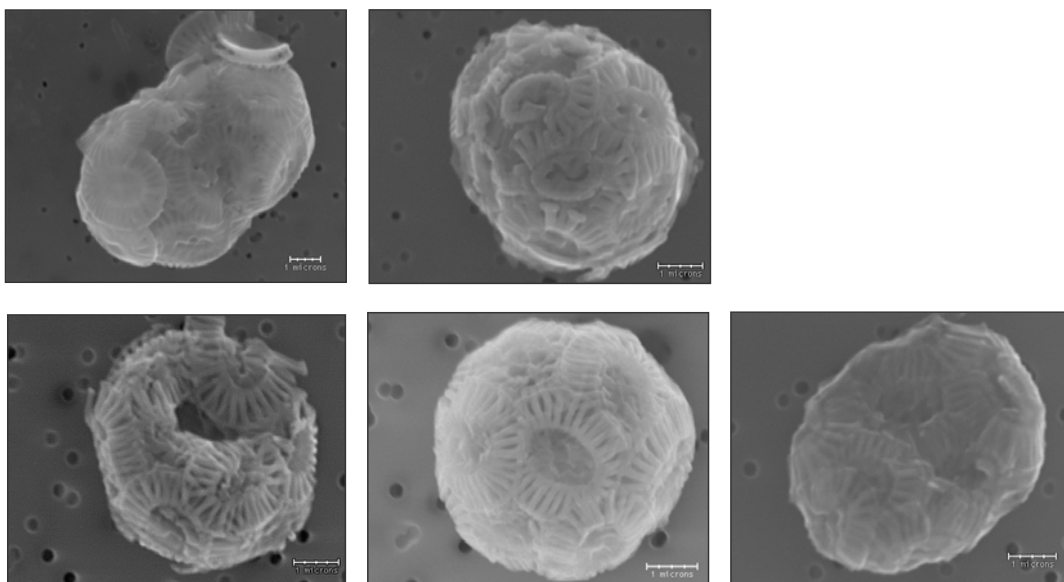
Figure 73. Malformed *E. huxleyi* observed at stations 4, 5 and 6 during the April-May 2003 Belgica cruise.

4.5.7 Kinetics of ^{14}C incorporation and size fractionation

^{14}C incorporation under constant light increased linearly during the first 12 hours of irradiance. The rate of ^{14}C incorporation in organic matter ranged between 0.24 and 0.28 $\mu molC.l^{-1}.h^{-1}$ on the continental shelf, except for station 12 (0.15 $\mu molC.l^{-1}.h^{-1}$). Lower values were obtained at station 12 (0.15 $\mu molC.l^{-1}.h^{-1}$) on the shelf and station 7 (0.19 $\mu molC.l^{-1}.h^{-1}$) on the slope. Station 4 exhibited a higher production (0.26 $\mu molC.l^{-1}.h^{-1}$).

The distinction between incorporation in organic and inorganic matter is based on acidification of filters and showed that calcification occurred preferentially at stations 5, 8, 10 and 12, situated on the continental shelf. Inorganic particulate carbon production (0.37 $\mu molC.l^{-1}.h^{-1}$) was comparable and even exceeded the primary production in surface waters of station 10 (Figure 74).
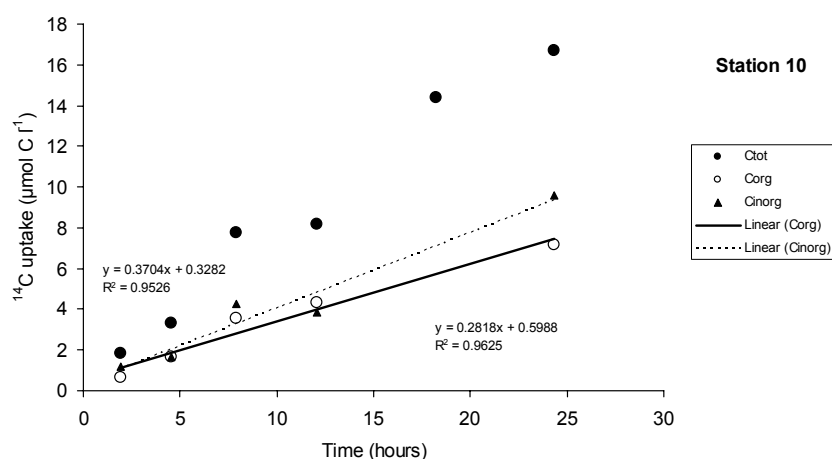
Figure 74. Kinetics of ^{14}C incorporation by the natural assemblages at station 10 (shelf break, in $\mu molC.l^{-1}$) under constant light (150 $\mu mol.m^{-2}.s^{-1}$). Black dots represent the total incorporation of ^{14}C while open dots represent incorporation in the organic compartment. The difference between the two values is defined as the rate of calcification (black triangles).

Incorporation of ^{14}C in the dark was very low, below 0.05 $\mu molC.l^{-1}$ and comparable to the level of poisoned (sodium azide, AZ) samples after 4 hours of incubation. After 12 hours of incubation, heterotrophic incorporation of ^{14}C seemed to occur but was one or two orders of magnitude lower than incorporation under light conditions.

Most of the primary production, in this survey, was due to phytoplanktonic algae smaller than 12 μm at 10 m depth with a dominant fraction of 0.2-2 μm (more than 50%, data not shown). In contrast, calcification was often observed in the [2-12 μm] range but sometimes occurred in smaller classes (probably due to detached coccoliths).
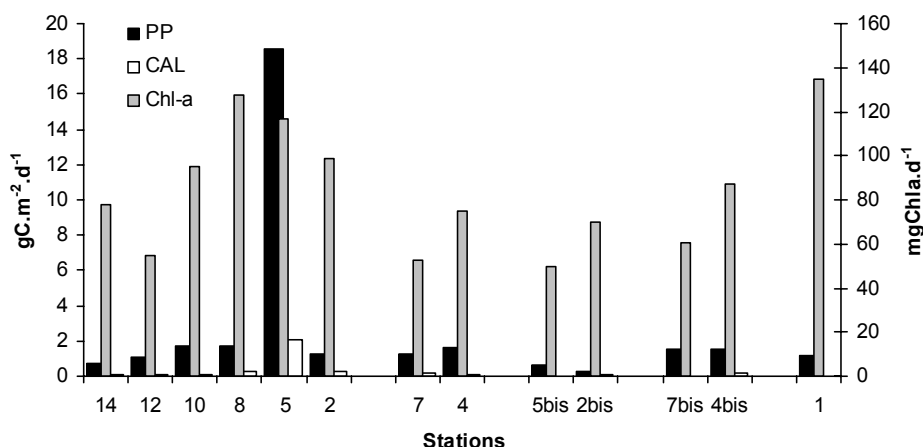
4.5.8 Integrated primary production and calcification

The rates of ^{14}C incorporation in the organic fraction did not exceed 2.0 gC m^{-2} d^{-1} in the survey, except for station 5, where up to 18.5 gC m^{-2} d^{-1} were taken up by the phytoplanktonic community (Figure 75). The continental shelf displayed primary production rates of 1.3 ± 0.4 gC m^{-2} d^{-1}, similar to that measured at station 1. They were slightly higher on the continental slope and at stations 7 (1.3 gC m^{-2} d^{-1}) and 4 (1.6 gC m^{-2} d^{-1}).

Calcification rates did not exceed 21 % of primary production rates, and ranged between 0.05 gC.m^{-2}.d^{-1} and 0.26 gC.m^{-2}.d^{-1}, at stations 10 and 2, respectively. A significant decrease in both primary production and calcification was observed on the continental shelf, at the revisited stations 5bis and 2bis, after 9 and 14 days, respectively. No particular trend was observed on the continental slope at stations 4bis and 7bis.

Since incorporation rates at station 2 were more than 10 times higher compared to the averaged incorporation rates into organic matter during the survey, the values must be considered with caution.

The integrated Chl-a concentration ranged between 50 and 135 mgChl-a.m^{-2} and averaged 85 ± 29 mgChl-a.m^{-2} in May 2003, at the continental margin. High phytoplanktonic biomass, in the range of 100 mgChl-a m^{-2} and above was measured on the southern continental shelf (stations 2, 5 and 8) and at station 1. A decrease was observed at the revisited stations 5bis and 2bis. A 50 % decrease was observed at station 5bis. Such a decrease was not observed on the continental slope between stations 4bis and 7bis.

Figure 75. Primary production and calcification rates (gC.m^{-2}.d^{-1}) determined during the April-May 2003 Belgica cruise. Integrated Chl-a (mg Chl-a.m^{-2}) gives an indication of the amount of organic matter at the different stations.

4.6   Field survey #3 (1 June – 17 June 2004)

In June 2004, a biogeochemical survey of a coccolithophore bloom in the Bay of Biscay was conducted onboard the *RV Belgica*. Real-time remote sensing allowed us to pinpoint coccolithophore blooms located on the continental shelf and along the continental margin as shown by the high reflectance patches (Figure 76).
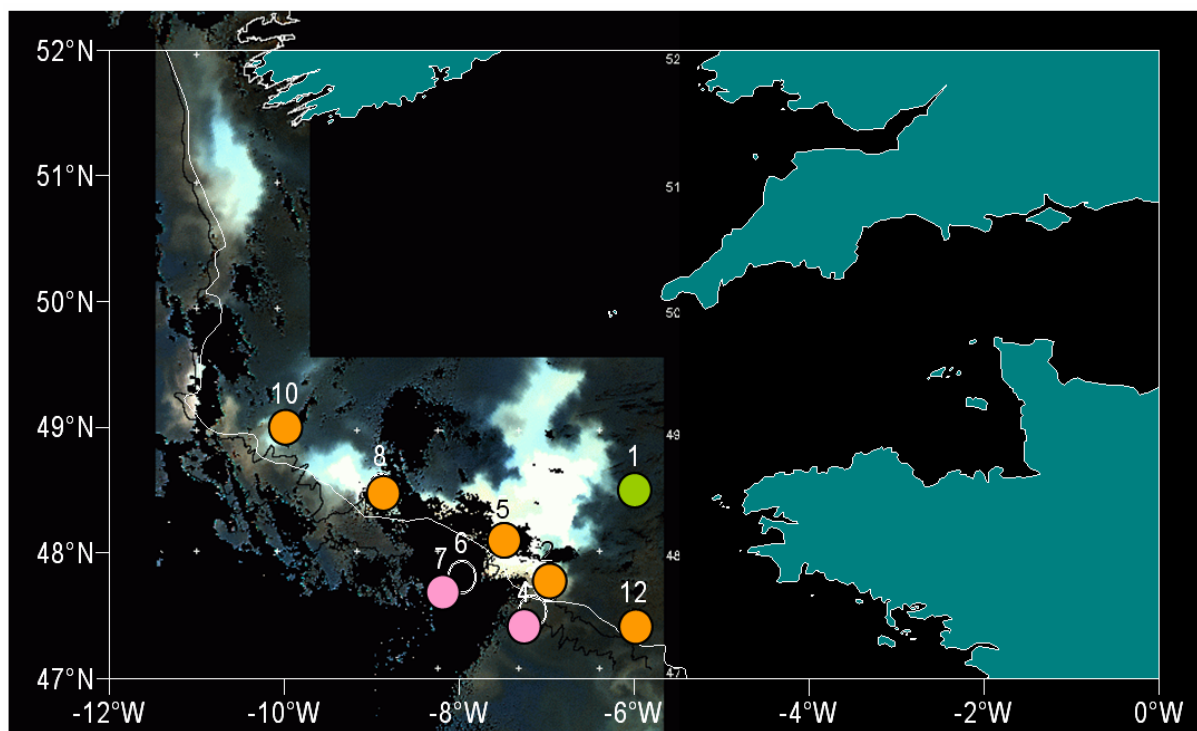
Figure 76. Reflectance satellite image on the 2nd of June 2004 where the sampling locations during the Belgica cruise are also indicated. The white line indicates the 200m isobath that separates oceanic waters from the continental shelf.

4.6.1 Temperature, salinity and nutrient profiles in the photic zone

The vertical profiles of **temperature** displayed rather constant values of 11-12°C at the base of the photic zone (Figure 77). A warming was observed up to 14-15°C at the top of the water column, accompanied by the formation of a thermocline below 20 m depth. The stations revisited during the second leg exhibited a significant warming of the surface layer above 16°C (stations Bis).

Salinity of surface waters was relatively constant and homogeneous around 35.6 until 150 m depth on the slope as well as on the continental shelf (Figure 78). The vertical distribution of salinities at station 1 was characteristic of its geographical position, close to the Ushant front.
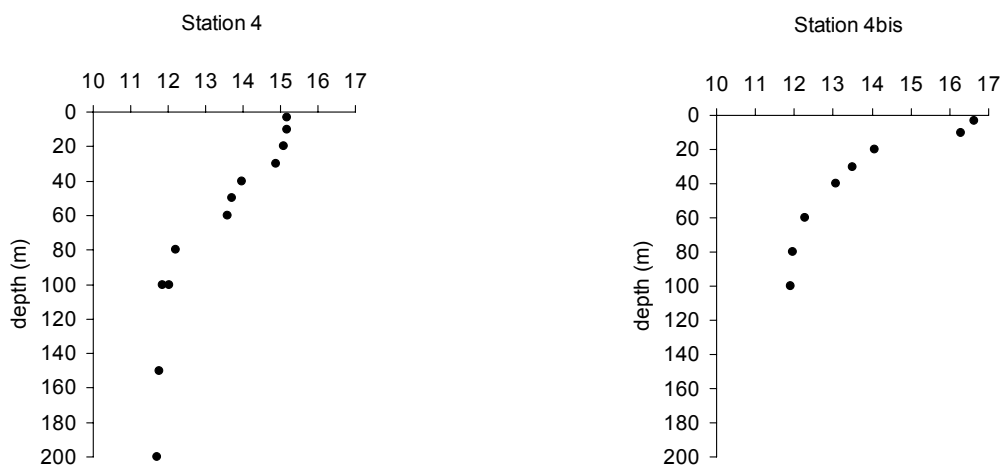
Station 4

Station 4bis

Figure 77. Temperature profiles at station 4, showing a warming of surface waters after 12 days during the June 2004 Belgica cruise.

St1ation 2
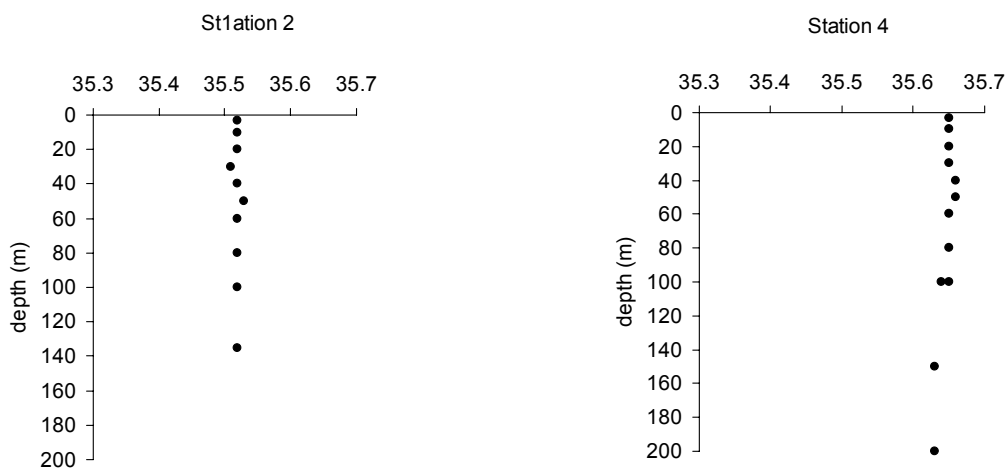
Station 4

Figure 78. Vertical distribution of salinity on the shelf break (station 2, left) and on the slope (station 4, right) during the June 2004 Belgica cruise.

The vertical distribution of **dissolved phosphate** in the water column indicated that this nutrient was being consumed at the time of the sampling (Figure 79). From concentrations of 0.4 $\mu mol.l^{-1}$ at the base of the photic zone, a drastic decrease towards the surface was generally observed. Such a decrease was noticeable both on the slope and on the continental shelf.

The lowest concentrations of **dissolved silica** in surface waters observed during this survey were generally in the range of 0-1 $\mu mol.l^{-1}$. While most stations displayed values close to 1, the concentration fell to zero at station 10 located in the northern part of the continental shelf. The vertical distribution of the concentrations of dissolved silica displayed rather constant values at the base of the photic zone (around 3 $\mu mol.l^{-1}$). A marked nutricline was generally observed on the continental

shelf at a depth between 20 m and 40 m (Figure 80). This nutricline was less pronounced on the rise and slope (stations 3, 4, 6 and 7) as the topographic discontinuity, in conjunction with sporadic internal waves, enhanced vertical mixing with nutrient-rich deeper waters. A deep (100 m) nutricline was observed at the station 4 but seemed to be dampened at the other deepest stations.
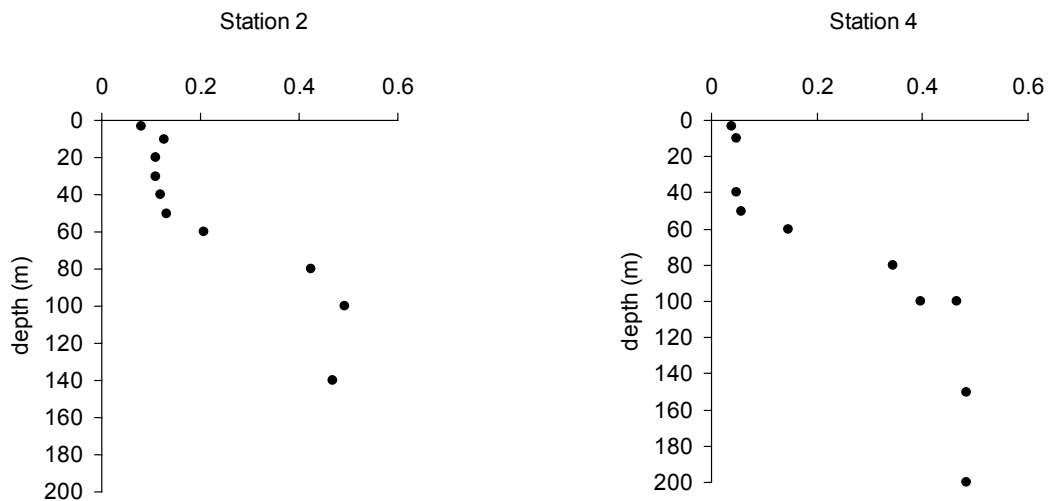
Figure 79. Vertical distribution of dissolved phosphate concentrations (µmol.l^{-1}) in the photic zone on the shelf break (station 2, left) and on the slope (station 4, right) during the June 2004 Belgica cruise.

Figure 80. Vertical distribution of dissolved silica concentrations (µmol.l^{-1}) in the photic zone on the shelf break (station 10, left) and on the slope (station 4, right) during the June 2004 Belgica cruise.

4.6.2 Photosynthetic pigments and dissolved oxygen
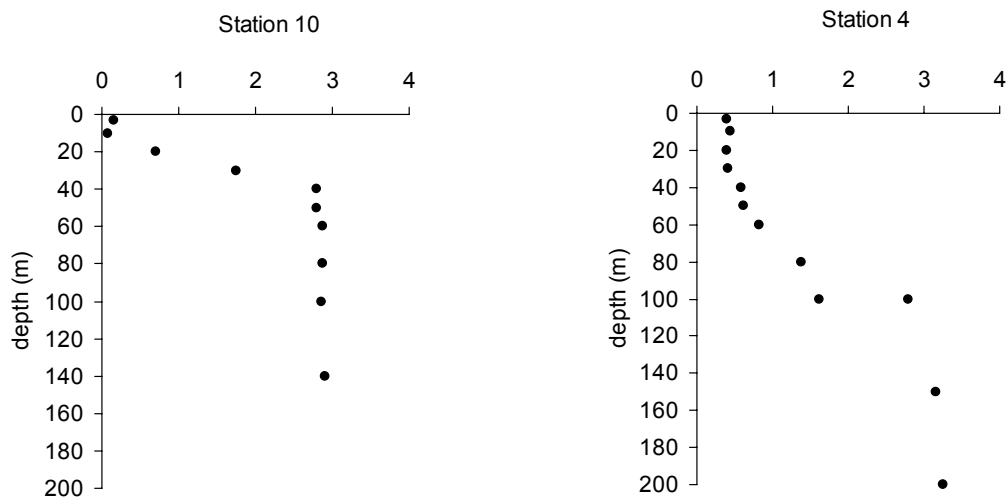
The concentrations of **Chl-a** in surface waters rarely exceeded 1 µg.l^{-1} during the survey. The thickness of the layer in which Chl-a was present never exceeded 60 m. Two contrasted features appeared when observing the various profiles: most of the profiles displayed a peak concentration at a depth of 20 m (i.e. stations 4, 5, 7, 8, 10 and 12), while the station 2 had its maximum at the surface. This general tendency was also observed during the second leg (Figure 81).
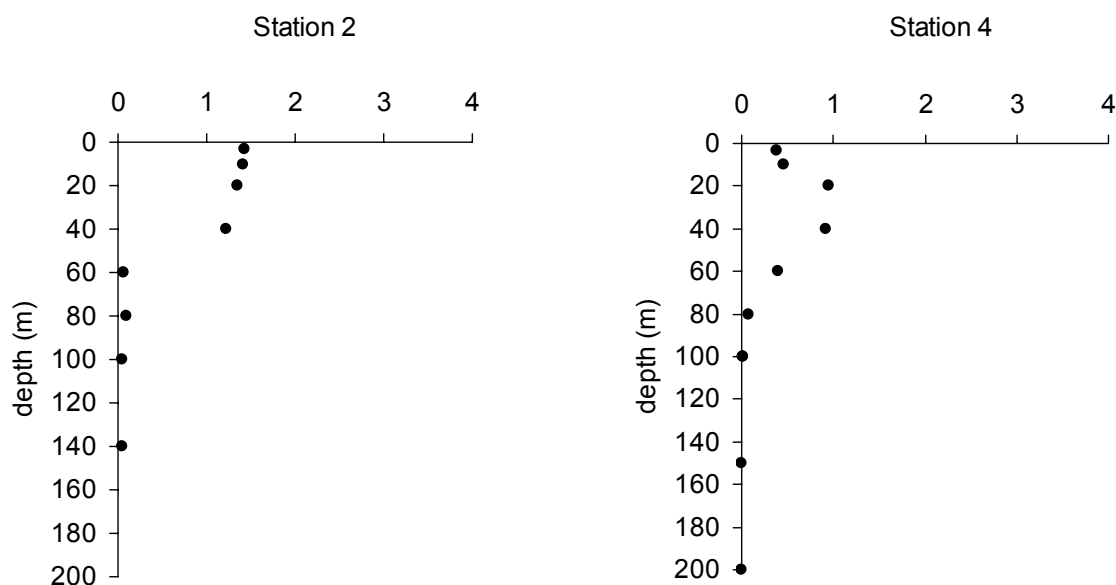
Figure 81. Vertical distribution of Chl-a concentrations (µg Chl-a.l^{-1}) in the photic zone on the shelf break (station 2, left) and on the slope (station 4, right) during the June 2004 Belgica cruise.

Phaeopigments were abundant in the area investigated during this cruise. Values in the range of 2 to 4 µg.l^{-1} were common among the stations and phaeopigments could be found down to 100 m depth (taken as the base of the photic zone in this region). Figure 82 exhibited maximum values at a depth of 20 m to 40 m (stations 4, 5, 7, 10) and a second peak was sometimes observed at around 80 m (stations 2, 12, 4bis and 7bis).

The surface waters were oversaturated with respect to **oxygen** concentration in the atmosphere by 10 % while it appeared to be undersaturated at the bottom of the photic zone (Figure 83).
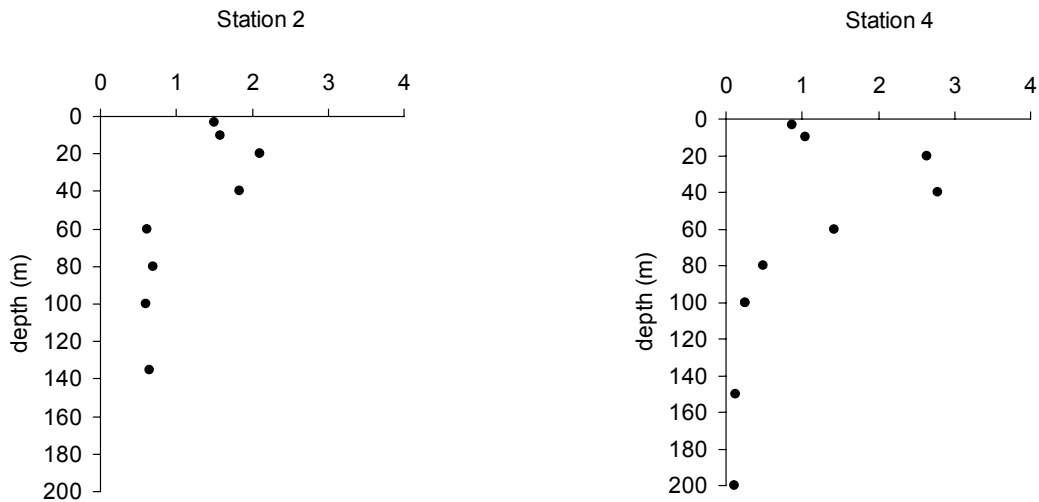
Figure 82. Vertical distribution of phaeopigments (μg.l^{-1}) in the photic zone on the shelf break (station 2, left) and on the slope (station 4, right) during the June 2004 Belgica cruise.
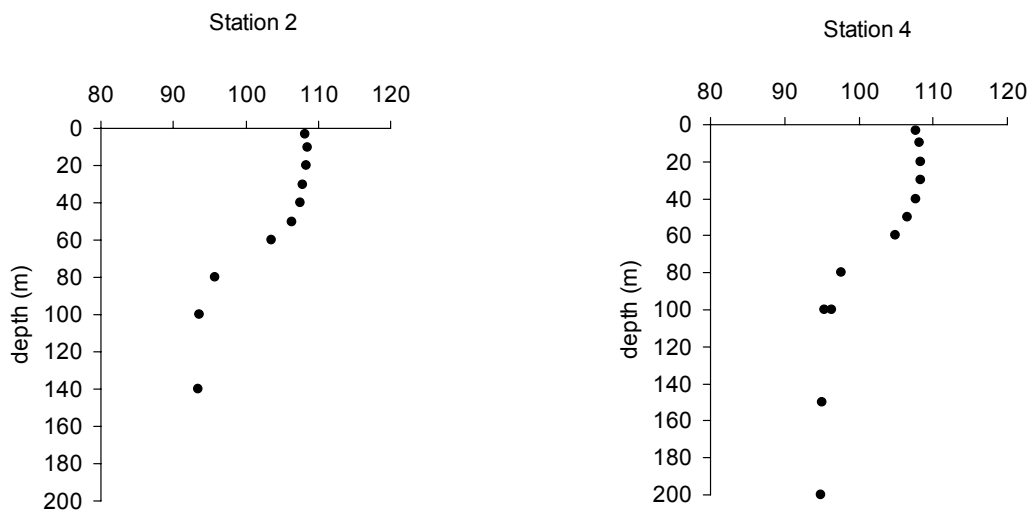
Figure 83. Oxygen saturation (%) in the photic zone on the shelf break (station 2, left) and on the slope (station 4, right) during the June 2004 Belgica cruise.

4.6.3 Inorganic carbon biogeochemistry

The **pH$_{(SWS)}$** of seawater varied between 8.05 and 8.15 in the photic zone and decreased to values close to 7.90 (Figure 84). Higher values were found in surface waters.

Surface waters were under-saturated with respect to atmospheric **pCO$_2$** by 50 to 75 ppmV (Figure 85) while the seawater pCO$_2$ at depth was greater than 400 ppmV (data not shown). The decrease of pCO$_2$ from depth towards the surface began at around 60-80 m. Comparison of the data of stations 5 and 5bis, a decrease in

surface values of pCO_2 between the 2 legs was observed. This was also noticeable, but to lesser extent, for the stations 4bis and 7bis.

Station 4

Figure 84. Vertical distribution of $pH_{(SWS)}$ at station 4 during the June 2004 Belgica cruise.
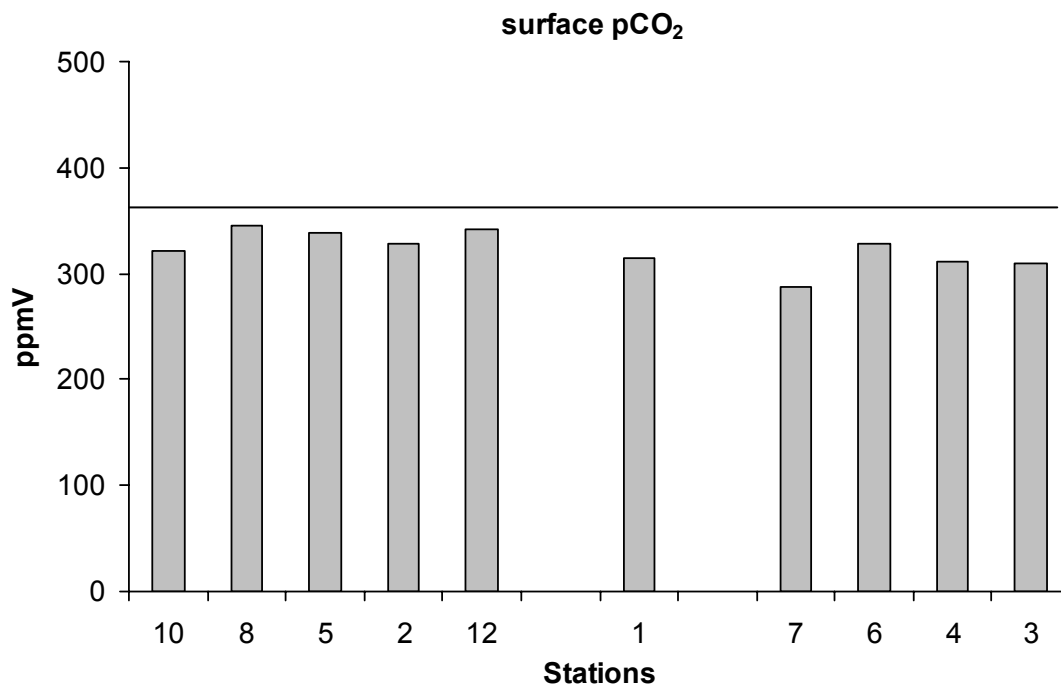
surface pCO$_2$

Figure 85. Surface distribution of pCO_2 (ppmV) along the 200 m isobath (continental shelf-break, stations 10 to 12), on the continental shelf (station 1) and on the slope (stations 7 to 3) during the June 2004 Belgica cruise. Straight line represents atmospheric saturation with respect to CO_2.

Total alkalinity, normalized to salinity 35, was generally about 2300 µmol.kg^{-1} at the bottom of the photic zone. Across the slope transect (Stations 5, 6, 7), a first minimum of total alkalinity was observed at 80 m depth, a second minimum is observed in surface (Figure 86). The lowest total alkalinity encountered here is 2284 µmol.kg^{-1} (Station 7) at 10 meters depth.
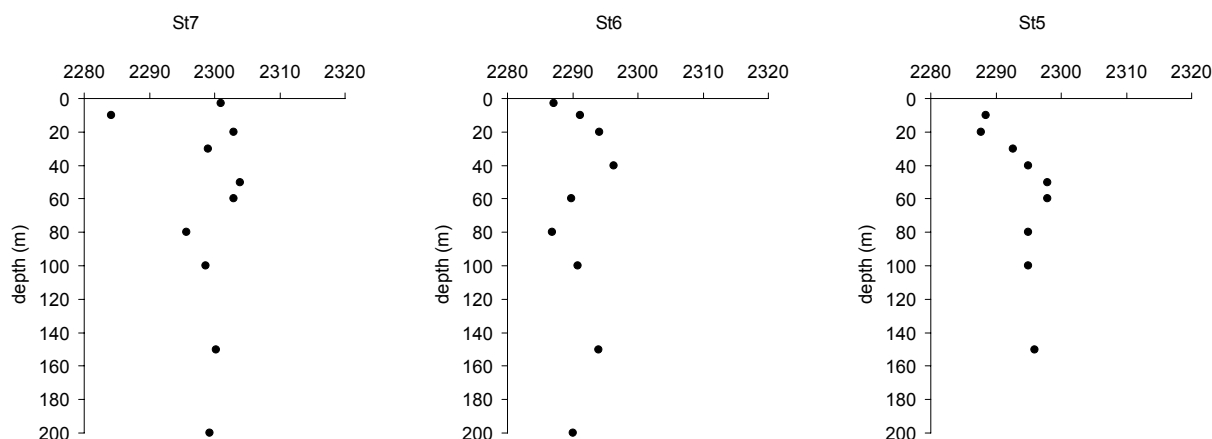
Figure 86. Vertical distribution of normalized (to salinity 35) total alkalinity (µmol.kg$_{SW}$$^{-1}$) along the transect across the slope during the June 2004 Belgica cruise.

4.6.4 Particulate matter distribution, composition and PIC:POC ratios

The **particulate matter** was most abundant at stations 4, 5, 7 and 8 with maximum concentrations ranging from 0.8 to 1.2 mg.l^{-1}. Stations 2, 5 and 12 exhibited lower values, around 0.5 mg.l^{-1}. The vertical profiles showed higher values in surface, which decreased with depth. A second peak, deeper than the pervious one, was also observable (Figure 87).

Figure 88 shows as an example of the vertical distribution of POC and PIC at station 10. The concentration of **POC** rarely exceeded 150 µgC.l^{-1}, except for the northern part (stations 8 and 10). POC in the water column decreased from surface to depth and was still present at 100 m depth and deeper. At certain stations, a second peak was observed at depth (i.e. stations 4, 10 and 12). In contrast, PIC was in general low or absent below 80 m depth (Figure 88), except in the northern part of the survey. Surface waters displayed concentrations varying from 25 (stations 1, 4, 8 and 12) up to 98 µg.l^{-1} at the station 5 (data not shown). The vertical distribution of PIC at station 4 was in contrast compared to other stations: concentrations were very low at the surface whereas a peak (above 25 µg.l^{-1}) was observed at 60 m depth.
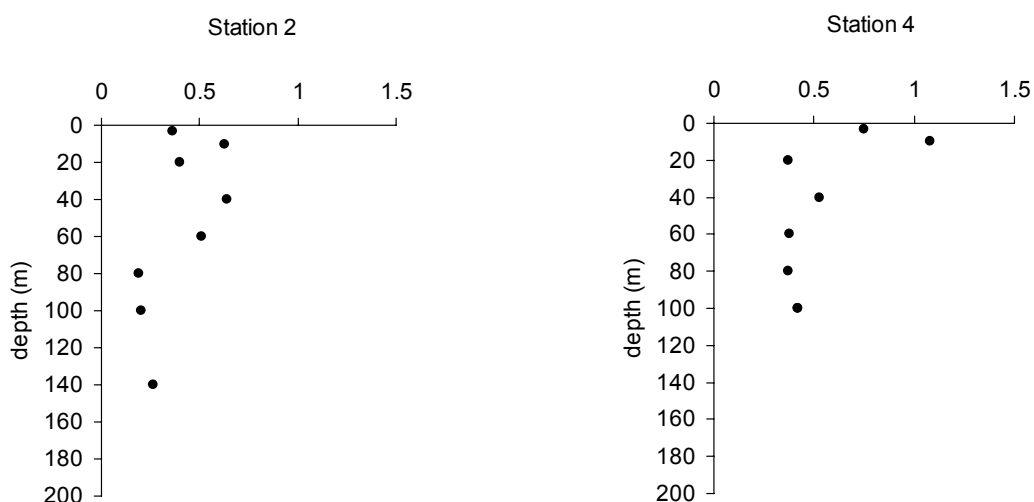
Figure 87. Vertical distribution of suspended matter (mg.l^{-1}) in the photic zone on the shelf break (station 2, left) and on the slope (station 4, right) during the June 2004 Belgica cruise.
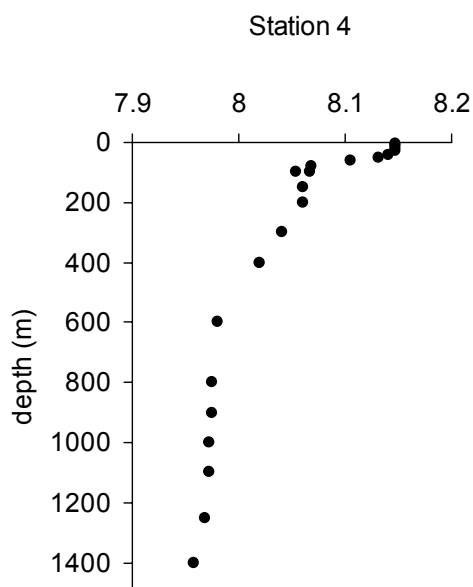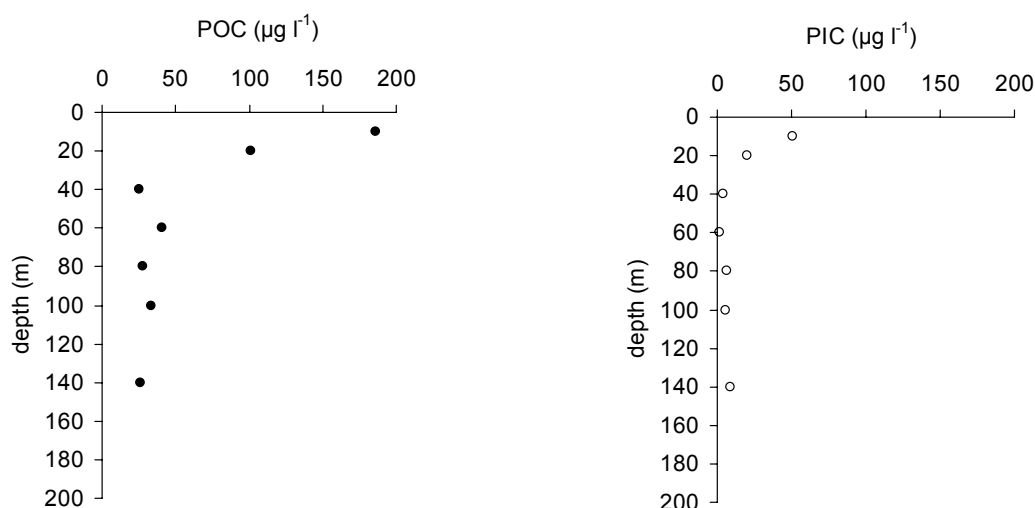

Figure 88. Vertical distribution of POC (black dots) and PIC (open dots) (both in µg.l^{-1}) in the northern part of the shelf break (station 10) during the June 2004 Belgica cruise.

The distribution of **carbon** in the suspended matter of surface waters was variable in the zone of study (Table 6). The contribution of carbon at station 1 was very low (5.6 % of weight), compared to other stations that ranged between 22.7 % (station 5) and 38 % (station 8) for the continental shelf, and between 32.3 % (station 4) and 54.7 % (station 4bis) on the slope. The contribution of the **inorganic fraction** to its total amount did not exceed 40 % (station 5) but was generally about 20 % on the shelf and could be lower (4.4 % at station 4) on the slope. These values globally yield a fraction of inorganic carbon in suspended matter ranging from 2.0 % (station 1) to 9.3 % (station 5) on the shelf, while they remained lower (1.4 % for station 4) on the

slope. The PIC:POC ratio was below unity for the stations investigated, the higher value (70 %) being found at station 5.

The **total nitrogen** to organic carbon ratio was found to be 5.63 $\pm$ 0.62 in the suspended matter of surface waters and the two parameters were strongly correlated ($r^2 = 0.97$, n = 10).

Table 6. Particulate carbon (organic and inorganic) and nitrogen contents in the suspended matter, expressed in % (wt/wt) for the June 2004 Belgica cruise.

Station	Ctot	Corg	Cinorg	Ntot	Corg/Ntot	Cinorg/Corg
12	29.46	25.85	3.60	5.17	5.00	0.14
1	5.77	3.78	1.99	0.56	6.81	0.53
2	30.76	23.65	7.11	4.29	5.52	0.30
5	22.73	13.40	9.33	2.55	5.26	0.70
8	38.02	31.66	6.35	6.67	4.75	0.20
10	27.06	21.35	5.70	3.36	6.36	0.27
4	32.33	30.90	1.43	5.27	5.86	0.05
4b	54.73	51.75	2.98	9.72	5.32	0.06
7	33.20	26.94	6.26	4.90	5.50	0.23
7b	32.08	26.15	5.93	4.44	5.89	0.23

4.6.5 Coccolith abundance and preservation

SEM analysis of samples showed that the investigated area was dominated by the Prymnesiophyte *E. huxleyi*, which could reach densities close to 10^7 cells.l^{-1} (e.g. station 5, at 10 m, Figure 89). The abundance of *E. huxleyi*, compared to other coccolithophores, was close to 65% at stations 10 and 8 and increased to more than 90% at stations 5, 2 and 7.

Various degrees of $CaCO_3$ preservation were observed by SEM for samples collected during the cruise (Figures 90 and 91), but overall they appeared to be well preserved (good-4 stars to excellent-5 stars). A contrario, bad preservation of coccoliths was encountered within the high reflectance patch, where 4 or 5 stars preservation index was rarely found in the top 40 m of the water column. Such a low preservation may represent dissolution of $CaCO_3$ above the lysocline, as shown by Wollast & Chou (1998) in the same area.
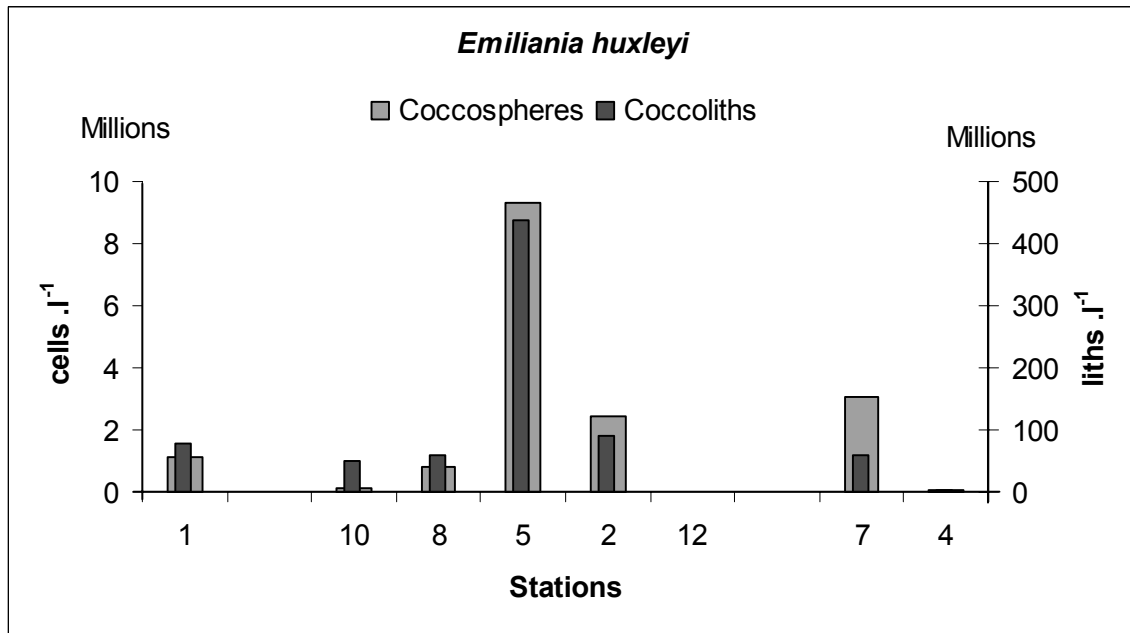
Figure 89. *E. huxleyi* cells (left Y-axis) and shed liths (right Y-axis) concentrations at 10 m depth for the continental plateau (station 1), the shelf-break (Stations 10 to 12) and the slope (stations 7 and 4). Data provided by C. Koch and J.R. Young (The Natural History Museum, London. U.K.).
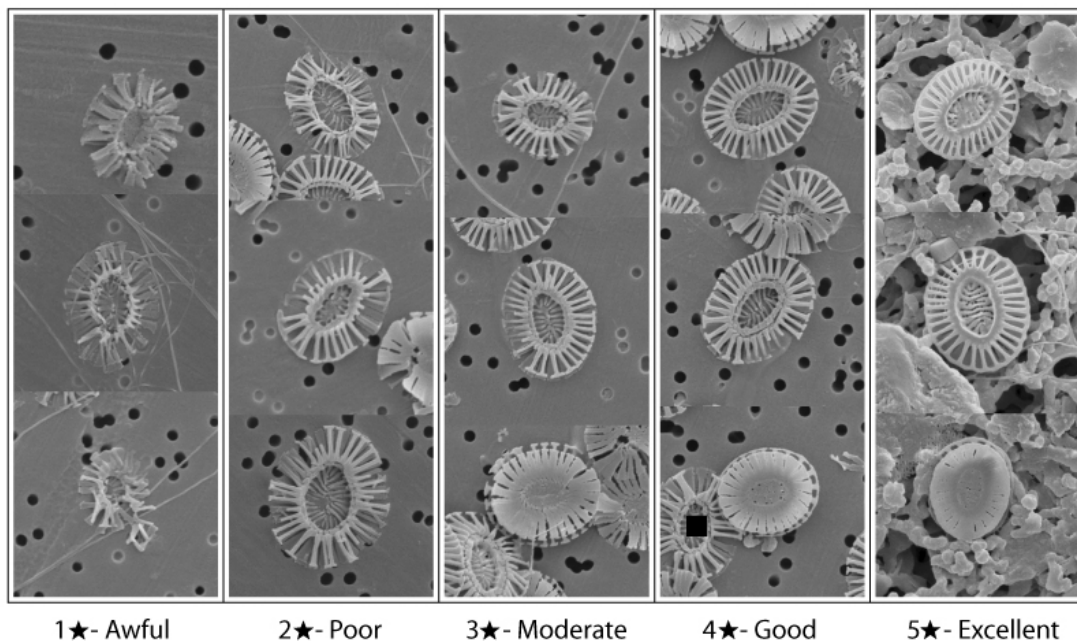
Figure 90. Index of coccolith preservation in samples based on morphological observations by SEM. Five stars correspond to intact coccoliths. Decreasing star numbers indicates a decrease in the preservation state of coccoliths. SEM micrographs provided by C. Koch and J.R. Young (The Natural History Museum, London, U.K.).
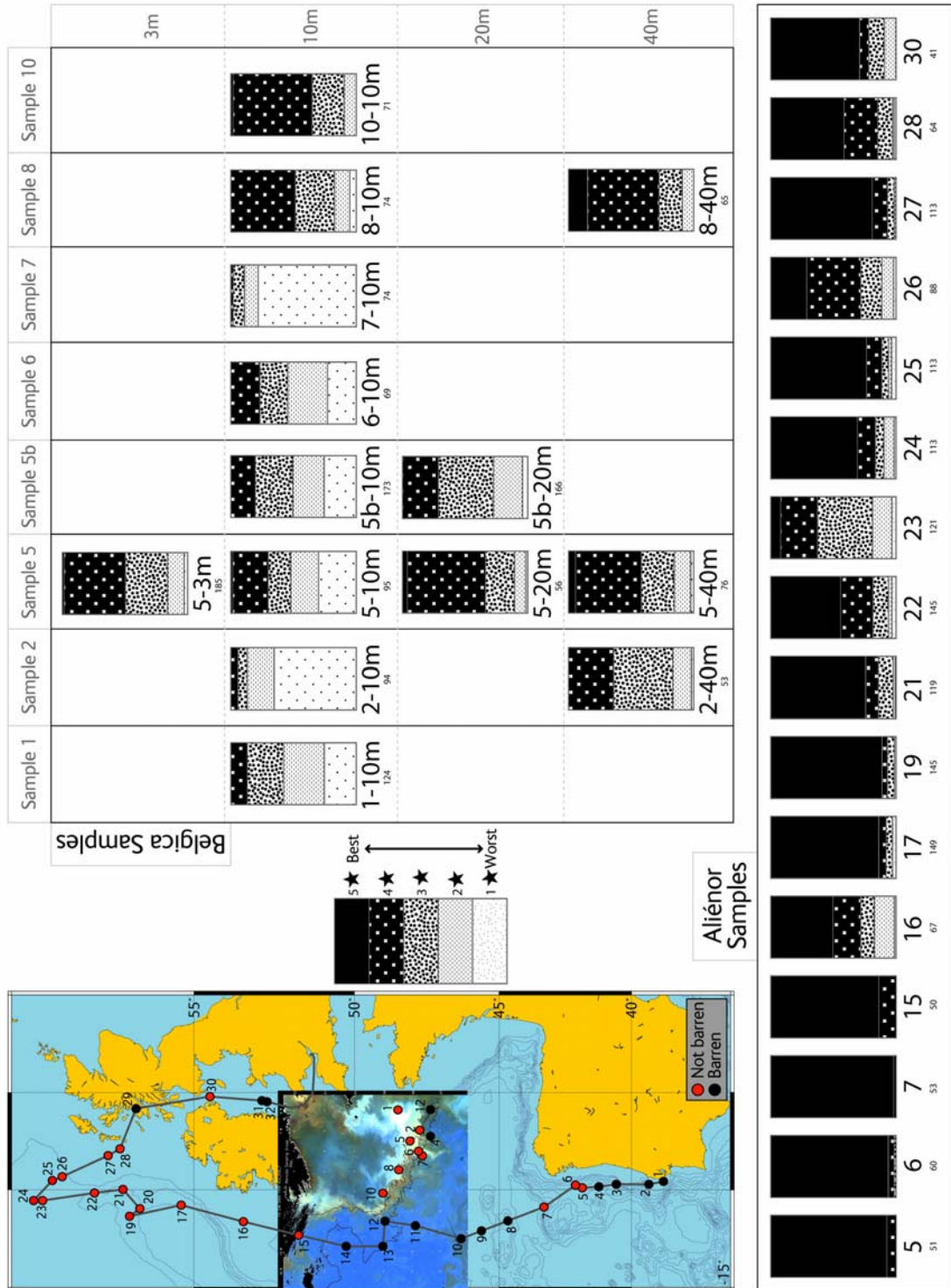
Figure 91. Diagram summarizing the degree of coccolith preservation in seawater (see figure 90 for explanation of the preservation index). 'Aliénor Samples' refer to samples collected in surface waters during the Aliénor cruise (7th June to 17th June 2004). 'Belgica Samples' refer to samples collected at various depth (from 3 m to 40 m, sample number corresponds to station number) during the Belgica cruise 2004/13 (1st June to 17th June 2004). Small numbers below each sample indicate numbers of coccoliths graded. Data provided by C. Koch and J.R. Young (The Natural History Museum, London, U.K.).

4.6.6 *Transparent exopolymer particles (TEP)*

TEP are formed from cellular releases during and after cellular growth. The aggregation of particles during the decay phase of a coccolithophore bloom is a mechanism that contributes to the export of particulate matter to depth and could lead to the formation of marine snow under certain conditions (Passow 2002b). The composition of the aggregates may be different if they come from cellular growth (labile) or bacterial growth (refractory) because bacterial polysaccharides are designed for sticking bacteria to their substrates (Azam et al., 1999; Passow, 2002a).

The concentration of TEP in seawater varied from 25 µg XGeq.l^{-1} to more than 100 µg XGeq.l^{-1} during the survey. The vertical profiles generally showed lower concentrations at the bottom of the photic zone. The concentrations were rather constant (around 35 µg XGeq.l^{-1}) with depth down to 1200 m (station 7). Only the upper photic zone (0-60 m) occasionally displayed higher concentrations of TEP at stations 2, 8 and 10 (shelf break). Station 8 showed the maximum TEP concentration at around 10 m depth. A noticeable increase was observed between the two legs at station 7 (Figure 92) that was not apparent for stations 4 and 5, probably due to a moving filament of the bloom.
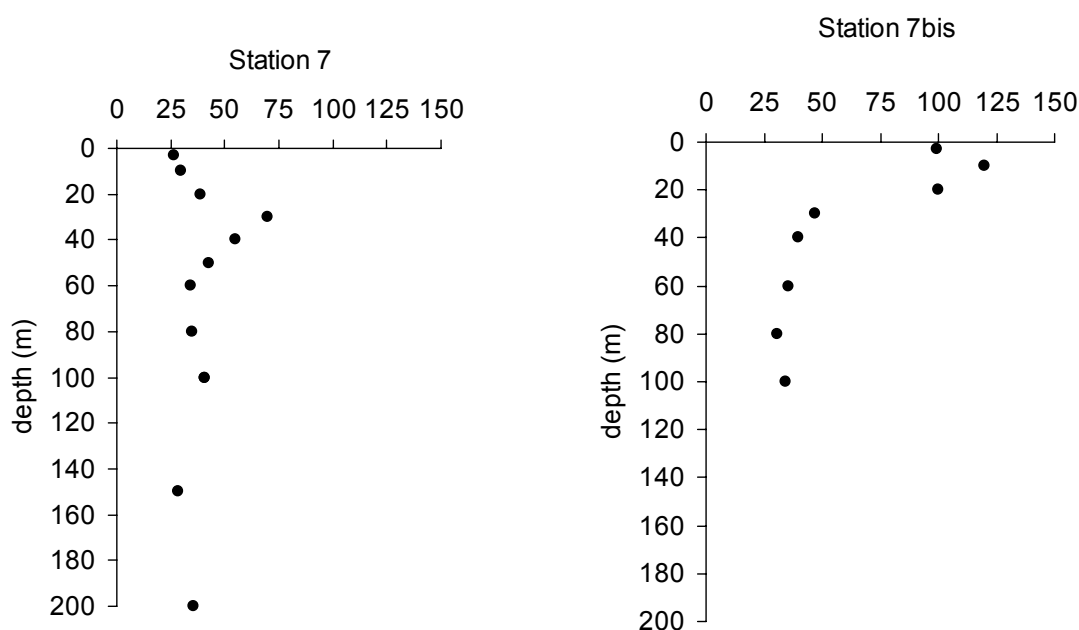
Figure 92. Vertical distribution of transparent exopolymer particles (µg XGeq.l^{-1}) in the photic zone at station 7 and station 7bis revisited after 10 days during the June 2004 Belgica cruise. An increase in the TEP concentration at the surface was observed during the two legs.

4.6.7 Bacterial density, distribution and production

Bacterial density ranged between 3 10^5 (station 1) and 3 10^6 cell.ml^{-1} (station 5) in the photic zone (Figure 93). Higher concentrations were found in surface waters and decreased with depth reaching very low values at depth (7 10^4 cell.ml^{-1} at 1200 m, station 7).
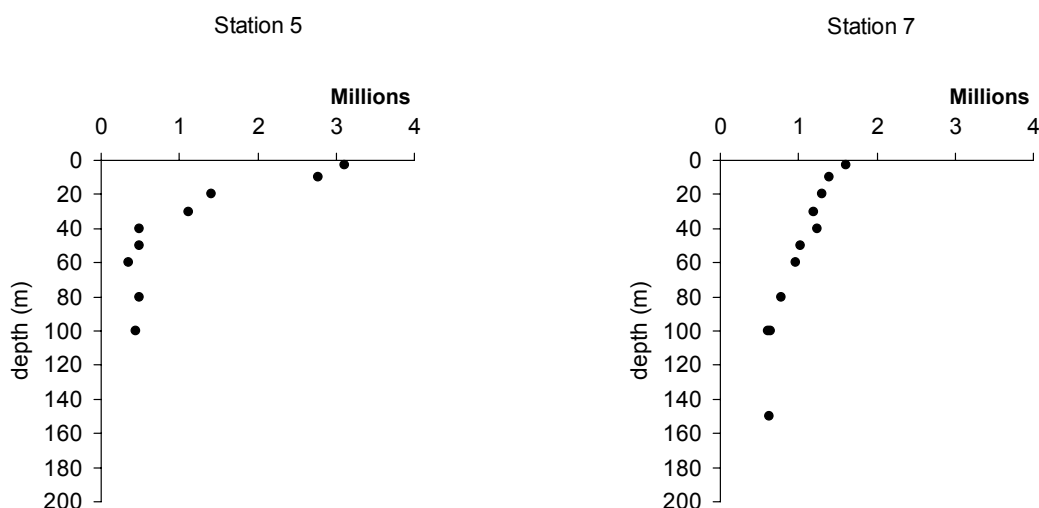
Figure 93. Vertical profiles of bacterial density (10^6 cell.ml^{-1}) at station 5 (shelf break) and station 7 (slope) during the June 2004 Belgica cruise.

Bacterial density in surface waters of the continental shelf increased from station 12 to station 5. Densities close to 1 10^6.ml^{-1} were found in the northern part of the survey (stations 8 and 10).

Dispersion on filters of bacteria in the water column varied visually (Figure 94). Free-living bacteria were generally encountered in the lower photic zone while they were stuck to particles at the surface and sometimes at the bottom. Unfortunately it was not possible to distinguish such dispersion with statistical analysis of data.

Bacterial production in surface waters displayed contrasted values between the continental shelf and the slope (Figure 95). The continental shelf was characterised by the higher range of daily production (> 15 µgC.l^{-1}.d^{-1}) with values as high as 26 µgC.l^{-1}.d^{-1} (stations 12 and 5). On the slope, daily bacterial production was around 10 µgC.L^{-1}.d^{-1} (stations 4 and 7). The time series of bacterial production at these stations was in the same range, contrasting with station 5 that showed a decrease (from 26 to 10 µgC.l^{-1}.d^{-1}) after 10 days. In the meantime, bacterial density decreased from 3.1 10^6 to 1.3 10^6 cell.ml^{-1}.

(a)

(b)

(c)
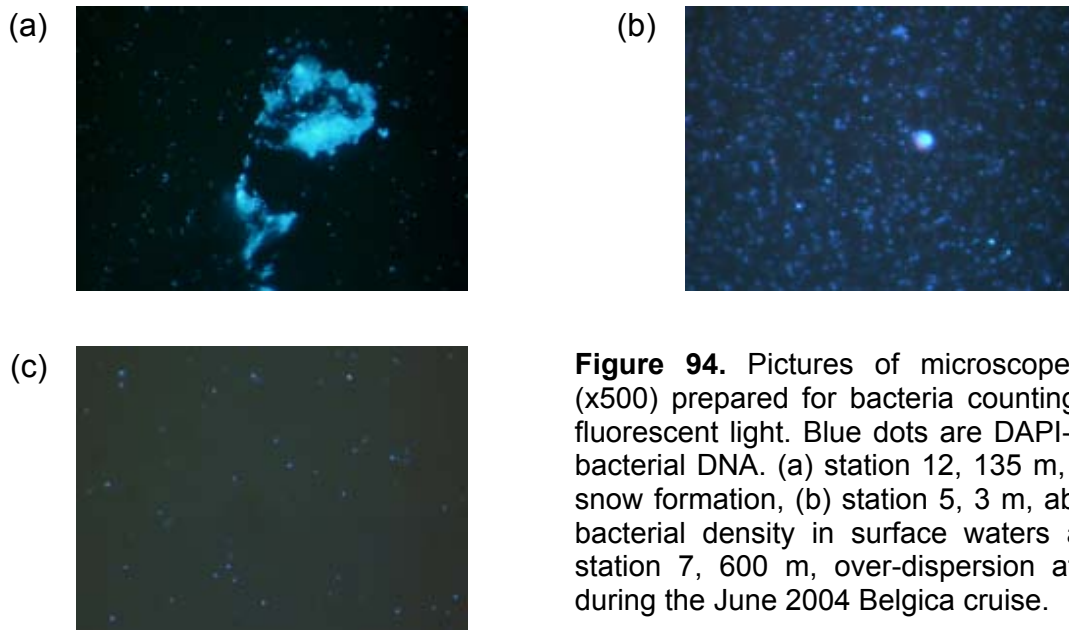
Figure 94. Pictures of microscope slides (x500) prepared for bacteria counting under fluorescent light. Blue dots are DAPI-stained bacterial DNA. (a) station 12, 135 m, marine snow formation, (b) station 5, 3 m, abundant bacterial density in surface waters and (c) station 7, 600 m, over-dispersion at depth during the June 2004 Belgica cruise.
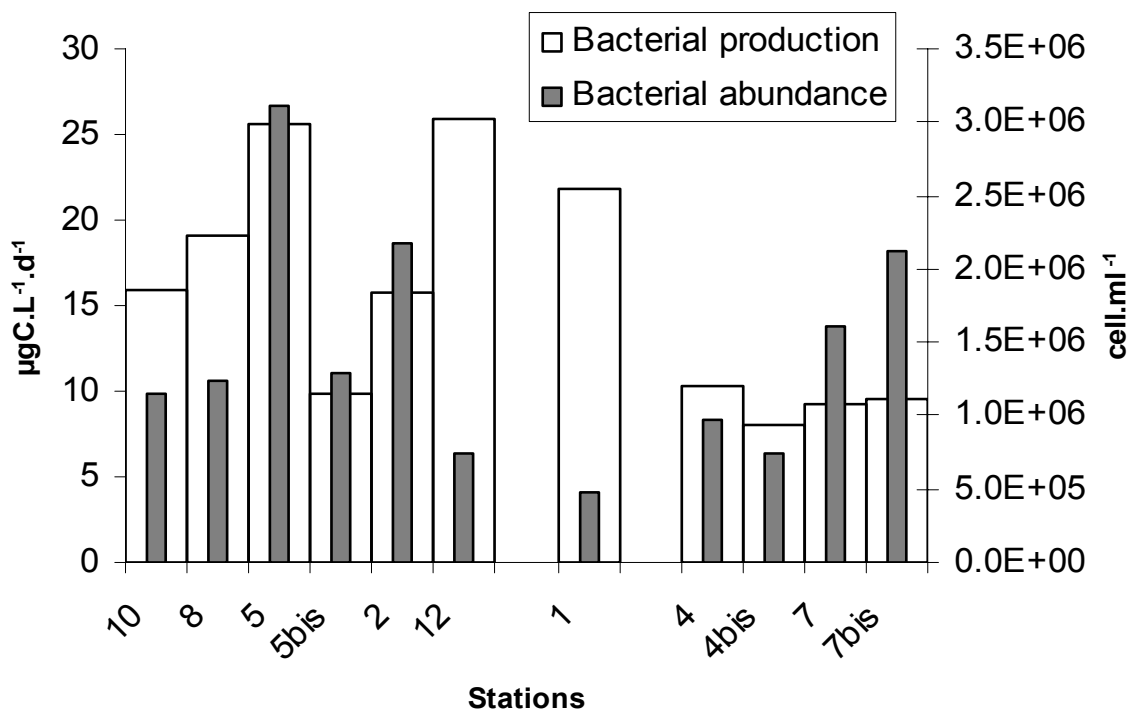
Figure 95. Bacterial production (converted into µg C.l^{-1}.d^{-1}) and density (cell.ml^{-1}) in surface waters (3 m) during the June 2004 Belgica cruise.
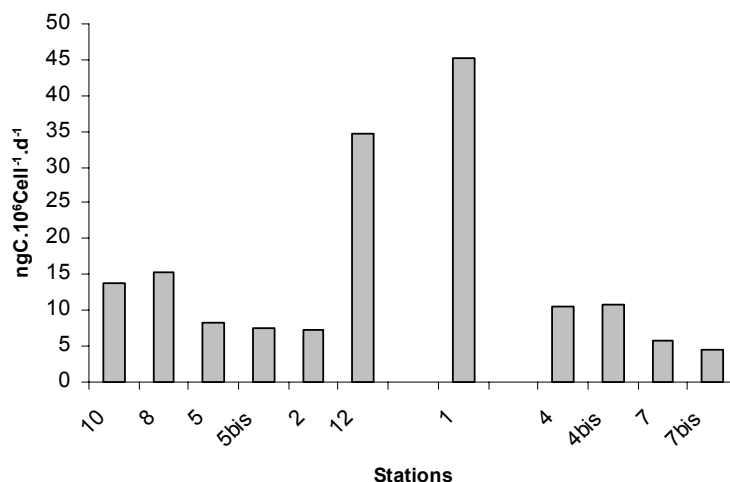
Figure 96. Specific bacterial production (in ng C.cell^{-1}.d^{-1}) in surface waters (3 m) during the June 2004 Belgica cruise.

The specific production suggests that the stations 12 and 1 were in a very active state, respectively taking up 34.7 and 45.2 ngC.(10^6 cell)$^{-1}$.d^{-1} (Figure 96). Stations 8 and 10 displayed values of around 15 ngC.(10^6 cell)$^{-1}$.d^{-1} while stations 4 and 7 on the slope, and stations 5 and 2 on the shelf took up approximately (or below) 10 ngC.(10^6 cell)$^{-1}$.d^{-1}.

4.6.8 Kinetics of ^{14}C incorporation and size fractionation

Incorporation of ^{14}C in inorganic particulate matter was very low during the survey. Southern stations displayed higher rates of ^{14}C incorporation in organic matter at 3 m depth along the shelf (0.32 and 0.27 µmolC.l^{-1}.h^{-1} at stations 12 and 2, respectively) and decreased towards the north (0.16 µmolC.l^{-1}.h^{-1} at station 10). Comparable rates were measured on the slope, in the range observed on the shelf with the same decreasing tendency (0.25 and 0.16 µmolC.l^{-1}.h^{-1} at stations 4 and 7, respectively). Very low rate of incorporation was found at station 1 (0.05 µmolC.l^{-1}.h^{-1} near the Ushant front). Organic production decreased by c.a. 50 % at station 4 (0.25 to 0.13 µmolC.l^{-1}.h^{-1}) after 10 days but increased slightly at station 7 during the same lag (0.16 to 0.19 µmolC.l^{-1}.h^{-1}). Incubations of deeper water showed lower organic matter production at stations 5, 8 and 10 (0.01 to 0.02 µmolC.l^{-1}.h^{-1}), compared to other stations of the continental shelf (0.10 and 0.13 µmolC.l^{-1}.h^{-1} at stations 12 and 2, respectively). Figures 97 and 98 show as an example of the kinetics of ^{14}C incorporation at station 2 respectively at 3 m and 60 m.

Incorporation of ^{14}C in organic matter in the dark was generally about or even below 0.05 µmolC.l^{-1} after 12 hours of incubation, and comparable with the one found for poisoned samples (sodium azide).

Few incorporation of carbon in organic matter was due to larger phytoplankton (> 12 µm) but rather to the size classes of [2-12 µm] and [0.2-2 µm] (data not shown).

St2 (3m)

$y = 0.32x - 0.13$
$R^2 = 0.95$
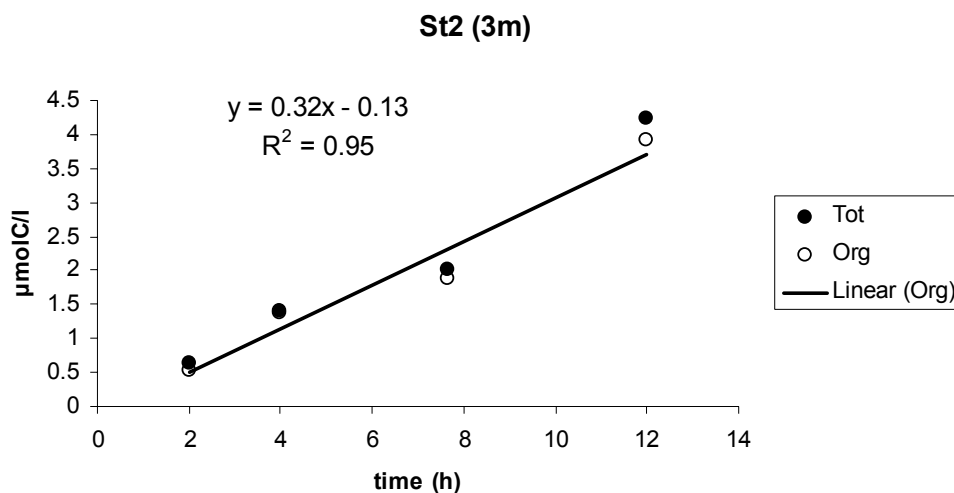
Figure 97. Kinetics of ^{14}C incorporation by natural assemblages in surface waters (3 m) at station 2 (shelf break, in µmolC.l^{-1}) under constant light (150 µmol.m^{-2}.s^{-1}) during the June 2004 Belgica cruise. Black dots represent the total incorporation of ^{14}C while open dots represent incorporation in the organic compartment. The difference between the two values is defined as the rate of calcification.

St2 (60m)

$y = 0.13x + 0.19$
$R^2 = 0.88$
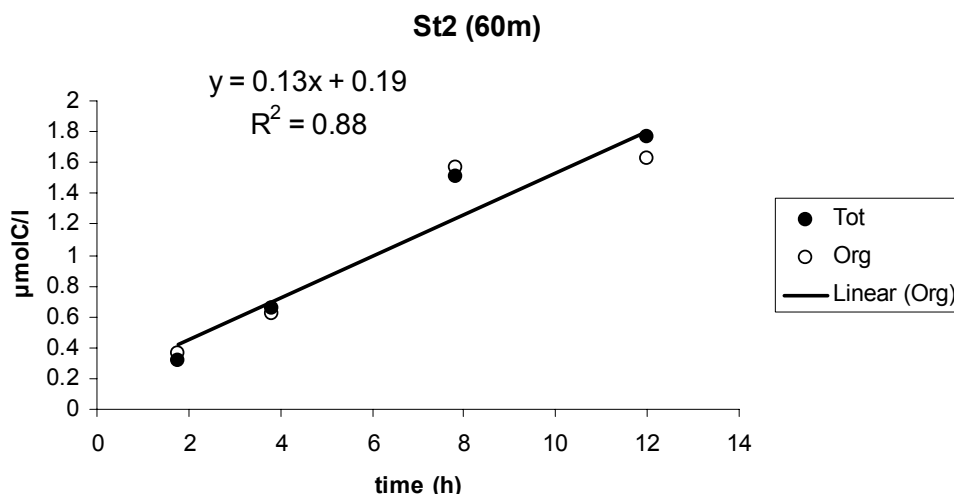
Figure 98. Kinetics of incorporation of ^{14}C by natural assemblages at depth (60 m) at station 2 (shelf break, in µmolC.l^{-1}) under constant light (150 µmol.m^{-2}.s^{-1}) during the June 2004 Belgica cruise. Black dots represent the total incorporation of ^{14}C while open dots represent incorporation in the organic compartment. The difference between the two values is defined as the rate of calcification.

4.6.9 Integrated primary production and calcification

The rates of ^{14}C incorporation in the organic fraction were generally lower than 0.7 $gC.m^{-2}.d^{-1}$ in the survey and ranged between 0.2 and 0.7 $gC.m^{-2}.d^{-1}$ on the continental shelf (Figure 99). No significant trend was observed on the continental slope, where the rates of incorporation were similar to those measured on the shelf (0.3 and 0.4 $gC.m^{-2}.d^{-1}$ at stations 7 and 4, respectively). A three-fold increase was however observed at the revisited station 5bis.

Calcification rates ranged between 1 % (station 12) and 31 % (station 2) of the primary production rates, and never exceeded 0.14 $gC.m^{-2}.d^{-1}$ (stations 2). The increase of C uptake rates in the organic fraction at station 5bis was accompanied by a lower but still noticeable increase in calcification, after 9 days. The rates decreased to 0.03 and 0.02 $gC.m^{-2}.d^{-1}$ at stations 4bis and 7bis, after 12 days and 10 days, respectively.

The integrated Chl-a concentration ranged between 23 and 83 $mgChl-a.m^{-2}$ and averaged 43 ± 19 $mgChla.m^{-2}$ in June 2004, at the continental margin. High phytoplanktonic biomass, in the range of 100 $mgChl-a\ m^{-2}$ was measured at station 12 and at the revisited station 5bis. In general, a decrease was observed at the revisited stations 5bis, 7bis and 4bis.
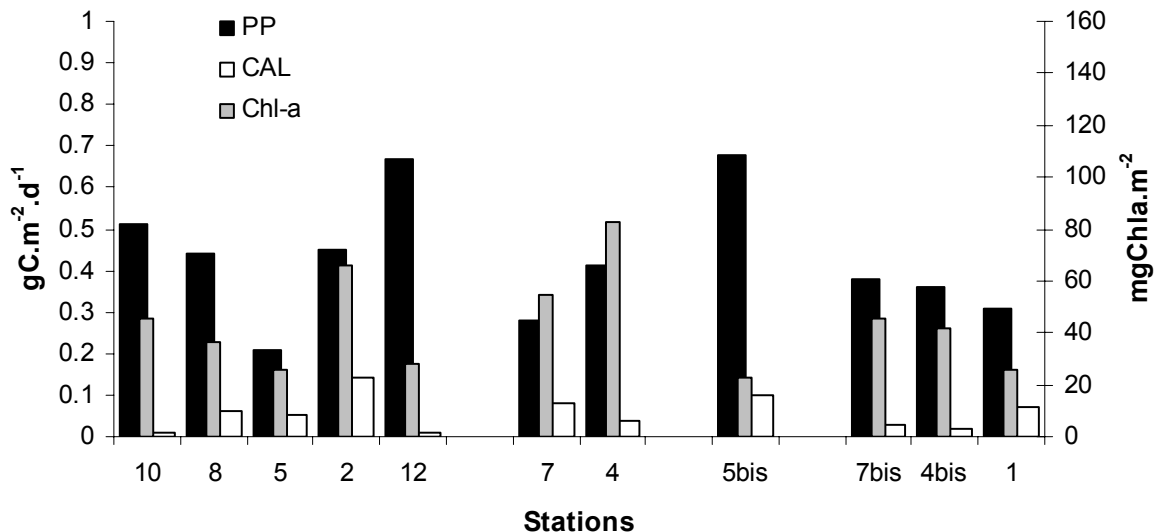
Figure 99. Primary production and calcification ($gC.m^{-2}.d^{-1}$) during the June 2004 Belgica cruise. Integrated Chl-a (mg $Chl-a.m^{-2}$) gives an indication of the amount of organic matter at the different stations.

4.7   Synthesis of field investigations

4.7.1 Watermass properties

Temperature-salinity (T-S) diagram of the top 1600 m, over the continental slope, shows the influence of the cold and low-salinity Labrador Sea Water (LSW) below the Mediterranean maximum, at salinities close to 35.7 and temperatures of 8 to 9°C (Hydes *et al.*, 2001). This inflexion of the T-S curve is characteristic of the Mediterranean Outflow Water (MOW) that flows poleward along the slope at approximately 1000 m depth. The mode water in the surface layer is the North Atlantic Central Water (NACW) that, despite a low range of salinities ranging between 35.5 and 35.6, exhibits a wide range of temperatures in its upper part as a result of surface warming and that suggests thermal stratification of the surface waters.
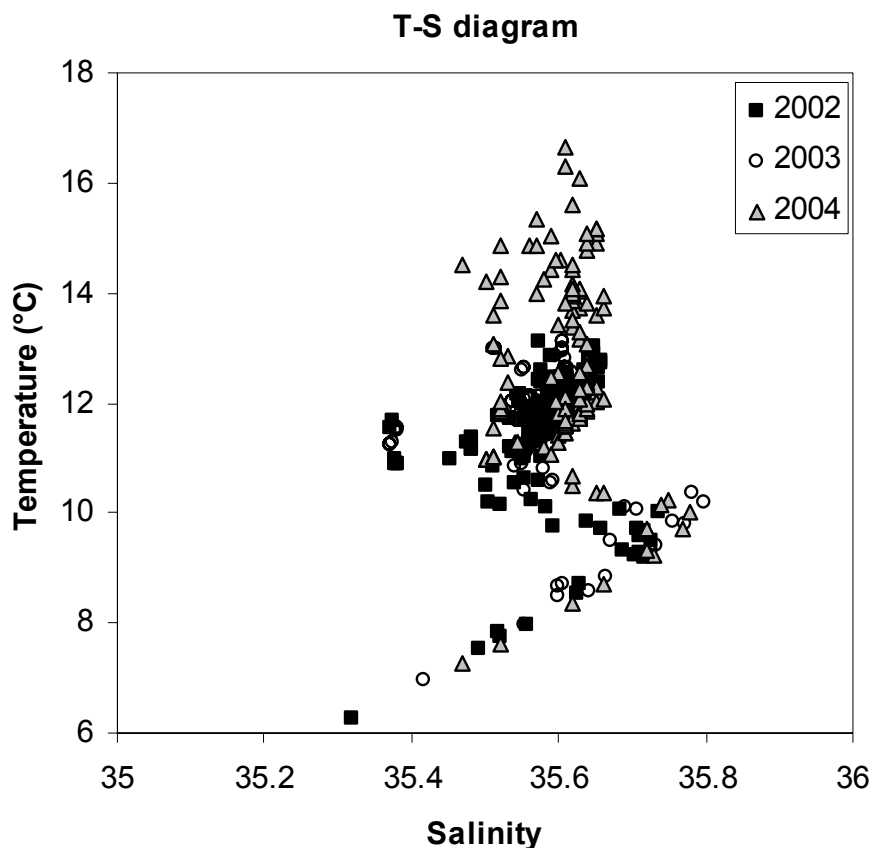
Figure 100. T-S diagram of vertical CTD profiles during the 2002, 2003 and 2004 cruises, down to 1600 m depth.

4.7.2 Analysis of time series

The analysis of time series of averaged OBPG SeaWiFS Chl-a concentrations (http://reason.gsfc.nasa.gov/OPS/Giovanni/) between 2002 and 2004 provides a good indication of seasonal changes in total phytoplankton biomass during the spring bloom (Figure 101). It however cannot be used as a quantitative descriptor since phytoplankton patchiness is important at the continental margin and the mesh of the area is too coarse (24500 km² and 40500 km² for the La Chapelle and the Goban Spur areas, respectively). Nevertheless, it appears that the region shows an overall increase in phytoplankton starting mid-March. Phytoplanktonic biomass returns to its pre-bloom level in August and shows two successive phases: an early increase at the beginning of the bloom period followed by a small decrease and a subsequent regain, approximately one and a half month later. The bloom occurs earlier at the Goban Spur than at the La Chapelle area, as also observed by Joint *et al.* (2001). The pioneer group to have a significant impact on Chl-a concentration in the phytoplanktonic succession during this period are diatoms (Taylor *et al.*, 1993) whose activity lasts until nutrients, and especially dissolved silica, are depleted. As a general scheme, coccolithophores bloom after diatoms and grow on reduced nitrate and phosphate standing stocks. The high-reflectance patches associated with coccolithophores, in this area (GREPMA, 1988; Garcia-Soto *et al.*, 1995) are generally observed at the end of the spring bloom, when thermal stratification occurs, and lasts until August (S. Groom, pers. comm.). The continental margin undergoes discontinuous nutrient inputs, as characterised by cool waters at the shelf break that result in the mixing of cool nutrient-rich water at the surface (Joint *et al.*, 2001). The nutrient inputs to the photic zone may sustain high rates of productivity by both diatoms and coccolithophores, so that they are often found together within the samples all over this period.

The temporal distribution of the three cruises with respect to the seasonal cycle of phytoplanktonic biomass covers distinct phases of the spring bloom (Figure 101). The cruise carried out in 2002 characterises an early-bloom situation, during which high rates of primary production are sustained. The subsequent cruises (2003 and 2004) occur after the first peak of phytoplanktonic biomass (2003) or during the late-stage of the bloom (2004) and show lower C incorporation in organic matter.

As observed for primary production, calcification is also sustained at different rates between the three cruises and follows the pattern of primary production (Figure 102). Nevertheless, averaged calcification to primary production ratio (C:P) was estimated to be 0.34 during the 2002 early-bloom period, and decreased to 0.11 and 0.16 in 2003 and 2004, respectively.
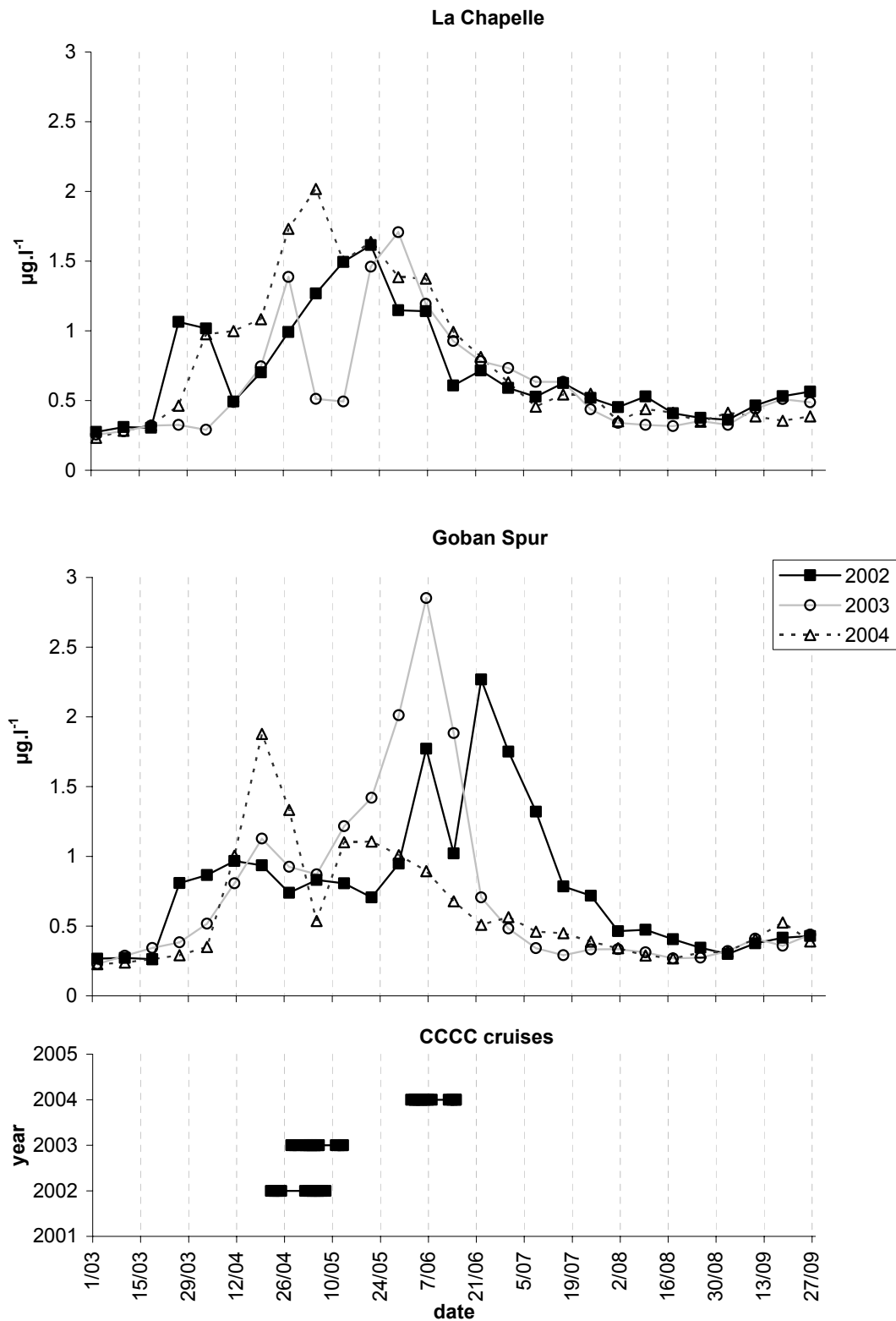
Figure 101. Temporal coverage of the three CCCC cruises and averaged OBPG SeaWiFS Chl-a concentrations (http://reason.gsfc.nasa.gov/OPS/Giovanni/) (in µg.l^{-1}) at the La Chapelle Bank (lat [47.0° N, 48.5° N]; long [8.0° W,6.0° W]) and the Goban Spur (lat [48.5° N, 51.0° N]; long [12.0° W, 10.0° W]) areas.
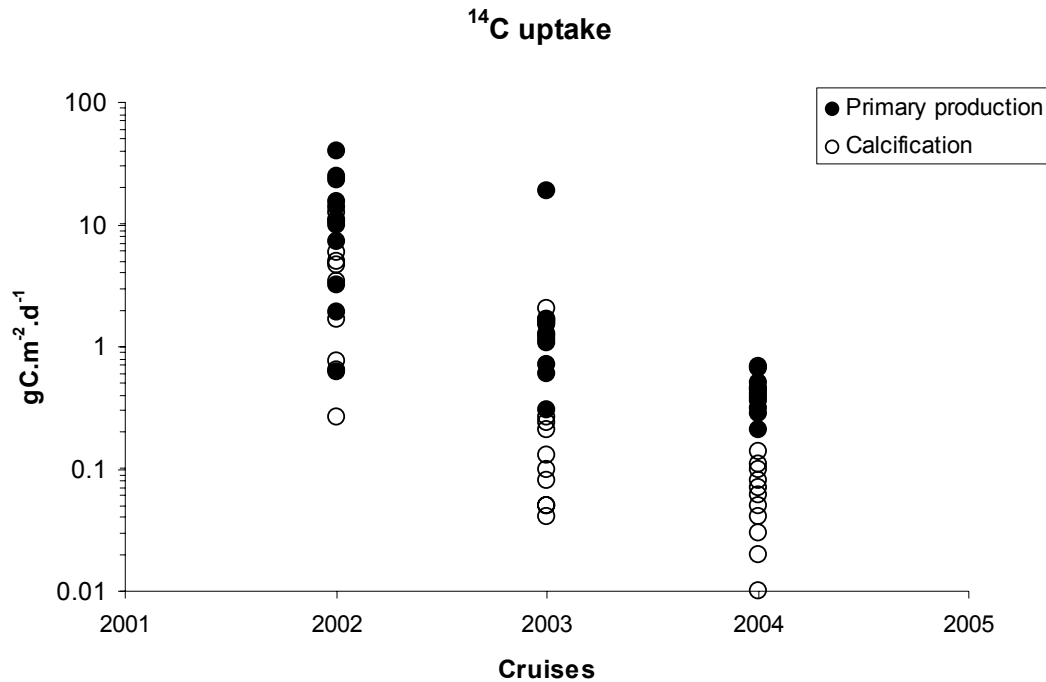
Figure 102. Comparison of ^{14}C uptake rates for primary production (solid dots) and calcification (open dots) in phytoplankton incubated during the three campaigns (2002, 2003 and 2004).

Seawater reflectance is due to suspended calcite in surface waters. Even if coccolith detachment occurs continuously during cell development (Fritz and Balch, 1996), this process is enhanced under nutrient depleted conditions, in the case of *E. huxleyi*, when the cells have achieved their exponential growth (Fritz, 1999). The high-reflectance patch is associated with the coccolithophorid post-stationary phases (late stage) and suggests that the coccolithophores have already bloomed a couple of weeks before they are observed on satellite pictures, according the dynamics of a bloom (Engel *et al.,* 2005).

The emphasis of pelagic calcification at the continental margin is also shown, here, by the non-conservative behaviour of TA with respect to salinity (Figure 103). Such a situation occurs when $CaCO_3$ precipitation has contributed to the removal of TA in stratified waters. A similar decrease of TA by 25 µmol.kg^{-1} was observed in both the early-(2002) and late-(2004) bloom periods. Nevertheless, the so-called TA anomaly technique (Chisholm and Gattuso, 1991), which allows the determination of the total amount of $CaCO_3$ produced by integrating TA concentrations over depth could not be used at the continental margin, where vertical mixing occurs.
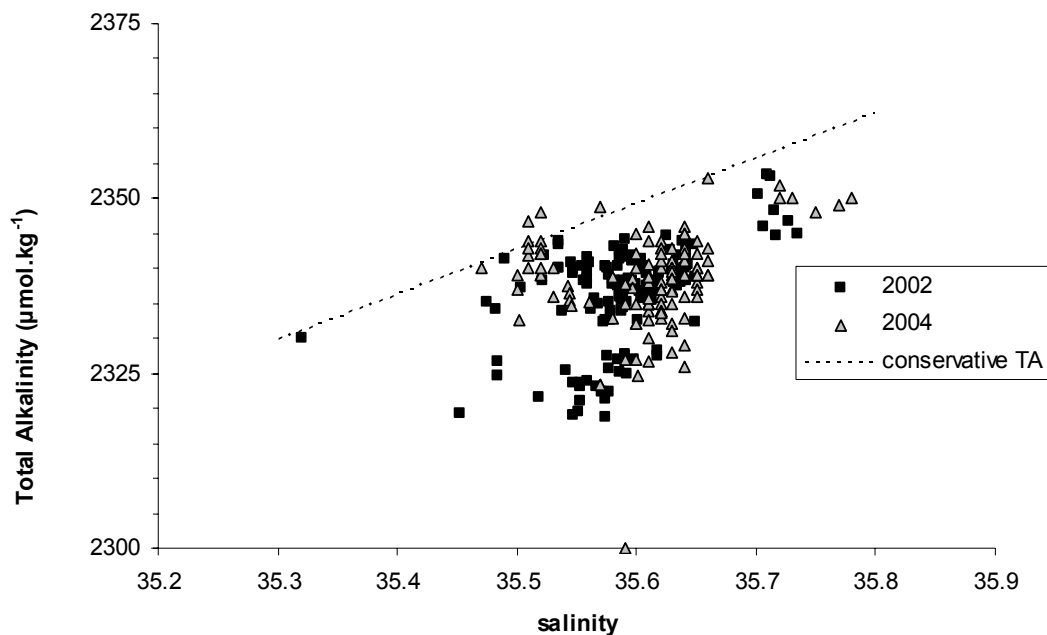
Figure 103. Total alkalinity (µmol.kg^{-1}) versus salinity in the photic zone (2002 and 2004) and conservative mixing of TA = 64.9*S + 38.8 (ULg, unpubl. Data.).

Based on C incorporation data, a tentative mass balance for C can be derived for the continental shelf and slope (Table 7 and Figure 104). The intensity of the biological pump is modulated by the carbonate counter-pump, which is enhanced in areas where coccolithophores develop important blooms. In early-stage conditions, the potential sequestration of C due to phytoplanktonic activity in surface waters averages 12.05 gC.m^{-2}.d^{-1} and the continental shelf behaves as a sink for atmospheric CO_2 by 8.09 gC.m^{-2}.d^{-1}. The oceanic sink decreased with aging of the phytoplanktonic bloom either on the shelf or on the slope. Nevertheless, the potential impact of TEP formation, as suggested by our results may play an important role in C sequestration since they may contribute to suspended matter aggregation and contribute to the export of C.

Table 7. Mass balance of C for the 2002, 2003 and 2004 cruises. Our approach discriminates the shelf and the slope areas but averages the variations with respect to the latitude.

	Continental shelf				*Continental slope*		
Flux	2002	2003	2004		2002	2003	2004
$(gC.m^{-2}.d^{-1})$							
1	10.07	3.59	0.49		23.38	1.33	0.36
2	3.96	0.40	0.08		6.02	0.13	0.04
3	1.98	0.20	0.04		3.01	0.07	0.02
4	12.05	3.79	0.53		26.40	1.40	0.38
5	8.09	3.39	0.45		20.37	1.27	0.34
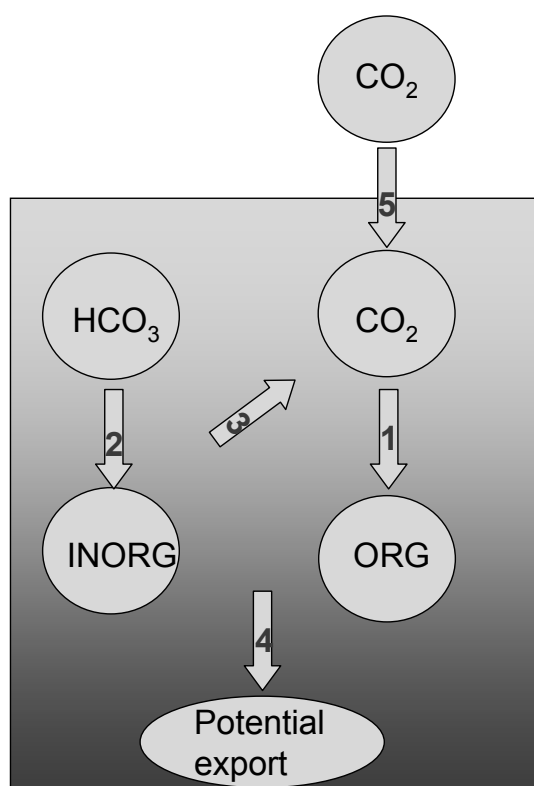
Figure 104. Fluxes are represented by numbers (in $gC.m^{-2}.d^{-1}$) and refer to Table 7. They are quoted as positive in the direction of the arrows.

5.   A CONCEPTUAL CARBON MODEL FOR THE COCCOLITHOPHORES

Because the end-product of the overall calcification process (i.e. calcium carbonate plates or coccoliths) is generally considered, most of the hypotheses dealing with a functional role of calcification by coccolithophores are contradictory and no study, to date, can ascertain the role of the calcite plates onto the cell surface (Brownlee & Taylor, 2004). It is established that the coccosphere cannot escape from zooplankton grazing (Nejstgaard *et al.*, 1997) nor provide a shelter against viruses (Jacquet *et al.*, 2002). *E. huxleyi* generally produces more coccoliths than needed for providing a physical protection (Fritz, 1999). The role of the calcite plates in cell buoyancy (Lecourt *et al.*, 1996) is contradictory with the lack of photoinhibition (Nanninga & Tyrrell, 1996) in *E. huxleyi* and their ability to grow under low phosphate concentrations (Riegman *et al.*, 2000); so does the photoprotective role of the coccosphere. One can consider coccolithophorid internal calcification in another way: the production of polysaccharides (Engel *et al.*, 2004) and especially of the acidic coccoliths-polysaccharides (CP) responsible for biomineralization would provide several metabolic advantages.

The absence of photoinhibition under irradiances higher than 1000 µmol.m^{-2}.s^{-1} not only provides *E. huxleyi* with a very important competitive advantage under high light intensities, for either coccoliths-bearing or naked cells, but also converges with the "overflow hypothesis" for the production of polysaccharides. It has been suggested by van der Wal *et al.* (1983) that naked cells of *E. huxleyi* would produce polysaccharides but that their inability to produce coccoliths was due to a deviant morphology of the apparatus through which coccoliths are formed (coccolith vesicle and base plate). Calcification was found to be light-dependent (e.g. Sikes *et al.*, 1980) and even highly energy consuming for the cell (Anning *et al.*, 1996). Such statements are in contrast with a real function of calcification, if reduced to the sole production of calcium carbonate. Rather than biomineralization by itself, the production of polysaccharides might then be an important pathway for coccolithophores. They represent an effective energetic cost since about 50 % of the C fixed by the cell is released as polysaccharides if a calcification to primary production (C:P) ratio of 1.0 is taken into account (Brownlee and Tyrrell, 2004). This proportion is prone to increase when the C:P ratio reaches values above 1, up to 2.2, as observed in the North Sea (van Bleijswijk *et al.*, 1994). They provide a route through which the excess energy is derived through the formation of by-products. Buitenhuis *et al.* (1999), Paasche (2001) and Rost and Riebesell (2004) have evoked a possible "trash-can" function for calcium carbonate which was associated with photosynthesis, as a possible cooperation of calcification in providing CO_2 to the RUBisCO. In this debate, we argue that calcification can effectively act as a "trash-can" for the cell, but not as a carbon concentration mechanism (CCM), as previously

suggested. It can be rather viewed as a way to expend the excess of solar energy. This function could be met by carbohydrate production when DIC is not limiting but low nutrient concentrations prevent from the production of structural and functional proteins. This also occurs when the structural and functioning pool of proteins is obtained.

The ability of CP to bind and drive calcium outside the cell and even "neutralize" the excess soluble intracellular Ca^{2+} by precipitating $CaCO_3$ also provides an efficient way to preserve homeostasis (i.e. low cytosolic $[Ca^{2+}]$ compatible with cell physiology) within the cell. Ca^{2+} can then be released outside, bound to polysaccharides or in the form of calcite. Ca^{2+} detoxification (Simkiss, 1977) is often neglected when attempting to inventory the various functions that internal calcification could represent for coccolithophores.

Therefore, the production of polysaccharides, which appears to be a common feature in coccolithophores, fulfils two important functions for the cell's physiology. Firstly, it allows the overflow of the excess energy provided by solar irradiance by producing simple carbon-rich molecules ("overflow mechanism") and, secondly, it provides a way to concentrate the excess of Ca^{2+} and drive it outside the internal medium (function of detoxification). The occurrence of "overflow mechanisms" for small unicellular algae, like *E. huxleyi*, is important because they are not capable of storing compounds in the internal medium, as usually do larger species, like diatoms. The storage vacuole, which permits nutrient hoarding, allows diatoms to outcompete coccolithophores in turbulent conditions (Tozzi *et al.*, 2004), while coccolithophores dominate under nutrient-limiting conditions as a consequence to low affinity for carbon (Nanninga & Tyrrell, 1996), nitrate and phosphate (Riegman *et al.*, 2000).

Such a conceptual model alternatively provides a certain degree of coupling between photosynthesis and calcification, as suggested in literature (Paasche, 2002) and allows the calcification rates to vary during the cell cycle (Figure 105). Internal calcification requires a high degree of saturation with respect to calcite in the compartment where precipitation occurs. The elevation of Ca^{2+} provided by the presence of the CP would contribute to the maintenance of such conditions within the cell in spite of a decrease in the ambient seawater Ω_{cal}, due to increased pCO_2 or decreased total alkalinity. The apparent internal Ω_{cal} would then be higher than but linked, to some extent, to the one measured externally and offset calcification under unfavourable conditions for thermodynamic precipitation in seawater. Pure calcite as produced by *E. huxleyi* is, in contrast with aragonite or Mg-calcite, the most widespread carbonate phases produced by marine organisms. Its high stability in seawater suggests a stronger energetic investment by *E. huxleyi* to produce this phase, compared to the more soluble Mg-calcites and aragonite. In this respect, the ability of coccolithophores to produce pure calcite is in phase with the energetic cost

required for its production and goes in favour of an overflow mechanism. Coccolithophorid calcification is then in contrast with the strictly structural function of aragonite or Mg-calcites in molluscs or corals.
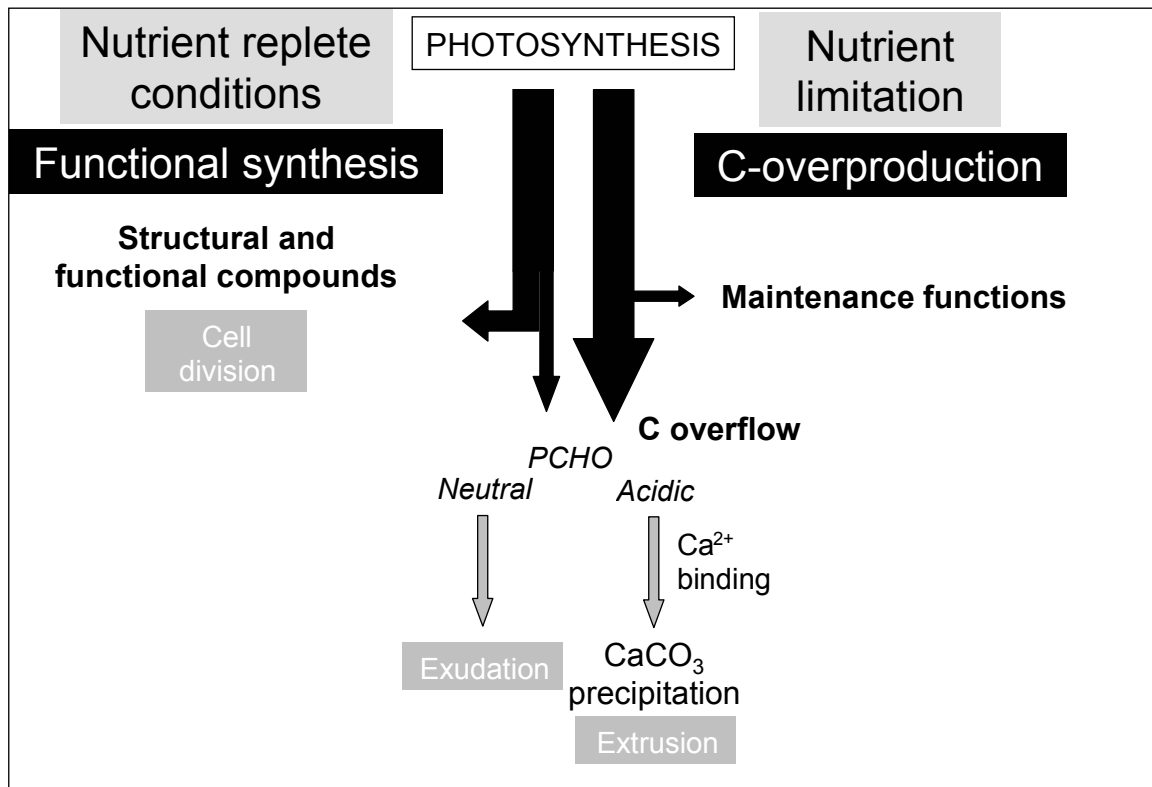
Figure 105. Schematic representation of the implication of the production of polysaccharides (PCHO) in the metabolism of *E. huxleyi*. The uptake of C under nutrient-replete conditions (left side) leads to the biosynthesis of functional and structural compounds that allows cells to divide during the exponential growth phase. After nutrient exhaustion (right side), the metabolic activity is sustained by photosynthesis (maintenance functions) and, in absence of photolimitation, the excess of C taken up by photosynthesis is exudated in the form of PCHO or other C-rich compounds (alkenons, lipids, esters, alcools…). Among this pool of PCHO, the acidic ones have a particular affinity for Ca^{2+} and allow $CaCO_3$ to precipitate internally. These polysaccharides are extruded with the coccoliths and are found in the external coating of the cells.

6.   CONCLUSIONS AND RECOMMENDATIONS

By combing laboratory experiments with field investigations, CCCC has contributed to an improved understanding of the role of calcifying planktonic organisms in sequestering CO_2. The major conclusions and achievements are presented. Perspectives for future research are also provided.

6.1   Laboratory chemostat experiments

Laboratory chemostat experiments were performed to investigate the effect of increasing pCO_2 on cellular calcification of a N-limited culture of *Emiliania huxleyi (E. huxleyi)*. Our investigation differed from previous studies by its regulation of pCO_2 based on the bubbling of gas mixtures and the maintenance of phytoplankton in the required steady-state conditions of nutrient limitation. The results obtained in this study indicated that a sudden doubling in pCO_2 had a rapid effect on the cell physiology, leading to a decrease in cellular calcification rates by 25 %, which took place within two generations. The magnitude of decrease in calcification rates in this work agrees with the results reported by Zondervan *et al*. (2002). The decrease of calcification rates in our study was not accompanied, however, by a significant decrease in the PIC:POC ratio as observed by Zondervan *et al.* (2002) for cultures grown in nutrient repleted conditions. This difference could be attributed to the nutrient status encountered in the two studies.

6.2   Mesocosm experiments

Primary production and calcification in response to different partial pressures of CO_2 (pCO_2) ("glacial," "present," and "year 2100" atmospheric CO_2 concentrations) were also investigated during a mesocosm bloom dominated by *E. huxleyi*. The net community production (NCP) and net community calcification (NCC) were assessed during the bloom development and decline, together with oxygen production and ^{14}C incorporation. No significant change in net NCP was observed with increasing pCO_2, while the NCC was reduced by 40%. The higher pCO_2 caused a delay in the onset of calcification. A change in the ratio of PIC to POC production and thus in export fluxes can be expected with rising atmospheric pCO_2.

6.3   Field investigations

Three field investigations, assisted by remote sensing, were carried during 2002-2004 onboard the *RV Belgica* in the Gulf of Biscay where the occurrence of frequent and recurrent coccolithophore blooms had been observed. Biogeochemical

parameters were measured and rates of primary production and calcification were determined. The three cruises with respect to the seasonal cycle of phytoplanktonic biomass covered distinct phases of the spring bloom. The cruise carried out in 2002 characterised an early-bloom situation, during which high rates of primary production were sustained. The subsequent cruises (2003 and 2004) took place after the first peak of phytoplanktonic biomass (2003) or during the late-stage of the bloom (2004) and showed a lower C incorporation in the organic matter. As observed for primary production, calcification was also sustained at different rates between the three cruises and followed the pattern of primary production. Averaged calcification to primary production ratio (C:P) was estimated to be 0.34 during the 2002 early-bloom period, and decreased to 0.11 and 0.16 in 2003 and 2004, respectively.

Various degrees of $CaCO_3$ preservation were observed by SEM for samples collected during the 2004 cruise, but overall they appeared to be well preserved. A contrario, bad preservation of coccoliths was encountered within the high reflectance patch, where good $CaCO_3$ preservation was rarely found in the top 40 m of the water column. Such a low preservation may represent dissolution of $CaCO_3$ above the lysocline, as previously evoked by Wollast & Chou (1998) for the same area.

Based on C incorporation data, a tentative mass balance for C can be derived for the continental shelf and slope in the Northern Gulf of Biscay area. The intensity of the biological pump is modulated by the carbonate counter-pump, which is enhanced in areas where coccolithophores develop important blooms. In early-stage conditions, the potential sequestration of C due to phytoplanktonic activity in surface waters is significant and the continental shelf behaves as a sink for atmospheric CO_2. The oceanic sink decreased with aging of the phytoplanktonic bloom either on the shelf or on the slope. Nevertheless, the potential impact of transparent exopolymer particle (TEP) formation, as suggested by our results may play an important role in C sequestration since they may contribute to suspended matter aggregation and hence to the export of C.

6.4   A conceptual carbon model for the coccolithophores

A conceptual model is proposed to describe the implication of the production of polysaccharides (PCHO) in the metabolism of the *E. huxleyi*. The uptake of C under nutrient-replete conditions leads to the biosynthesis of functional and structural compounds that allows cells to divide during the exponential growth phase. After nutrient exhaustion, the metabolic activity is sustained by photosynthesis (maintenance functions) and, in absence of photolimitation, the excess of C taken up by photosynthesis is exuded in the form of PCHO or other C-rich compounds. Among this pool of PCHO, the acidic ones have a particular affinity for Ca^{2+} and allow

$CaCO_3$ to precipitate internally. These acidic polysaccharides are then extruded with the coccoliths and are found in the external coating of the cells.

6.5 Perspectives for future research

Biogenic calcification responds positively to changes of saturate state of seawater with respect to calcium carbonate. It is therefore intuitive to consider that decreases in calcification rates in response to increases of pCO_2 would be a general feature. The overall response of calcification mediated by organic matter growth is however difficult to assess when pCO_2 increases. As we have seen in this study, the response of biology depends on various parameters such as, among others, environmental conditions (nutrient status, irradiance variations, seawater chemistry, …) and genetic variability. To better evaluate the behaviour of calcifying organisms in a high CO_2 environment, further investigations, either experimental or modelling, are needed.

The results of our field investigations show that the history of the coccolithophore bloom development in natural environments has an impact on whether the ecosystem could act as a sink for CO_2. Thus the rates of various biogeochemical processes associated with the bloom need to be better assessed at various blooming stages and their link better understood. Our study stresses also the importance in understanding the carbon dynamics of natural phytoplankton assemblages through an interdisciplinary approach.

7. ACKNOWLEDGEMENTS

8.   REFERENCES

Anning T., Nimer N. A., Merrett M. J., and Brownlee C. (1996) Costs and benefits of calcification in coccolithophorids. *J. Mar. Syst.* **9**, 45-56.

Balch W.M. and Kilpatrick K. (1996) Calcification rates in the equatorial Pacific along 140°W. Deep-Sea Research II 43, 971-994.

Bates et al. (1996) Alkalinity changes in the Sargasso Sea: Geochemical evidence of calcification ? Marine Chemistry 51, 3347-358.

Beardall J., Johnston A. M., and Raven J. A. (1998) Environmental regulation of CO2-concentrating mechanisms in microalgae. *Can. J. Bot.* **76**, 1010-1017.

Benthien A., Zondervan I., Engel A., Hefter J., Terbruggen A., and Riebesell U. (2007) Carbon isotopic fractionation during a mesocosm bloom experiment dominated by Emiliania huxleyi: Effects of CO2 concentration and primary production. *Geochimica et Cosmochimica Acta* **71**, 1528-1541.

Bishop J.K.B., Collier R.W., Kettens D.R. and Edmond J.M. (1980) The chemistry, biology and vertical flux of particulate matter from the upper 1500 m of the Panama Basin. Deep-Sea Research 27A, 615-640.

Bondarenko I., Treiger B., Van Grieken R., and Van Espen P. (1996) IDAS: a Windows based software package for cluster analysis. *Spectrochimica Acta Part B: Atomic Spectroscopy* **51** , 441-456.

Buitenhuis E. T., de Baar H. J. W., and Veldhuis M. (1999) Photosynthesis and calcification by *Emiliania huxleyi* (Prymnesiophyceae) as a function of inorganic carbon species. *J Phycol* **35**, 949-959.

Chisholm J. R. M. and Gattuso J.-P. (1991) Validation of the alkalinity anomaly technique for investigating calcification and photosynthesis in coral reef communities. *Limnol. Oceanogr.* **36**, 1232-1239.

Danbara A. and Shiraiwa Y. (1999) The requirement of selenium for the growth of marine coccolithophorids, Emiliania huxleyi, Gephyrocapsa oceanica and Helladosphaera sp (Prymnesiophyceae). *Plant Cell Physiol.* **40**, 762-766.

DeLille B., Harlay J., Zondervan I., Jacquet S., Chou L., Wollast R., Bellerby R. G. J., Frankignoulle M., Borges A. V., Riebesell U., and Gattuso J.-P. (2005) Response of primary production and calcification to changes of pCO(2) during experimental blooms of the coccolithophorid *Emiliania huxleyi*. *Glob. Biogeochem. Cycl.* **19**, GB2023.

Dickson A. G. (1990) Thermodynamics of the dissociation of boric acid in synthetic seawater from 273.15 to 318.15 K. *Deep Sea Research Part A. Oceanographic Research Papers* **37**, 755-766.

DOE (1994) *Handbook of methods for the analysis of the various parameters of the carbon dioxide system in sea water*. (electronic version 2.1).

Dong L. F., Nimer N. A., Okus E., and Merrett M. J. (1993) Dissolved inorganic carbon utilization in relation to calcite production in Emiliania huxleyi (Lohmann) Kamptner. *New Phytol.* **123**, 679-684.

Gattuso J.P., Frankignoulle M., Smith S.V., Ware J.R. and Wollast R. (1996) Coral Reefs and Carbon Dioxide, Science 271, 1298-1300.

Eilers P. H. C. and Peeters J. C. H. (1988) A model for the relationship between light intensity and the rate of photosynthesis in phytoplankton. *Ecol. Model.* **42**, 199-215.

Elzenga J. T. M., Prins H. B. A., and Stefels J. (2000) The role of extracellular carbonic anhydrase activity in inorganic carbon utilization of Phaeocystis globosa (Prymnesiophyceae): A comparison with other marine algae using the isotopic disequilibrium technique. *Limnol. Oceanogr.* **45**, 372-380.

Engel A. (2004) Distribution of transparent exopolymer particles (TEP) in the northeast Atlantic Ocean and their potential significance for aggregation processes. *Deep Sea Research Part I: Oceanographic Research Papers* **51**, 83-92.

Engel A., DeLille B., Jacquet S., Riebesell U., Rochelle-Newall E., Terbruggen A., and Zondervan I. (2004) Transparent exopolymer particles and dissolved organic carbon production by *Emiliania huxleyi* exposed to different CO_2 concentrations: a mesocosm experiment. *AME* **34**, 93-104.

Engel A. and Passow U. (2001) Carbon and nitrogen content of transparent exopolymer particles (TEP) in relation to their Alcian Blue adsorption. *Marine Ecology-Progress Series* **219**, 1-10.

Engel A., Thoms S., Riebesell U., Rochelle-Newall E., and Zondervan I. (2004) Polysaccharide aggregation as a potential sink of marine dissolved organic carbon. *Nat.* **428**, 929-932.

Engel A., Zondervan I., Aerts K., Benthien A., Chou L., DeLille B., Gattuso J.-P., Harlay J., Heemann C., Hoffmann L., Jacquet S., Nejstgaard J., Pizay M.-D., Rochelle-Newall E., Schneider U., Terbrueggen A., and Riebesell U. (2005) Testing the direct effects of CO_2 concentration on marine phytoplankton: A mesocosm experiment with the coccolithophorid Emiliania huxleyi. *Limnol. Oceanogr.* **50**, 493-507.

Fritz J. J. (1999) Carbon fixation and coccolith detachment in the coccolithophore *Emiliania huxleyi* in nitrate-limited cyclostats. *Marine Biology* **133**, 509-518.

Fritz J. J. and Balch W. M. (1996) A light-limited continuous culture study of *Emiliania huxleyi*: a determination of coccolith detachment and its relevance to cell sinking. *Journal of Experimental Marine Biology and Ecology* **207**, 127-147.

Garcia-Soto C., Fernandez E., Pingree R. D., and Harbour D. S. (1995) Evolution and structure of a shelf coccolithophore bloom in the Western English Channel. *J. Plankton Res.* **17** , 2011-2036.

Gattuso J.-P., Frankignoulle M., Bourge I., Romaine S., and Buddemeier R. W. (1998) Effect of calcium carbonate saturation of seawater on coral calcification. *Global and Planetary Change* **18**, 37-46.

Gran G. (1952) Determination of the equivalence point in potentiometric titrations. *Analyst (Part II)* 661-667.

Grasshoff K., Ehrhardt M., and Kremling K. (1983) *Methods of seawater analysis*. Verlag Chemie.

GREPMA. Satellite (AVHRR:NOAA-9) and ship studies of a coccolithophorid bloom in the western English Channel. Viollier, M., Sournia, A., Birrien, M.-J., Chrétiennot-Dinet, P., Le Borgne, P., Le Corre, P., Morin, P., and Olry, J. P. Marine Nature 1[1], 1-14. 1988. Ref Type: Generic

Guillard R. R. L. and Ryther J. H. (1962) Studies of marine planktonic diatoms. I. Cyclotella nana Hustedt and Detonula confervacea Cleve. *Can. J. Microbiol.* **8**, 229-239.

Hansen R.B., Ducklow H.W. and Field J.G. Editors (2000) The Changing Ocean Carbon Cycle: a midterm synthesis of the Joint Global Ocean Flux Study. International Geosphere-Biosphere Programme book Series 5, Cambridge University Press, 514p.

Hydes D. J., Le Gall A. C., Miller A. E. J., Brockmann U., Raabe T., Holley S., Alvarez-Salgado X., Antia A. N., Balzer W., and Chou L. (2001) Supply and demand of

nutrients and dissolved organic matter at and across the NW European shelf break in relation to hydrography and biogeochemical activity. *Deep Sea Research Part II: Topical Studies in Oceanography* **48**, 3023-3047.

Iglesias-Rodriguez M. D., Brown C. W., Doney S. C., Kleypas J., Kolber D. D., and Kolber Z. (2002) Representing key phytoplankton functional groups in ocean carbon cycle models: Coccolithophorids. *Glob. Biogeochem. Cycl.* **16**, 1100-doi:10.1029/2001GB001454.

IPCC (1995) Climate Change 1995, Contribution of Working Group I to the Second Assessment Report of the Intergovernmental Panel on Climate Change. J.T. Houghton, L.G. Meira Filho, B.A. Callander, N. Harris, A. Kattenberg and K. Maskell (eds). Cambridge University Press, 572p.

Israel A. and Hophy M. (2002) Growth, photosynthetic properties and Rubisco activities and amounts of marine macroalgae grown under current and elevated seawater CO_2 concentrations. *Global Change Biology* **8**, 831-840.

Lewis E. and Wallace D. W. R. Program Developed for CO_2 System Calculations. ORNL/CDIAC[105]. 1998. Carbon Dioxide Information Analysis Center, Oak Ridge National Laboratory, U.S. Department of Energy, Oak Ridge, Tennessee. Ref Type: Data File

Merrett M. J., Dong L. F., and Nimer N. A. (1993) Nitrate availability and calcite production in *Emiliania huxleyi* Lohmann. *Eur. J. Phycol.* **28**, 243-246.

Millero F. J., Lee K., and Roche M. P. (1998) Distribution of alkalinity in the surface waters of the major oceans. *Mar. Chem.* **60**, 111-130.

Milliman J. D., Troy P. J., Balch W. M., Adams A. K., Li Y. H., and Mackenzie F. T. (1999) Biologically mediated dissolution of calcium carbonate above the chemical lysocline? *Deep-Sea Research I* **46**, 1653-1669.

Murphy J. and Riley J. P. (1962) A modified single solution method for the determination of phosphate in natural waters. *Anal. Chim. Acta* **27**, 31-36.

Nanninga H.J., and Tyrrell T. (1996) Importance of light for the formation of algal blooms by *Emiliania huxleyi*. *Mar. Ecol. Prog. Ser.* **136**, 195-203.

Nimer N. A. and Merrett M. J. (1993) calcification rate in *Emiliania huxleyi* Lohmann in response to light, nitrate and availability of inorganic carbon. *New Phytol.* **123**, 673-677.

Obata T. et al. (2005) Change in the cellular composition of elements during selenium-deficient culture in a marine-calcifying alga, *Emiliania huxleyi* (Prymnesiophyceae). *Abstract* 1 (abstr.).

Paasche E. (1998) Roles of nitrogen and phosphorus in coccolith formation in Emiliania huxleyi (Prymnesiophyceae). *Eur. J. Phycol.* **33**, 33-42.

Paasche E. (1999) Reduced coccolith calcite production under light-limited growth: a comparative study of three clones of *Emiliania huxleyi* (Prymnesiophyceae). *Phycol.* **38**, 508-516.

Passow U. and Alldredge A. L. (1995) A dye-binding assay for the spectrophotometric measurement of transparent exopolymer particles (TEP). *Limnol. Oceanogr.* **40**, 1326-1335.

Riebesell U., Zondervan I., Rost B., Tortell P. D., Zeebe R. E., and Morel F. M. M. (2000) Reduced calcification of marine plankton in response of increased atmospheric CO_2. *Nat.* **407**, 364-367.

Riegman R., Stolte W., Nooderloos A. A. M., and Slezak D. (2000) Nutrient uptake and alkaline phosphatase (ec 3:1:3:1) activity of *Emiliania huxleyi* (prymnesiophyceae) during growth under N and P limitation in continuous cultures. *J Phycol* **36**, 87-96.

Rochelle-Newall E., DeLille B., Frankignoulle M., Gattuso J.-P., Jacquet S., Riebesell U., Terbruggen A., and Zondervan I. (2004) Chromophoric dissolved organic matter in experimental mesocosms maintained under different pCO2 levels. *Mar. Ecol. Prog. Ser.* **272**, 25-31.

Rost B., Riebesell U., Brukhardt S., and Slütemeyer D. (2003) Carbon acquisition of bloom-forming marine phytoplankton. *Limnol. Oceanogr.* **48**, 55-67.

Roy R. N., Roy L. N., Vogel K. M., Porter-Moore C., Pearson T., Good C. E., Millero F. J., and Campbell D. M. (1993) The dissociation constants of carbonic acid in seawater at salinities 5 to 45 and temperatures 0 to 45[degree sign]C. *Mar. Chem.* **44**, 249-267.

Sabine C.L. and Mackenzie F.T. (1993) Bank-derived carbonate sediment transport and dissolution in the Hawaiian Archipelago. Aquatic Chemistry 1, 189-230.

Schippers P., Lürling M., and Scheffer M. (2004) Increase of atmospheric CO2 promotes phytoplankton productivity. *Ecology Letters* **7**, 446-451.

Sciandra A., Harlay J., Lefèvre D., Lemée R., Rimmelin P., Denis M., and Gattuso J.-P. (2003) Response of coccolithophorid *Emiliania huxleyi* to elevated partial pressure of CO2 under nitrogen limitation. *Mar. Ecol. Prog. Ser.* **261**, 111-122.

Serpette,A.; Le Cann,B.; Colas,F. (2006) Lagrangian circulation of the North Atlantic Central Water over the abyssal plain and the continental slopes of the Bay of Biscay: description of selected mesoscale features. Scientia Marina 70S1, 27-42.

Sherrell R.M., Field M.P. and Gao Y. (1998) Temporal variability of suspended mass and composition in the northeast Pacific water column: relationship to sinking flux and lateral advection. Deep-Sea Research II 44, 733-761.

Smith D. C., Steward G. F., Long R. A., and Azam F. (1995) Bacterial mediation of carbon fluxes during a diatom bloom in a mesocosm. *Deep Sea Research Part II: Topical Studies in Oceanography* **42**, 75-97.

Takahashi T., Olaffson J., Goddard J. G., Chipman D. W., and Sutherland S. C. (1993) Seasonal variation of CO2 and nutrients in the high-latitude surface oceans: a comparative study. *Glob. Biogeochem. Cycl.* **7**, 843-878.

Taylor A. H., Harbour D. S., Harris R. P., Burkill P. H., and Edwards E. S. (1993) Seasonal succession in the pelagic ecosystem of the North Atlantic and the utilization of nitrogen. *J. Plankton Res.* **15**, 875-891.

Volk T. and Hoffert M.I. (1985) Ocean carbon pumps: Analysis of relative strengths and efficiencies in ocean-driven atmospheric CO2 changes. In: E.T. Sundquist and W.S. Broecker (eds) The Carbon Cycle and Atmospheric CO2: Natural Variations Archean to Present. Geophys. Monogr. Ser. 32, pp. 99-110., AGU, Washington, D.C.

Wollast R. and Chou L. (1998) Distribution and fluxes of calcium carbonate along the continental margin in the Gulf of Biscay. Aquatic Chemistry 4, 369-393. The Chave Memorial Volume.

Yentsch, C. S., and Menzel, D. W. (1963). A method for the determination of phytoplankton chlorophyll and phaeophytin by fluorescence. *Deep-Sea Res*. **10**, 221-231.

Zondervan I., Rost B., and Riebesell U. (2002) Effect of CO2 concentration on the PIC/POC ratio in the coccolithophore Emiliania huxleyi grown under light-limiting conditions and different daylengths. *Journal of Experimental Biology and Ecology* **272**, 55-70.

Zondervan I., Zeebe R. E., Rost B., and Riebesell U. (2001) Decreasing marine biogenic calcification: A negative feedback on rising atmospheric pCO$_2$. *Glob. Biogeochem. Cycl.* **15**, 507-516.

SPSD II (2000-2005)

BELGIAN SCIENCE POLICY

HEAD OF THE DEPARTMENT 'RESEARCH PROGRAMMES': DOMINIQUE FONTEYN

CONTACT PERSON: MARTINE VANDERSTRAETEN